

CALCIUM TRIGGERED SYNAPTIC VESICLE EXOCYTOSIS

APPROVED BY SUPERVISORY COMMITTEE

Thomas C. Südhof, M.D., Advisor

Kimberly Huber, Ph.D., Committee Chair

Ilya Bezprozvanny, Ph.D.

Micheal Rosen, Ph.D.

To my wife Yan Lin & Prof. Ji-Shuo Li

CALCIUM TRIGGERED SYNAPTIC VESICLE EXOCYTOSIS

by

ZHIPING PANG

DISSERTATION

Presented to the Faculty of the Graduate School of Biomedical Sciences

The University of Texas Southwestern Medical Center at Dallas

In Partial Fulfillment of the Requirements

For the Degree of

DOCTOR OF PHILOSOPHY

The University of Texas Southwestern Medical Center at Dallas

Dallas, Texas

August, 2007

Copyright
by
Zhiping Pang, 2007

All Rights Reserved
Copyright

ACKNOWLEDGEMENTS

I would like to thank my mentor, Dr. Thomas C. Südhof, who is also my scientific hero. Over the past four years, he encouraged me, made excellent suggestions and supported me in both my research and career development. I have always felt fortunate to be his student working with him and in his lab. His insightful opinions about scientific questions, and his rigor and perseverance in the endeavor of science always inspired me.

I would also want to give my thanks to the members of the Sudhof's lab. Without their support the completion of my thesis would have been impossible. Over the years, I had tremendous help from Drs. Ok-Ho Shin, Anton Maximov, Pascal Kaeser, Peter Bronk, Jiong Tang, Gowan Tervo and others. I would specially want to thank the technical support team, including Iza Kornblum, Andre Roth, Jason Mitchell, Lin Fan and Ewa Borowicz for their continuous supports.

The Department of Neuroscience at Dallas offered me a unique environment for my graduate studies. The state-of-art facilities and the enthusiastic young faculty created a nurturing workplace. I especially want to thank Dr. Jianyuan Sun and his postdoctoral fellow Dengkui Qin. We had a fruitful collaboration on Ca^{2+} -triggered asynchronous release that greatly enriched my graduate degree. I would also thank Dr. Weichun Lin and his lab members.

I would also like to thank Dr. Roberto Adachi and his associates, for providing us Synaptotagmin-2 KO mice.

Finally, I would like thank my thesis committee members: Drs. Kimberly Huber, Ilya Bezprozvanny and Michael Rosen. Their insightful comments and help greatly improved my thesis.

CALCIUM TRIGGERED SYNAPTIC VESICLE EXOCYTOSIS

Publication No. _____

Zhiping Pang Ph.D.

The University of Texas Southwestern Medical Center at Dallas, 2007

Supervising Professor: Thomas C. Südhof, M.D.

Neurotransmitter release is triggered by the action potential induced influx of Ca^{2+} into nerve terminals. One of the central questions in neuroscience is how Ca^{2+} promotes synaptic vesicles from rest to fusion leading to release of neurotransmitters. In this thesis, I first addressed if synaptogmin-1/SNARE binding is important for synaptic vesicle release. Using two knock-in mouse lines each with single amino-acid substitution, namely D232N and D238N in synaptotagmin-1, combined with electrophysiology, I found evoked release in D232N mutant neuronal cultures is significantly increased, whereas in D238N cultures release is slightly but significantly decreased. Ca^{2+} titration curves indicated the apparent

Ca^{2+} -affinity for vesicle release significantly increased in D232N synapses. These data are consistent with biochemical studies that showed that the D232N substitution in synaptotagmin-1 increases Ca^{2+} -dependent SNARE bindings but leaves phospholipid binding unchanged, whereas the D238N mutant slightly decreased phospholipid binding but leaves SNARE binding insignificantly changed. Second, I addressed if synaptotagmin-2 is another Ca^{2+} -sensor for synaptic vesicle release. I and my colleagues used two mouse lines: one contains a single amino acid mutation in synaptotagmin-2 (I377N) and one has synaptotagmin-2 ablated from the genome. By using a combination of biophysical, biochemical and functional techniques, we determined that synaptotagmin-2 is a fast synchronous Ca^{2+} -sensor. Third, in collaboration with Jianyuan Sun, we explored the biophysical properties of the slow Ca^{2+} -sensor in the Calyx of Held. Using Ca^{2+} -uncaging combined with electrophysiology, we mapped increasing Ca^{2+} concentrations in relation to neurotransmitter release and built a comprehensive mathematical model for the Ca^{2+} control of synaptic vesicle fusion. We found compelling evidence for the existence of two Ca^{2+} -sensors: one (synaptotagmin-2 in the Calyx of Held) is responsible for fast synchronous release, and the other one is responsible for slow delayed synaptic release. Surprisingly, we found the two Ca^{2+} -sensors have similar apparent Ca^{2+} affinities. This study showed clearly that synaptotagmin-2 is a fast Ca^{2+} -sensor, and gave us a prediction that narrows down the potential candidate for the slow Ca^{2+} -sensor.

TABLE OF CONTENTS

COMMITTEE SIGNATURES	i
DEDICATION	ii
TITLE PAGE	iii
ACKNOWLEDGEMENTS	v
ABSTRACTS	vi
TABLE OF CONTENTS	ix
PRIOR PUBLICATIONS	xiv
LIST OF FIGURES	xv
LIST OF TABLES	xviii
LIST OF ABBREVIATIONS	xix
CHAPTER I: Introductions.....	1
1.1 Overview of neurons and synapses.....	1
1.2 Anatomy of chemical synapses.....	3
1.3 Calcium-induced vesicle exocytosis.....	5
1.4 Essential proteins for membrane fusion.....	7
1.4.1 SNARE proteins (soluble N-ethylmaleimide-sensitive factor attachment protein receptor)	7
1.4.2 The SNARE core complex and membrane fusion.....	9
1.5 Ca ²⁺ -sensors for synaptic vesicle release.....	11
1.5.1 Synaptotagmins and synaptic transmission	11
1.5.2 Structure and functions of synaptotagmin-1	13

1.5.3 Synaptotagmin-1 is a phospholipid-binding module	15
1.5.4 Synaptotagmin-1 interact with SNAREs	16
1.5.5 Mechanism of synaptotagmin-1 functions: Phospholipid bindings vs. SNARE binding	17
1.6 Synaptotagmin-2	18
1.7 Other isoforms of synaptotagmin.....	20
1.8 Other Ca^{2+} binding proteins, possible Ca^{2+} -sensors?	22
1.9 Central questions.....	24
CHAPTER II: A gain-of-function mutation in synaptotagmin-1 reveals a critical role of Ca^{2+} -dependent SNARE-complex binding in synaptic exocytosis	26
2.1 Introductions	26
2.2 Materials and Methods.....	28
2.2.1 Mouse breedings.....	28
2.2.2 Co-immunoprecipitations.	28
2.2.3 Phospholipid binding.	29
2.2.4 Electrophysiological recordings from cortical neurons cultured at high density.	30
2.2.5 Electrophysiology from microisland cultures of hippocampal neurons.	31
2.2.6 Statistics.	32
2.3 Results.....	32
2.3.1 The D232N-mutation increases Ca^{2+} -dependent but not Ca^{2+} -independent SNARE-binding by synaptotagmin-1	32

2.3.2 Effect of the D232N- and D238N-mutations on Ca ²⁺ -dependent phospholipid binding	36
2.3.3 The D232N-mutation increases fast synchronous Ca ²⁺ -triggered release in inter-neuronal synapses	38
2.3.4 The D232N-mutation increases the apparent Ca ²⁺ -sensitivity of release in excitatory autapses	44
2.4 Discussion	50
CHAPTER III: Genetic Analysis of Synaptotagmin-2 in Spontaneous and Ca ²⁺ -Triggered Neurotransmitter Release.....	56
3.1 Introductions	56
3.2 Materials and methods	58
3.2.1 Generation, breeding and analysis of Synaptotagmin-2I377N mutant mice.	58
3.2.2 Behavioral Assays.....	58
3.2.3 Expression and purification of recombinant proteins.	59
3.2.4 Centrifugation pospholipid binding assays.	59
3.2.5 Circular Dichroism Spectra.....	59
3.2.6 Immunoprecipitations	59
3.2.7 Immunofluorescence labeling.....	60
3.2.8 Brain slicing and whole-cell recordings from MNTB neurons.	60
3.2.9 Neuromuscular junction recordings.	60
3.2.10 Neuronal cortical cultures.....	61
3.2.11 Statistical analysis.....	61

3.3 Results.....	61
3.3.1 An ataxic mouse harboring a point mutation in synaptotagmin-2.....	61
3.3.2 The synaptotagmin-2I377N mutant C2B-domain is unstable but functional.	62
3.3.3 Neurotransmitter release in WT and synaptotagmin-2I377N mutant neurons.	67
3.3.4 Release evoked by AP stimulus trains.	72
3.3.5 Spontaneous neurotransmitter release in WT and synaptotagmin-2I377N mutant neurons.	74
3.3.6 Deletion of synaptotagmin-1 also increases mini-frequency.	77
3.4 Discussion.....	79
CHAPTER IV: Synaptotagmin-2 is Essential for Survival and Contributes to Ca ²⁺ -Triggering of Neurotransmitter Release in Central and Neuromuscular Synapses	86
4.1. Introductions	86
4.2 Materials and Methods.....	88
4.2.1 Generation and maintenance of synaptotagmin-2 knockout mice.....	88
4.2.2 X-gal (β-Galactosidase) staining	89
4.2.3 Electrophysiological analyses of cultured striatal neurons.....	90
4.2.4 Electrophysiological analysis of the neuromuscular junction	91
4.2.5 Immunohistochemistry	92
4.2.6 Miscellaneous procedures.....	92
4.2.7 Statistical analysis.....	93
4.3 Results.....	93
4.3.1 Generation of synaptotagmin-2 knockout (KO) mice	93

4.3.2 Synaptotagmin-2 KO mice are postnatally lethal and have motor defects	95
4.3.3 Expression pattern of synaptotagmin-2 in mice.....	96
4.3.4 Synaptotagmin-2 expression in the NMJ.....	100
4.3.5 Evoked synaptic release in cultured neurons from the neostriatum	103
4.3.6 Spontaneous neurotransmitter release in NMJs.....	107
4.3.7 Evoked synaptic responses in synaptotagmin-2 deficient NMJs.....	108
4.3.8 Desynchronization of evoked vesicle release during repetitive stimulation.....	111
4.4 DISCUSSION.....	115
CHAPTER V: A two Ca^{2+} -sensor model for neurotransmitter release in the calyx of held	
synapse.....	122
5.1 Introduction.....	122
5.2 Material and Methods	125
5.2.1 Synaptotagmin-2 KO mice	125
5.2.2 Immunofluorescence labeling.....	125
5.2.3 Slice electrophysiology.....	125
5.2.3 Ca^{2+} -uncaging and Ca^{2+} -imaging.....	127
5.2.4 Data processing and modeling.....	128
5.2.5 Modeling.....	129
5.3. Results.....	131
5.3.1 Synaptotagmin-2 deletion blocks synchronous release in calyx terminals.....	131
5.3.2 Synaptotagmin-2 deletion does not alter Ca^{2+} -currents and readily-releasable pool sizes.....	135

5.3.3 Ca^{2+} -dependence of synchronous and asynchronous release.....	138
5.3.4 A two Ca^{2+} -sensor model of neurotransmitter release.....	143
5.4 Discussions	145
CHAPTER VI: Discussion and Conclusions	148
6.1 Ca^{2+} -dependent Synaptotagmin 1/SNARE binding is important for synaptic vesicle release	149
6.2 Synaptotagmin is a fast Ca^{2+} -sensor for synaptic vesicle release in Calyx and Neuromuscular junctions	149
6.3 A two- Ca^{2+} -sensor model for synaptic vesicle release	151
6.5. Future directions in searching for slow asynchronous Ca^{2+} -sensor(s)	152
Bibliography	155
Vitae.....	171

PRIOR PUBLICATIONS

1. Sun JY, Pang ZP, Qin DK, Fahim AT, Adachi R, Südhof TC. A Two Ca^{2+} -Sensor Model for Neurotransmitter Release in the Calyx of Held Synapse, Submitted
2. Maximov A*, Pang ZP*, Tervo DGT, Südhof TC. Monitoring Synaptic Transmission in Primary Neuronal Cultures Using Extracellular Stimulation. *J. Neurosci. Method*, 2007 161:75-87. * equal contribution
3. Pang ZP, Melicoff E, Padgett D, Liu Y, Teich A, Dickey B, Lin W, Adachi R, Südhof TC. Synaptotagmin-2 is essential for survival and contributes to Ca^{2+} -triggering of neurotransmitter release in central and neuromuscular synapses. *J. Neurosci.* 2006 26:13493-13504.
4. Pang ZP*, Shin OK*, Meyer A*, Rosenmund C, Südhof TC. A gain-of function mutation in synaptotagmin-1 reveals a critical role of Ca^{2+} -dependent SNARE-complex binding in synaptic exocytosis. *J. Neurosci.* 2006, 26:12556-12565. * equal contribution
5. Pang ZP*, Sun J*, Rizo J, Maximov A, Südhof TC. Genetic analysis of synaptotagmin-2 in spontaneous and Ca^{2+} -triggered neurotransmitter release. *EMBO J*, 2006, 25:2039-2050. * equal contribution
6. Nagy G, Kim JH, Pang ZP, Matti U, Rettig J, Südhof TC, Sorensen JB. Different effects on fast exocytosis induced by synaptotagmin-1 and 2 isoforms and abundance but not by phosphorylation. *J. Neurosci.* 2006, 26:632-43.

LIST OF FIGURES

Figure 1-1 Cortical neurons stained using Golgi methods.....	2
Figure 1-2 Nerve endings at the light- (left panel) and electro- (right panel) microscopy level.	4
Figure 1-3 Reaction sequence and timing of synaptic transmission.....	6
Figure 1-4 Structures of the neuronal SNARE proteins.	8
Figure 1-5 Model of the neuronal SNAREs assembling.	11
Figure 1-6 Ribbon diagrams of the C ₂ A- and C ₂ B-domains of synaptotagmin-1.	14
Figure 1-7 Comparison of biochemical properties between synaptotagmin 1 and synaptotagmin-2.....	19
Figure 1-8 Sequence comparison of mouse synaptotagmins 1 and 2.	20
Figure 1-9 Domain structures of synaptotagmins 1-13: relation of protein domains to the intron/exon organization of the human genes	21
Figure 2-1 Immunoprecipitation analysis of native wild-type and mutant synaptotagmin-1 binding to SNARE complexes using polyclonal syntaxin-1 antibodies.	34
Figure 2-2 Immunoprecipitation analysis of synaptotagmin-1 binding to SNARE complexes using monoclonal synaptobrevin-2 antibodies.....	35
Figure 2-3 Comparison of Ca ²⁺ -induced phospholipid binding by equivalent fragments of recombinant and native synaptotagmin-1.	37
Figure 2-4Ca ²⁺ -dependent binding of native wild-type or mutant synaptotagmin-1 to liposomes.	39
Figure 2-5 Evoked IPSCs in synapses containing wild-type or mutant synaptotagmin-1.....	40
Figure 2-6 Ca ²⁺ dependency of synaptic responses in D232N and D238N mutant synapses.	42
Figure 2-7 Short-term synaptic plasticity in synapses containing wild-type or mutant synaptotagmin-1.....	43
Figure 2-8 Effect of D232N- and D238N-mutations on asynchronous release during and following a 10 Hz stimulus train.....	45

Figure 2-9 Evoked EPSCs in autapses formed by D232N- and D238N-mutant neurons.	46
Figure 2-10 Determination of the apparent Ca^{2+} -affinity of release from excitatory synapses in autapses from D232N- and D238N-mutant mice.	47
Figure 3-1 Characterization of synaptotagmin-2 ^{I377N} mutant mice.	63
Figure 3-2 Biochemical characterization of synaptotagmin-2 ^{I377N} mutant protein.	64
Figure 3-3 Synaptotagmin-2 but not synaptotagmin-1 is present in Calyx terminals.	66
Figure 3-4 Kinetics of release in Calyx synapses in response to a 50 ms presynaptic depolarization.	69
Figure 3-5 Release evoked by single APs or hypertonic sucrose in Calyx synapses at postnatal day P14.	71
Figure 3-6 EPSCs evoked by a 50 Hz AP train.	73
Figure 3-7 Spontaneous neurotransmitter release in WT and synaptotagmin-2 ^{I377N} mutant neurons (mEPSCs).	75
Figure 3-8 Spontaneous neurotransmitter release at the NMJ.	77
Figure 3-9 Spontaneous release in synaptotagmin-1-deficient cortical neurons.	80
Figure 4-1 Generation of synaptotagmin-2 KO mice by homologous recombination.	94
Figure 4-2 Weight and survival of synaptotagmin-2 KO mice.	96
Figure 4-3 Expression pattern of synaptotagmin-2 in forebrain.	99
Figure 4-4 Expression pattern of synaptotagmin-2 in caudal brain.	101
Figure 4-5 Immunostaining of synaptotagmin-1 and-2 in NMJ.	102
Figure 4-6 Synaptic release in striatal neuronal cultures.	105
Figure 4-7 Spontaneous miniature synaptic responses in NMJ.	107
Figure 4-8 Evoked synaptic responses in NMJ.	108
Figure 4-9 Paired-pulse facilitation.	110
Figure 4-10 Short-term plasticity of evoked endplate potentials (EPP) in NMJ.	112
Figure 4-11 Desynchronization of EPPs during high-frequency stimulus trains in synaptotagmin-2 deficient NMJs.	113

Figure 5-1 Calyx synapses in synaptotagmin-2 deficient mice	132
Figure 5-2 Synaptic transmission evoked by isolated action potentials	134
Figure 5-3 RRP size, Ca^{2+} -currents, and release kinetics in synaptotagmin-2 deficient calyx synapses	136
Figure 5-4 Dependence of peak vesicular release rates on $[\text{Ca}^{2+}]_i$ in calyx terminals.....	139
Figure 5-5 A two Ca^{2+} -sensor model for neurotransmitter release.....	141
 Figure 6- 1 A molecular hypothesis describing the two Ca^{2+} -sensor model of neurotransmitter release.	153

LIST OF TABLES

Table 2-1 Ca^{2+} affinities in excitatory and inhibitory synapses..... 49

Table 4-1 Levels of synaptic proteins in synaptotagmin-2 knockout mice 104

LIST OF ABBREVIATIONS

3V	Third ventricle
ANOVA	Analysis of variance
AP	Action potential
BSA	Bovine serum albumin
CALI	Chromophore assisted light inactivation
CASK	Calmodulin-associated serine/threonine kinase
CC	Central canal
CD	Circular dichroism
Cg	Cingulated cortex
CNS	Central nervous system
CPu	Caudate putamen
Cpx	Complexin
CSP	Cysteine-string protein
Ctx	Cortex
DC	Dorsal cochlear nucleus
Df	Dorsal fasciculus
DG	Dentate gyrus
DH	Dorsal horn
DMEM	Dulbecco's modified eagle medium
EPI	External plexiform layer of olfactory bulb

EPP	Endplate potential
EPSC	Excitatory postsynaptic current
G	Glomeruli
GC	Ganglion cell layer
Gi	Gigantocellular reticular nucleus
Gr	Granular layer
GrO	Granular cell layer of olfactory bulb
GST	Glutathione-S-transferase
IC	Inferior colliculus
INL	Inner nuclear layer
IPSC	Inhibitory postsynaptic current
KO	Knock-out
Lat	Lateral cerebellar nucleus
Lf	Lateral fasciculus
LGP	Lateral globus pallidus
LV	Lateral ventricle
mEPP	Miniature endplate potential
Mi	Mitral cell layer of olfactory bulb
Mlf	Medial longitudinal fasciculus
MNTB	Medial nucleus of the trapezoid body
Mol	Molecular layer
NMJ	Neuromuscular junction

NSF	N-ethylmaleimide-sensitive factor
PAGE	Polyacrylamide gel electrophoresis
PC	Phosphocholine
PE	Phosphatidylethanolamine
PEp	Pigment epithelium
PIP	Phosphatidylinositolphosphate
PIP ₂	Phosphatidylinositol biphosphate
PKC	Protein kinase C
Pkj	Purkinje cells
PnC	Caudal pontine reticular nucleus
PnV	Ventral pontine reticular nucleus
PS	Phosphoserine
R & C	Layer of rods and cones
RMg	Raphe magnus nucleus
RRP	Readily-releasable pool
Rt	Reticular thalamic nucleus
SCAMP	Secretory carrier membrane proteins
SDS	Sodium dodecyl sulfate
sIPSC	Spontaneous inhibitory postsynaptic current
SNAP	Soluble NSF attachment protein
SNAP-25	Synaptosome-associated protein of 25 kda
SNARE	Soluble NSF attachment receptor element

SNARE core complex	SNARE complex containing only SNARE motifs
SO	Stratum oriens
Sp5	Interpolar subnucleus of the spinal trigeminal nucleus
SR	Stratum radiatum
Syb 2	Synaptobrevin 2
Synt	Syntaxin 1A
Syp	Synaptophysin
Syt 1	Synaptotagmin-1
Syt 2	Synaptotagmin-2
TMR	Transmembrane region
TTX	Tetrodotoxin
Tz	Nucleus of trapezoid body
VAMP	Vesicle associated membrane protein
VH	Ventral horn
VMH	Ventromedial hypothalamic nucleus
WM	White matter.
WNK	With-no-lysine kinase
WT	Wild-type
ZI	Zona incerta

CHAPTER I: INTRODUCTIONS

1.1 Overview of neurons and synapses

The nervous system is divided into central and peripheral parts. The central nervous system is composed of the brain and the spinal cord. Nervous tissue is composed of two main cell types, termed **neurons** and **glial cells**. The fine structure of the nervous system, especially neurons, was first described by Ramón y Cajal using histological staining developed by Camillo Golgi (Cajal, 1937)(Figure 1-1). Using this method, Cajal postulated that the nervous system is made up of billions of separate neurons and that the neurons are highly polarized (Cajal, 1937). He suggested that these cells communicate with each other via specialized junctions, termed "synapses". This concept became the basis of the neuron doctrine, which states that the individual unit of the nervous system is a single neuron (Cajal, 1937).

The **neuron** is a functional unit of the nervous system. There are more than 10^{11} neurons in human brain, which can be divided into hundreds even thousands of subgroups depending on location, size, and shape. All neurons are polarized with three parts: soma or cell body, dendritic tree and axons. The soma contains the nucleus of the cell, mitochondria and other organelles; dendrites are cell extensions with many branches, receiving incoming information from other neurons; axons send signals to other neurons.

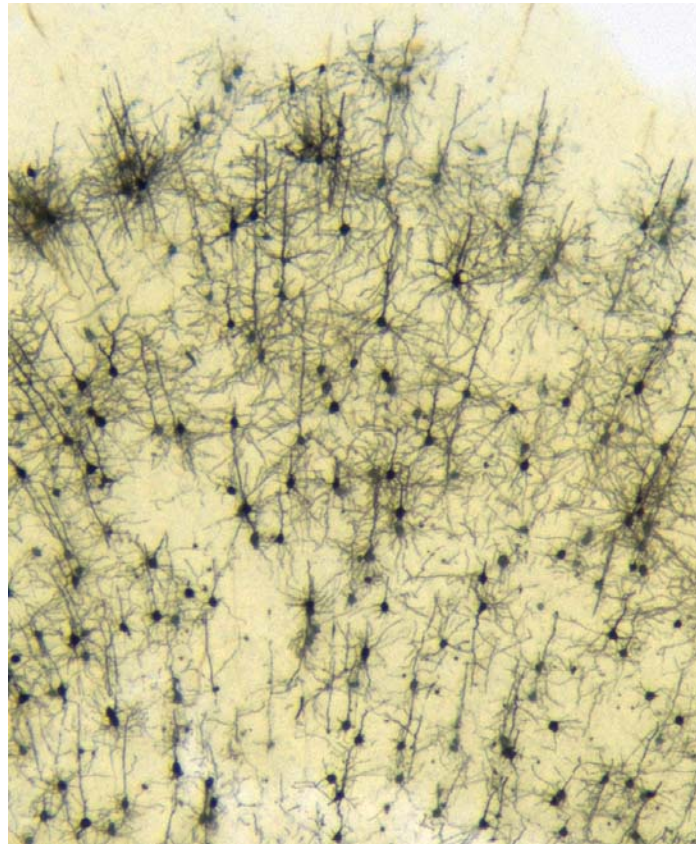


Figure 1-1 Cortical neurons stained using Golgi methods.
Courtesy of Xinran Liu.

As Cajal and Sherrington suggested, neurons communicate with each other through synapses. Neuronal synapses can be divided into two types depending on how they function, **chemical synapses** and **electric synapses**.

Chemical synapses are specialized junctions through which the cells of the nervous system signal to each other and to non-neuronal cells such as those in muscles or glands. Chemical synapses allow the neurons of the central nervous system to form interconnected neural circuits. They are thus crucial to the biological computations that underlie perception and thought. They provide the means through which the nervous

system connects to and controls the other systems of the body. A chemical synapse between a motor neuron and a muscle cell is called a neuromuscular junction; this type of synapse is well-understood.

An Electric synapse is a mechanical and electrically conductive link between two abutting neurons that is formed at a narrow gap between the pre- and postsynaptic cells known as a gap junction. At gap junctions, cells are about 3.5 nm apart (Kandel et al., 2000), a much shorter distance than the 20 to 40 nm distance that separates cells at chemical synapses (Connors and Long, 2004).

My thesis is focused on chemical synapses, upon which I would like to elaborate in terms of their structure and functions.

1.2 Anatomy of chemical synapses

At the light microscopy level, the synaptic bouton can be revealed by traditional silver staining (Figure 1-2, left panel), or by using more advanced technology, such as Fei Mao (FM) dye staining (Betz et al., 1996) or cell-filling fluorophores in combination with fluorescence microscopy. Synaptic endings can be found on dendrites, the cell body, and even on axons (Kandel et al., 2000). A typical synapse, such as those found on dendritic spines, usually involves a mushroom-shaped bud or varicosity from the axon of the presynaptic neuron that caps the dendritic spine of the postsynaptic counterpart.

At the ultrastructure level, synapses have presynaptic terminals, a synaptic cleft, and a postsynaptic density (Figure 1-2, right panel). Imaged using an electron microscope, the synapse can be seen to be highly asymmetric. The presynaptic terminal contains

hundreds of synaptic vesicles in addition to early endosomal structures (Sudhof, 2004). The presynaptic membrane has electron-dense projections that make up active zone, which can be seen using special staining, and synaptic vesicles are supposed to release from this active zone. The synaptic cleft is about 20 nm in distance, and while the composition of the synaptic cleft is unclear, it probably contains cell adhesion molecules and extracellular matrix proteins. The postsynaptic membrane also has electron-dense structures, most likely clustered scaffolding proteins that are important for postsynaptic receptor positioning. The postsynaptic cell need not be a neuron, and can also be a gland, muscle cell, or glia.

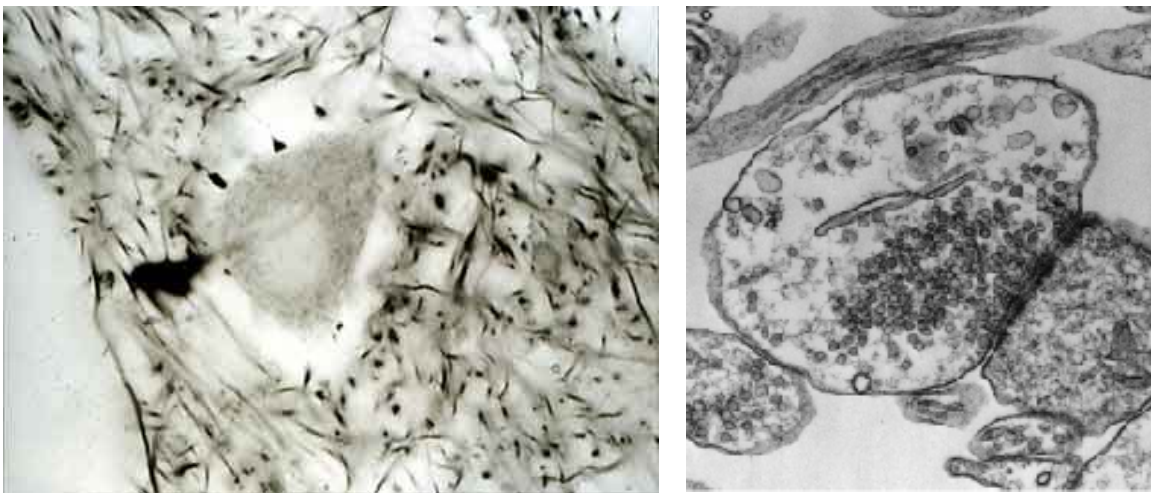


Figure 1-2 Nerve endings at the light- (left panel) and electro- (right panel) microscopy level.

Left panel: a high-magnification view of a motor neuron cell body, surrounded by a mass of axonal and dendritic processes. Synaptic endings can be seen adhering to the plasma membrane of the cell body. Right panel: an electronmicrograph of synapses. The presynaptic terminal contains synaptic vesicles. The synaptic cleft is the space between the two membrane structures. The postsynaptic membrane has an electron-dense structure termed the postsynaptic density.

(<http://millette.med.sc.edu/images/F%20images/f3.jpg>, and Curtesy of Xinran Liu)

1.3 Calcium-induced vesicle exocytosis

From the 1950s to the 1970s, Sir Bernard Katz, together with his colleagues, made a fundamental discovery that helped to unravel the mechanism of neurotransmitter release from presynaptic terminals (Katz, 1966). By using intracellular recordings from neuromuscular preparations, they found that in the absence of any form of stimulation there are randomly recurring discrete events that they termed miniature end-plate potentials (Katz, 1966). The amplitude of each event is only on the order of 0.5 mV, but shares similar properties to endplate potentials evoked by stimulating the nerves terminating on the muscle: they show the same sharp rise and slow decay, and have the character of a discrete all-or-none phenomena, but are much smaller in amplitude (Katz, 1966). Based on these observations, Katz devised a quantal mechanism of neurotransmitter release (Katz, 1966). Another of Katz's contribution was the finding of ionic requirements of synaptic transmitter release, especially the requirement for Ca^{2+} (Katz and Miledi, 1967a, b).

We now know that when an action potential invades a nerve terminal, Ca^{2+} influx induces neurotransmitter release with an exquisite temporal specificity. A central question is to understand the tight coupling between the increase in intracellular Ca^{2+} through the opening of presynaptic Ca^{2+} -channels upon the arrival of an action potential, and the activation of the exocytotic synaptic vesicle fusion machinery. The probability of vesicle fusion increases drastically in the 200 μs following Ca^{2+} influx and returns to much lower levels within 1 msec (Meinrenken et al., 2003)(Figure 1-3). In order to ensure the temporal fidelity of synaptic transmission, Ca^{2+} regulated neurotransmitter release is

uniquely rapid and precise, a fact that distinguishes it from other membrane trafficking processes. Intensive studies of synaptic proteins by multiple approaches have yielded insights into the molecular basis of the various steps that lead to neurotransmitter release (Jahn et al., 2003; Lin and Scheller, 2000; Rizo and Sudhof, 2002).

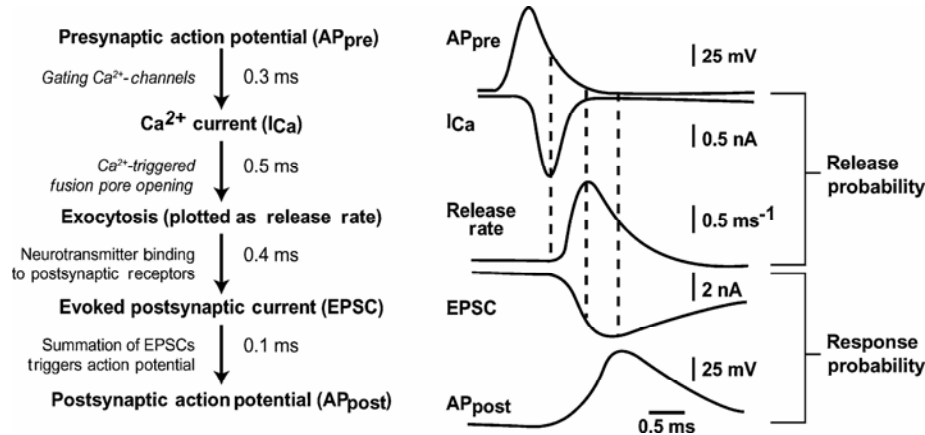


Figure 1-3 Reaction sequence and timing of synaptic transmission.

The principal reactions with the associated time constants are shown on the left, and traces from the corresponding reactions in the calyx of Held synapses are illustrated on the right. The time calibration bar at the bottom applies to all traces. (Meinrenken et al., 2003; Sudhof, 2004)

Action potential-evoked vesicle release has at least two components, a fast synchronous component that dominates at low-frequency stimulation, and a slower asynchronous component that dominates at high-frequency stimulation. Compared to other Ca^{2+} -regulated biological processes, both components of release are rapid, because Ca^{2+} triggers synchronous release in as little as 100 μsecs , and asynchronous release in 10-50 msec. Both release components are Ca^{2+} -dependent, with similar apparent Ca^{2+} -cooperativities but different apparent Ca^{2+} -affinities, suggesting that multiple Ca^{2+} -sensors control release (Shin et al., 2003).

A number of key proteins involved in exocytosis have been discovered (Sudhof, 2004), but many aspects of the mechanism of exocytosis and its regulation by Ca^{2+} remain obscure. Soluble NSF attachment receptor proteins (SNAREs) are composed of the vesicle protein synaptobrevin and the membrane proteins syntaxin and SNAP-25. These presynaptic SNAREs are essential for synaptic transmission. They form a four-helix core complex during exocytotic processes. Ca^{2+} -sensors interact with SNAREs to promote synaptic exocytosis (Jahn et al., 2003; Sudhof et al., 1993). Thus, the identification of Ca^{2+} -sensors is crucial for unveiling the mechanisms governing synaptic transmission. Synaptotagmin-1 is currently one of the best characterized proteins shown to act as a major Ca^{2+} -sensor that triggers exocytosis in the forebrain (Fernandez-Chacon et al., 2001; Geppert et al., 1994).

1.4 Essential proteins for membrane fusion

1.4.1 SNARE proteins (soluble N-ethylmaleimide-sensitive factor attachment protein receptor)

The SNARE protein family has more than sixty members in yeast and mammalian cells. They share a common motif known as a SNARE motif which is composed of about sixty amino acids and has a high tendency to form coiled coil domains (Jahn and Sudhof, 1999; Rizo and Sudhof, 2002). SNAREs can be divided into two categories based on their primary localization in the cell: vesicle or v-SNAREs, which are incorporated into the membranes of transport vesicles, including synaptic vesicles; and target or t-SNAREs, which are located on the target plasma membrane.

The neuronal SNAREs for synaptic vesicle fusion include: synaptic vesicle protein synaptobrevin/VAMP (vesicle associated membrane protein, a v-SNARE); the plasma membrane protein syntaxin and membrane associated protein SNAP-25 (synaptosomal-associated protein of 25kD, at-SNAREs). SNAP-25 has two SNARE motifs. All four SNARE motifs from these three proteins can form a very tight SNARE core complex (Fig 1.4).

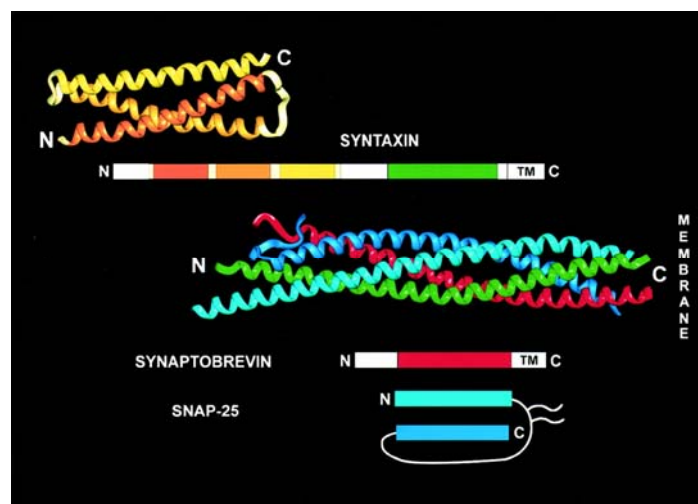


Figure 1-4 Structures of the neuronal SNARE proteins.

Syntaxin has three N-terminal Habc domains that can fold automatically (depicted in the upper left corner) and a C terminal SNARE motif (green). Middle panel, ribbon diagram of core complex composed of all four SNARE motifs from syntaxin, SNAP-25 and Synaptobrevin. Bottom carton shows the domain structure and relative position of the SNARE motif within synaptobrevin (red) and SNAP-25 (dark and light blue). For comparison, the linear arrangement of the domains is shown for each protein in like colors. (Jahn and Sudhof, 1999)

Synaptobrevin: The SNARE motif of synaptobrevin is flanked by a C'-terminal transmembrane region and a short N'-terminal proline-rich sequence that do not form independent domains.

Syntaxin: The SNARE motif of syntaxin is located towards the C'-terminus. The N'-terminus of syntaxin has conserved sequences (Habc domains) among different species from *C. elegans* to mammals, which can form a tight complex with the neuronal

Sec1/Munc18-1 (SM proteins) (Fernandez et al., 1998) (Fig 1-4). In isolated syntaxin 1, the Habc domains, in conjugation with Munc 18-1 (mouse uncoordinated 18-1), fold back onto the SNARE motif, forming a “closed conformation” that prevents syntaxin from forming the core complex with synaptobrevin and SNAP-25. Thus, syntaxin-1 must have a conformational change to switch between its complex with Munc18-1 and the core complex. Munc13 has been proposed as a candidate to promote this conformational change (Betz et al., 1997).

Synaptosome-associated protein of 25,000 daltons (SNAP-25) contains two SNARE motifs (the N-terminal and the C-terminal SNARE motifs designated as SNN and SNC, respectively). Although SNAP-25 doesn't have a transmembrane domain, it can still attach to the plasma membrane through four palmitoylated cysteine residues in the linker region between SNN and SNC. The linker region is quite long in order to ensure the parallel alignment of the two SNARE motifs in SNAP-25 when forming the core complex.

1.4.2 The SNARE core complex and membrane fusion

The SNARE core complex is hypothesized to be the fusion machinery of synaptic vesicles (reference to SNARE hypothesis). It is formed by one SNARE motif from the v-SNARE, synaptobrevin, one SNARE motif from the t-SNARE, syntaxin, and two SNARE motifs from SNAP-25. All these proteins have little obvious structure in isolation, but they form a very tight parallel four helix bundle upon assembly (Sutton et

al., 1998). The SNARE core complex is sodium dodecyl sulfate (SDS) resistant and also resilience to proteolysis by botulinum and tetanus neurotoxins (Hayashi et al., 1994).

Structural studies reveal that the core complex is highly twisted, with salt bridges on the surface and conserved leucine-zipper-like layers at the center (Sutton et al., 1998). Both the interior residues and the whole helix structure of the bundle are highly conserved throughout the SNARE family (Fasshauer et al., 1998; Rizo and Sudhof, 2002; Sutton et al., 1998). Embedded within these leucine-zipper layers is an ionic layer (called the zero layer) consisting of one arginine and three glutamine residues that are contributed from each of the four alpha-helices (R from synaptobrevin and Q from syntaxin and SNAP-25). This led to the definition of Q- and R- SNAREs (Fasshauer et al., 1998; Sutton et al., 1998) and the proposal that all core complexes consist of four-helix bundles formed by three Q-SNAREs and one R-SNARE. This proposal is supported by reconstitution studies (McNew et al., 2000; Parlati et al., 2000) and especially the crystal structure of the endosomal SNARE complex, which is remarkably similar to that of the neuronal complex (Antonin et al., 2002).

The functions of SNAREs in synaptic transmission were first revealed by the actions of clostridial neurotoxins, which inhibit synaptic transmission by cleavage of SNARE proteins. Genetically, when SNARE proteins are deleted, the evoked synaptic transmission is totally abolished (Schoch et al., 2001; Washbourne et al., 2002). In a working model of SNARE-mediated membrane fusion, the formation of the stable SNARE complex overcomes the energy barrier of the two membrane structures and directly causes vesicle fusion (Jahn et al., 2003). *In vitro* reconstitution experiments with

SNAREs incorporated into separate liposomes showed that the SNARE complex itself can drive vesicles to fuse (Weber et al., 1998). In addition, cells expressing interacting domains on their surfaces can fuse spontaneously, demonstrating that SNAREs are sufficient to fuse biological membranes (Hu et al., 2003). However, the low efficiency and long time scale cannot fully represent the fusion event of synaptic vesicle fusion, and thus other factors might also control the last step of membrane fusion.

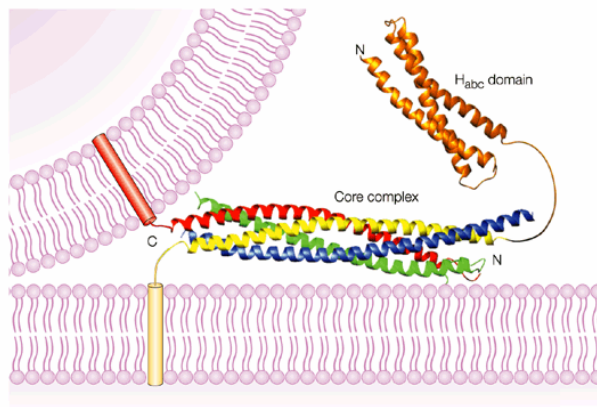


Figure 1-5 Model of the neuronal SNAREs assembling.

SNARE assembled into the core complex and positions of a synaptic vesicle in close proximity to the plasma membrane. The ribbon diagrams depict the crystal structure of the core complex and the NMR structure of the N-terminal Habc domain of syntaxin 1. The Habc domain is colored in orange and the SNARE motifs are color coded as follows: synaptobrevin, red; syntaxin 1, yellow; SNAP-25 amino terminus, blue; SNAP-25 carboxyl terminus, green. The cylinders represent the transmembrane regions of synaptobrevin and syntaxin 1, which are inserted into the synaptic vesicle and plasma membrane, respectively. (Rizo and Sudhof, 2002)

1.5 Ca^{2+} -sensors for synaptic vesicle release

1.5.1 Synaptotagmins and synaptic transmission

Synaptotagmins constitute a family of fifteen membrane-trafficking proteins that are characterized by an N-terminal transmembrane region (TMR), two C_2 domains (e.g. C_2A and C_2B) that are homologous to the C_2 regulatory region of protein kinase C (PKC),

and a variable linker region between the TMR and the C₂A-domain (Sudhof, 2002). The two C₂ domains of synaptotagmins are involved in both Ca²⁺-dependent and Ca²⁺-independent interactions. Synaptotagmins exhibit Ca²⁺/phospholipid binding activity with a concentration dependence and specificity for Ca²⁺ resembling that of the neurotransmitter release reaction (Brose et al., 1992; Davletov and Sudhof, 1993; Perin et al., 1990). In addition, synaptotagmin specifically interacts with several synaptic proteins: 1) syntaxin (Bennett et al., 1992), SNAP-25 (Schiavo et al., 1997; Wilson et al., 1996) and SNARE complexes; 2) clathrin assembly protein-2, a protein with an essential role in endocytosis of synaptic vesicles (Zhang et al., 1994); 3) soluble NSF attachment protein (α -SNAP) (Schiavo et al., 1995); and 4) N-type Ca²⁺ channels (Kim and Catterall, 1997; Sheng et al., 1997). Furthermore, Ca²⁺ promotes the oligomerization of synaptotagmin molecules (Chapman et al., 1996; Chapman et al., 1998; Osborne et al., 1999; Perin et al., 1991; Sugita et al., 1996). Thus, synaptotagmin plays central roles in both lipid-protein and protein-protein interactions in processes leading to exo- and/or endocytosis.

Synaptotagmin-1 is well established as a Ca²⁺-sensor for fast synchronous neurotransmitter release (DiAntonio et al., 1993; Fernandez-Chacon et al., 2001; Geppert et al., 1994; Littleton et al., 1993a). It was initially proposed to be a Ca²⁺-sensor based on its Ca²⁺-dependent phospholipid binding properties (Brose et al., 1992; Davletov and Sudhof, 1993; Perin et al., 1990). Subsequently, it was shown in both *Drosophila* and *C. elegans* that synaptotagmin-1 is essential for Ca²⁺-activated neurotransmitter release (Littleton et al., 1993a; Nonet et al., 1993). In synaptotagmin-1 null mutant mice, the fast synchronous synaptic release in the hippocampus is impaired, while the slow

asynchronous release remains unaffected (Geppert et al., 1994; Nishiki and Augustine, 2004). Moreover, studies in mice bearing point mutations within the C₂A domain of synaptotagmin-1, in which R233 or K236 were substituted by glutamine (R233Q and K236Q, respectively) demonstrated that synaptotagmin-1 is a Ca²⁺-sensor. The synaptotagmin-1 R233Q that decreases the apparent Ca²⁺ affinity by a factor of two also decreases the Ca²⁺ sensitivity of neurotransmitter release by a factor of two, while the K236Q mutation has no effect on synaptic transmission. A recent study using acute photoinactivation of synaptotagmin-1 by chromophore assisted light inactivation (CALI) demonstrated the involvement of synaptotagmin-1 in the fusion process of docked vesicles (Marek and Davis, 2002).

1.5.2 Structure and functions of synaptotagmin-1

Synaptotagmin-1 is an abundant synaptic vesicle protein that was discovered by two monoclonal antibodies raised against rat synaptic membrane proteins. Based on its apparent molecular weight in SDS-PAGE (~65 kDa), it was initially named p65 (Matthew et al., 1981). The molecular weight of synaptotagmin-1 is ~47.3 kDa if calculated based on the amino acid sequences. Due to N-terminal glycosylation, the apparent molecular weight is shifted to ~65 kDa. Synaptotagmin-1 is a type I membrane protein which has a short intravesicular N-terminus followed by a transmembrane region, linker region, and two C₂ domains (C₂A and C₂B) which are homologous to the second

domain of protein kinase C (Perin et al., 1991). Synaptotagmin-1 is a highly conserved across all species from *C elegans* to human.

Both the C₂A and C₂B domains of synaptotagmin-1 contain eight β -strands that form a β -sandwich structure and three loop regions from both the top and bottom ends (Figure 1-6). Calcium selectively binds to the top loops 1 and 3. As determined by structural studies, the C₂A domain binds three Ca²⁺ ions via five aspartates and one serine, which are widely separated in the primary sequence (Ubach et al., 1998). Without the serine on loop3, the C₂B domain only binds two Ca²⁺ ions (Fernandez et al., 2001). In addition, the C₂B domain of synaptotagmin-1 has two additional α -helices, one between the 7th and 8th β -strands, and the other at the very end(Fernandez et al., 2001).

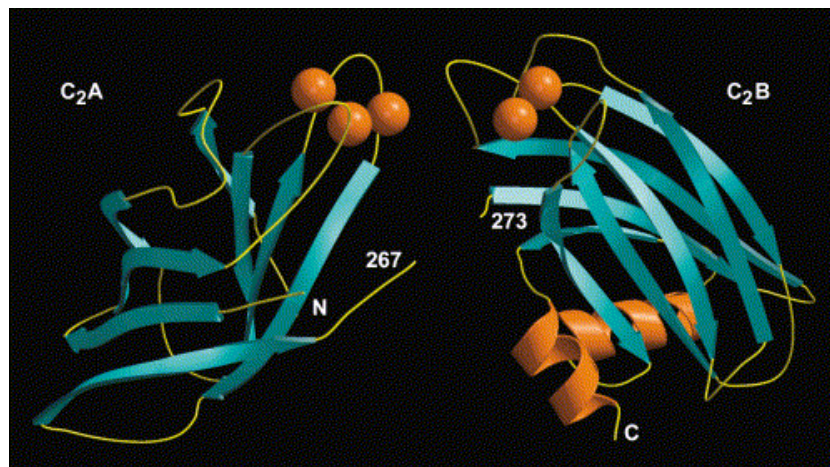


Figure 1-6 Ribbon diagrams of the C₂A- and C₂B-domains of synaptotagmin-1. The C₂A and C₂B domains are oriented with their Ca²⁺ binding sites in close proximity. The proximity of the C-terminus of the C₂A-domain (267) to the N terminus of the C₂B-domain (273) shows that this orientation can be easily reached. (Fernandez et al., 2001)

1.5.3 Synaptotagmin-1 is a phospholipid-binding module

The intrinsic Ca^{2+} binding affinities of synaptotagmin-1 C_2 domains are very low ($K_d > 1$ mM for C_2A and > 0.3 mM for C_2B -domain). However, in the presence of negatively charged phospholipids, the Ca^{2+} affinity can be tremendously enhanced ($\sim 10,000$ fold), which is probably due to lipids providing additional coordination sites for the incomplete calcium-binding sphere (Fernandez et al., 2001). Upon Ca^{2+} binding to the upper loop of the C_2 domain, a combination of electrostatic interactions between basic residues and the phospholipid head groups coordinates the Ca^{2+} ions and mediates insertion of hydrophobic residues into the lipid bilayer (Bai et al., 2004; Gerber et al., 2002; Zhang et al., 1998). The basic residues and the hydrophobic residues located at the top loops are important for phospholipid binding. For example, the mutant R233Q displays decreased phospholipid binding affinity in the presence of Ca^{2+} (Fernandez-Chacon et al., 2001), while a mutation increasing hydrophobicity (6W) will increase the binding affinity of synaptotagmin-1 for lipids in the presence of Ca^{2+} (Rhee et al., 2005). There is no significant conformational change in the C_2 domains, suggesting that the C_2 domains function as electrostatic switches (Fernandez et al., 2001; Ubach et al., 1998). Ca^{2+} binding to synaptotagmin-1 triggers the simultaneous penetration of the C_2A and C_2B domain (Hui et al., 2006), and both C_2A and C_2B have similar orientations with deeper penetration into the bilayer interior compared to that of a single C_2 domain (Frazier et al., 2003; Herrick et al., 2006; Rufener et al., 2005). Other metal ions such as Ba^{2+} and Sr^{2+} can also bind to the upper loop region of synaptotagmin-1 and trigger phospholipid binding (Shin et al., 2003). At the same time, the composition of lipids can

also affect the phospholipid binding of synaptotagmin-1. It has been shown that PIP and PIP₂ can increase both Ca²⁺-dependent and -independent phospholipid binding, and the latter is mediated by the polybasic region of the C₂B domain (Bai et al., 2004; Li et al., 2006).

1.5.4 Synaptotagmin-1 interact with SNAREs

Biochemically, in addition to forming a Ca²⁺-dependent complex with phospholipids, synaptotagmin-1 also binds to SNARE proteins. For SNARE monomers, synaptotagmin-1 has no interaction with synaptobrevin (Schiavo et al., 1997; Tang et al., 2006), but synaptotagmin-1 can bind to syntaxin in calcium-dependent manner (Chapman et al., 1995; Li et al., 1995a; Shin et al., 2003) and bind to SNAP-25 in both Ca²⁺-dependent and -independent manner (Schiavo et al., 1997). It has been reported that both N-terminal Habc domain and a C-terminal SNARE motif of syntaxin have calcium-dependent interactions with synaptotagmin-1 separately in different assays, but cannot be detected together (Chapman et al., 1995; Kee and Scheller, 1996; Shao et al., 1997). In addition, SNARE heterodimers and core complexes have also been shown to have both Ca²⁺-dependent and -independent interactions with synaptotagmin-1 (Bai et al., 2004; Ernst and Brunger, 2003; Rickman and Davletov, 2003; Schiavo et al., 1997; Zhang et al., 2002). The detail binding region of synaptotagmin-1 to SNAREs is still not completely clear. The C₂A domain of synaptotagmin-1 is involved in syntaxin and SNAP-25 binding, but no direct interaction with synaptobrevin 2 has been detected (Shin et al., 2003). It has

been suggested that the polybasic region of the C₂B domain is responsible for the calcium-independent binding of synaptagmin-1/SNAREs (Rickman et al., 2004), the possibility that this could be mediated by the contaminated proteins sticking to the polybasic region has raised questions (Ubach et al., 2001). Further studies including synaptotagmin-1/SNAREs complex structure may help solve the detailed interactions.

1.5.5 Mechanism of synaptotagmin-1 functions: Phospholipid bindings vs. SNARE binding

Genetic deletion of synaptotagmin 1 causes impairments in action potential evoked synaptic transmission in all organisms investigated, from *C. elegans* to *Drosophila* to mouse (Broadie et al., 1994; Geppert et al., 1994; Littleton et al., 1993b). Biochemically, synaptotagmin 1 binds to Ca²⁺, phospholipids and SNARE proteins. Moreover, a point mutation (R233Q) in the synaptotagmin-1 C₂A domain that decreases the overall apparent calcium affinity by half also induces the same shift in the calcium affinity for exocytosis (Fernandez-Chacon et al., 2001). Thus, synaptotagmin-1 is a well-established Ca²⁺-sensor of synaptic vesicle release machinery involved in fast neurotransmission.

Biochemically, synaptotagmin-1 binds to phospholipids in a Ca²⁺-dependent manner, it can also binds to SNAREs in both Ca²⁺-independent and –dependent ways. Both calcium-dependent phospholipid binding and SNARE complex binding could be the driving force for vesicle fusion. Although some results favor phospholipid binding of synaptotagmin-1 as essential (Fernandez-Chacon et al., 2001; Shin et al., 2003; Shin et al.,

2002), the importance of SNARE complex binding is not clear (Bai et al., 2004). A key problem is finding mutants of synaptotagmin-1 which selectively affect only one of the interactions. Moreover, synaptotagmin-1 may bind simultaneously to the SNARE complex and membrane to trigger release, although the opposite result has also been reported (Arac et al., 2003; Davis et al., 1999).

1.6 Synaptotagmin-2

Among all synaptotagmins, synaptotagmin-2 has the highest homology to synaptotagmin-1 (88% sequence identity in the C₂-domains). Biochemically, C₂ domains of synaptotagmins 1 and 2 bind Ca²⁺ in a complex with phospholipids at micromolar concentrations, and associate with SNARE complexes in a calcium- independent manner (Sugita et al., 2001; Sugita et al., 2002) (Figure 1-7). In addition, expression of synaptotagmin-2 in synaptotagmin-1 KO hippocampal neurons or chromaffin cells can rescue impaired calcium-evoked vesicle release (Nagy et al., 2006; Stevens and Sullivan, 2003). Based on the biochemical similarity, synaptic vesicle localization and the ability of synaptotagmin-2 to substitute for synaptotagmin-1, it is proposed that synaptotagmin-2 functions as an alternate Ca²⁺-sensor for fast synchronous release, but acts prominently in caudal synapses lacking synaptotagmin-1. However, this notion has yet to be experimentally validated.

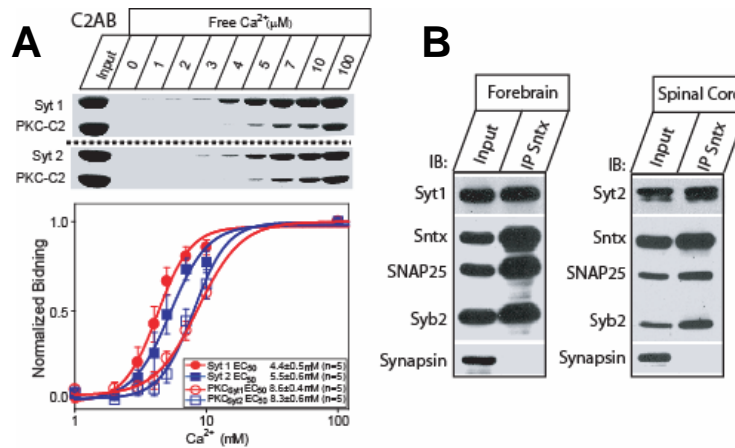


Figure 1-7 Comparison of biochemical properties between synaptotagmin 1 and synaptotagmin-2.

A. Recombinant double C₂ domains of either synaptotagmin-1 (Syt 1) or synaptotagmin 2 (Syt 2) bind to phospholipids in the presence of Ca²⁺. The binding affinity to Ca²⁺ of Syt 2 C₂AB domain is slightly lower than Syt 1. PKC-C₂ domain was included as an internal control. B. SNARE complexes with synaptotagmins-1 or 2 were immunoprecipitated using syntaxin antibodies (U6251 polyclonal antibody in the left panel; HPC-1 monoclonal antibody in the right panel). Both Syt 1 and Syt 2 are co-immunoprecipitated with SNARE proteins.

There are major differences between synaptotagmins-1 and 2. First, synaptotagmins 1 and 2 are differentially distributed in the CNS in a mutually exclusive pattern. Synaptotagmin-1 is expressed predominantly in rostral brain while synaptotagmin-2 is found in more caudal brain regions and spinal cord (Berton et al., 1997; Marqueze et al., 1995; Ullrich et al., 1994). Second, the N-terminal sequences have only ~40% homology between synaptotagmins 1 and 2 (Figure 1-8). Third, the linker region between the TMR and C₂A domain of synaptotagmin-1 can be phosphorylated by Ca²⁺/calmodulin-dependent kinase II (CaMKII), casein kinase II, and PKC (Davletov et al., 1993; Herrick et al., 2006; Popoli, 1993). However, synaptotagmin-2 lacks the corresponding threonine residue (T112, highlighted in green, Fig. 1.8) that is phosphorylated by CaMKII and PKC in synaptotagmin-1 (Herrick et al., 2006). A recent report showed that two threonines (T202 and T386, present in the C₂A and C₂B domains,

respectively) of synaptotagmin-2 could be phosphorylated by WNK1 protein kinase. These phosphorylations increased the requirement of Ca^{2+} for liposome binding. Mutations of T202 partially prevented this change (Lee et al., 2004). These findings suggested that the phosphorylation of synaptotagmin-2 can regulate Ca^{2+} sensing and subsequently Ca^{2+} -dependent interactions with other proteins or lipids. However, whether synaptotagmin-2-mediated exocytosis is regulated is unknown. In addition, the fact that synaptotagmin-1 KO mice die at postnatal day 1 (Geppert et al., 1994), and synaptotagmin-2 KO mice die at ~P19-20 (see Chapter IV), suggests that these two proteins display differential phenotypes when knocked out and cannot simply compensate for each other.

```

mSyt1, MVSASR-----PEALAAPVTTVATLVPHNATEPASPGEGKEDAFSKLKQKFMNELHKIPLPPWALIAIAIV 66
mSyt2, MRNIFKRNQEPNVAPATTATMPLAPVAPADNSTESTGPGESQEDMFAKLKEKFFNEINKIPLPPWALIAMAVV 74

mSyt1, AVLLVVTCCFCVCKKCLFKKKKKKKGKEKGGKNAINMKDVKDLGKIMKDQALKDDDAETGLTIDGE-EKEEPKEE 139
mSyt2, AGLLLLTCCFCICKKCCCKKKKKKKEKGMKNAMNMKDMK-----GGQ--DDDDAETGLTEGEGEGEEKEP 140
                                     -loop 1-                               loop 2
mSyt1, EKLGLQYSLDYDFQNNQLLVGIIQAELPALDMGGTSDPYVKVFLLPDKKKKFETKVHRKTLNPFVNEQFTFK 213
mSyt2, ENLGLQYSLDYDFQANQLTVGVLQAELPALDMGGTSDPYVKVFLLPDKKKKYETKVHRKTLNPAFNETFTFK 214
                                     --loop 3-
mSyt1, VPYSELGGKTLVMAVYDFDRFSKHDIIIGEFKVPMTVDVFGHVTEEWRDLQSAEKEEQEKLGDICFSLRYVPTAG 287
mSyt2, VPYQELAGKTLVMAIYDFDRFSKHDIIIGEVKVPMTVDLGPPIEWRDLQGGEKEEPEKLGDICTSLRYVPTAG 288
                                     -loop 1-                               loop 2
mSyt1, KLTVVILEAKNLKKMDVGGLSDPYVKIHLMQNGKRLKKKTTIKKNTLNPYNESFSFEVPFEQIQKVQVVVTV 361
mSyt2, KLTVCILEAKNLKKMDVGGLSDPYVKIHLMQNGKRLKKKTTTVKKKTLNPFNFESFSFEIPFEQIQKVQVVVTV 362
                                     --loop 3--
mSyt1, LDYDKIGKNDIAGKVFVGYNSTGAELRHWSMLANPRRPIAQWHTLQVEEEVDAMLAVKK 421
mSyt2, LDYDKLGKNEAIGKIFVGSNATGTEL RHWSMLANPRRPIAQWHTLQVEEEVDALLGKNK 422

```

Figure 1-8 Sequence comparison of mouse synaptotagmins-1 and 2.

mSyt1: mouse synaptotagmin-1; mSyt2: mouse synaptotagmin-2; transmembrane regions are highlighted in blue; sequence in red is C₂A region; sequence in blue is C₂B region; top loops are indicated in italics above the sequences; residues that are presumably Ca^{2+} binding sites are highlighted in black; reported phosphorylated residues (Davletov et al., 1993; Hilfiker et al., 1999; Popoli, 1993) (T112 in synaptotagmin-1, T202 & T386 in synaptotagmin-2) are highlighted in green.

1.7 Other isoforms of synaptotagmin

As discussed above, there are thirteen more isoforms of synaptotagmin in the mouse genome apart from synaptotagmin-1 and 2. According to sequence similarity and properties, they can be classified into several groups (Figure 1-9). The functions of most of the synaptotagmins are unknown. Synaptotagmin-7 is alternatively spliced and is mainly expressed on plasma membrane in brain. Although synaptotagmin-7 C₂ domains have 10-20 fold higher calcium affinity than synaptotagmin-1, its function in synaptic transmission is still unclear. Synaptotagmin-4 has a conserved substitution of an aspartate for a serine in the C₂A domain, which abolishes calcium binding for rat synaptotagmin-4. But *Drosophila* synaptotagmin-4 still binds calcium and can functionally replace synaptotagmin-1 in *Drosophila* (Robinson et al., 2002). Synaptotagmin-12 can be phosphorylated by PKA and is important for spontaneous synaptic vesicle fusion (Maximov et al., 2007b).

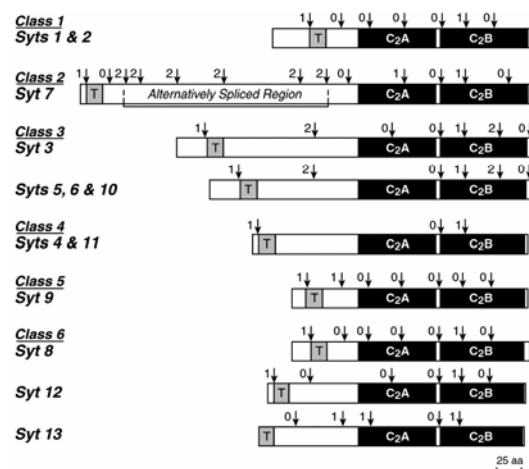


Figure 1-9 Domain structures of synaptotagmins 1-13: relation of protein domains to the intron/exon organization of the human genes.

Each diagram shows a single or several closely related synaptotagmins as identified on the *left*. Arrows indicate positions of introns in the corresponding human genes as identified in the human genome sequence.² The numbers next to the arrows describe the position in the codon at which the coding sequence is interrupted by the intron (0, at the codon junction; 1 and 2, after the first and second codon position, respectively). The N-terminal TMR is marked with a T, and the C₂A- and C₂B-domains are labeled. (Sudhof, 2002)

1.8 Other Ca^{2+} binding proteins, possible Ca^{2+} -sensors?

There are hundreds of proteins in the mammalian genome that bind to Ca^{2+} , including C_2 domain-containing proteins; E-F hand motif containing proteins and others. Most C_2 domain proteins serve either as signal transduction enzymes, such as protein kinase C, or as membrane trafficking proteins, such as synaptotagmin-1. C_2 domain-containing proteins that are important for signal transduction, from ubiquitin ligases to kinases to various phospholipases, are usually soluble and contain a single C_2 domain. On the other hand, membrane trafficking proteins with C_2 domains, such as synaptotagmins and ferlins, generally include at least two C_2 domains. However, a few proteins at the active zone that might be important for vesicle release, such as RIMs, and some splice variants of piccolo/aczonin and intersctin, contain only a single C_2 domain (Fenster et al., 2000; Pucharcos et al., 2001; Wang et al., 1999; Wang and Sudhof, 2003).

Among C_2 domain-containing proteins aside from mentioned above, ferlins, including dysferlin and otoferlin, are a family of proteins with six C_2 domains (Shin et al., 2005). Otoferlin has been suggested to be essential for exocytosis at the auditory ribbon synapses (Roux et al., 2006); MCTPs (multiple C_2 domain and transmembrane region proteins) is a novel family of evolutionarily conserved C_2 domain proteins that bind to Ca^{2+} , but without interaction with negatively charged or neutral phospholipids in the presence or absence of Ca^{2+} (Shin et al., 2005); E-Syts, another C_2 domain-containing protein family, contain an N-terminal transmembrane region, a central juxtamembranous domain that is conserved from yeast to human, and multiple C_2 domains (5 in E-Syt1; 3 in E-Syt2 and E-Syt3). The first C_2 domain of the E-Syts is required for Ca^{2+} binding.

Recombinant protein fragments of the C₂A domain of E-Syt2 binds to phospholipids in the presence of Ca²⁺. E-Syts are ubiquitously expressed, but enriched in brain (Roux et al., 2006).

In vertebrate genomes, proteins containing EF-hand Ca²⁺-binding sites are more common than C₂ domain proteins. However, Ca²⁺ binding in EF-hand proteins often does not serve a direct regulatory function but instead acts in Ca²⁺ buffering (*e.g.* parvalbumin and calbindin) or subserves a structural role (Lewit-Bentley et al., 2000; Muller et al., 2007). Among the EF-hand proteins with a regulatory Ca²⁺-binding site, one particular protein, calmodulin, appears to mediate more Ca²⁺-dependent regulatory actions than all other EF-hand proteins combined and is in fact expressed as an identical sequence from multiple independent genes (Means, 2000; Toutenhoofd and Strehler, 2000).

Neuronal Ca²⁺-sensor-1 (NCS-1) is another member of EF-hand protein family. NCS-1 is mainly expressed in neuronal and neuroendocrine cells, and it has been shown that NCS-1 enhances neurotransmission and Ca²⁺-dependent exocytosis (Chen et al., 2001; Gromada et al., 2005; McFerran et al., 1998; Pongs et al., 1993; Rivosecchi et al., 1994; Sippy et al., 2003). NCS-1 binds to Ca²⁺, and can regulate short-term plasticity (Sippy et al., 2003), most likely by increasing the Ca²⁺ buffering capacity of presynaptic terminals. In addition, NCS-1 probably participates in Ca²⁺-regulated exocytosis, because it also interacts with and regulates the activity of phosphatidylinositol 4-kinase β (Hendricks et al., 1999; Rajebhosale et al., 2003; Taverna et al., 2002; Zhao et al., 2001), which in turn regulates the synthesis of PI4,5-bisphosphate (PI_{4,5}P₂) and regulates Ca²⁺-dependent secretion (Aikawa and Martin, 2003; Holz et al., 2000; Milosevic et al., 2005).

Given the fact that Ca^{2+} -dependent vesicle release remains after synaptotagmin-1 deletion, it is important to figure out the molecular nature of the slow Ca^{2+} -sensor(s). Any of the Ca^{2+} binding proteins in the genome that localize to presynaptic terminals can potentially serve as a Ca^{2+} -sensor for membrane trafficking.

1.9 Central questions

There are several central questions that remain elusive. First, as I discussed above, synaptotagmin-1 binds to SNARE proteins and phospholipids in a Ca^{2+} -dependent manner. However, it is unclear if the SNARE/synaptotagmin-1 binding or the SNARE/lipid binding is important. To address this question, we used a knock-in mouse containing a point mutation in synaptotagmin-1, which we found increased the Ca^{2+} -dependent Syt1/SNARE binding without much influence on synaptotagmin-1/phospholipid binding (see Chapter II).

Second, there are fifteen members of the synaptotagmin family in the mouse genome and hundreds of other Ca^{2+} -binding proteins. Is synaptotagmin-1 the only Ca^{2+} -sensor for fast synaptic vesicle release? Synaptotagmin-2 is the closest relative of synaptotagmin-1, with ~76% protein sequence homology, and has long been suspected to act as another fast Ca^{2+} -sensor at synapses lacking synaptotagmin-1. However, this proposal has never been addressed directly. To address this hypothesis, we utilized two mouse lines: one with a chemical-induced point mutation in synaptotagmin-2 and the other a synaptotagmin-2 KO mouse (Chapter III and IV).

Third, if syt 1 and syt 2 are the fast Ca^{2+} -sensor, what is the slow Ca^{2+} -sensor? We don't know the molecular identity of the slow Ca^{2+} -sensor yet, however, using the synaptotagmin-2 KO mice, we addressed the biophysical properties of the slow Ca^{2+} -sensors (Chapter V).

CHAPTER II: A gain-of-function mutation in synaptotagmin-1 reveals a critical role of Ca^{2+} -dependent SNARE-complex binding in synaptic exocytosis

2.1 Introductions

Neurotransmitter release is mediated by synaptic vesicle exocytosis in a reaction that is catalyzed by SNARE complex assembly, and is triggered by Ca^{2+} -binding to the two C_2 -domains of the synaptic vesicle protein synaptotagmin-1 (Brunger, 2005; Sorensen, 2005; Sudhof, 2004). *In vitro*, Ca^{2+} -binding causes synaptotagmin-1 to form complexes with both phospholipids and with SNARE complexes (Banerjee et al., 1996; Bennett et al., 1992; Bowen et al., 2005; Chapman et al., 1995; Chapman and Jahn, 1994; Davletov and Sudhof, 1993; Fernandez et al., 2001; Lee et al., 2004; Li et al., 1995b; Rickman et al., 2004; Rickman and Davletov, 2003; Schiavo et al., 1997; Yoshida et al., 1992). *In vivo*, mutations that selectively decrease synaptotagmin-1 phospholipid-binding cause a corresponding decrease of release (Fernandez-Chacon et al., 2001; Li et al., 2006), whereas mutations that enhance phospholipid-binding produce an increase of release (Rhee et al., 2005). These data demonstrated that Ca^{2+} -binding to synaptotagmin-1 triggers neurotransmitter release, and that Ca^{2+} -dependent phospholipid binding is an essential component of the Ca^{2+} -triggering reaction.

In contrast to phospholipid binding, however, SNARE binding by synaptotagmin-1 has been difficult to examine. No synaptotagmin-1 mutation is known that selectively

enhances or depresses SNARE-binding without changing phospholipid binding, precluding an *in vivo* analysis of SNARE-binding by synaptotagmin-1. A large body of indirect evidence, primarily based on transfected cells, supports the importance of SNARE-binding by synaptotagmin-1 (Bai et al., 2004; Shin et al., 2003; Wang et al., 2001; Zhang et al., 2002), but no *in vivo* data confirming this importance are available. Thus a major question is now whether synaptotagmin-1 acts primarily as a Ca^{2+} -dependent phospholipid-binding protein in triggering exocytosis, with its SNARE-binding having a separate role (possibly in priming vesicles for subsequent release), or whether the interactions of synaptotagmin-1 with both SNAREs and phospholipids collaborate in Ca^{2+} -triggering of neurotransmitter release.

We previously analyzed two aspartate-to-asparagine substitutions in the Ca^{2+} -binding site of the C₂A-domain (D232N- and D238N) that interfere with Ca^{2+} -binding to the C₂A-domain in slightly different ways, but do not alter its atomic structure, and have little effect on Ca^{2+} -dependent phospholipid binding by synaptotagmin-1 (Fernandez-Chacon et al., 2002). In knockin mice, the D238N-mutation produced no major change in synaptic function, but the D232N-mutation caused an unexplained increase of synaptic depression during repetitive stimulation (Fernandez-Chacon et al., 2002). Moreover, a separate study using rescue experiments of synaptotagmin-1 KO neurons with D232N-mutant synaptotagmin-1 suggested that the D232N-mutation may increase the Ca^{2+} -sensitivity of evoked responses (Stevens and Sullivan, 2003), although again no biochemical basis for the changes was identified.

To clarify these puzzling observations and to search for a potential mechanism to account for the unexplained electrophysiological phenotype of the D232N-mutation, we have analyzed the effect of the D232N- and D238N-mutations on the biochemical properties and physiological functions of native synaptotagmin-1 expressed in knockin mice at physiological levels. This approach avoids artifacts produced by recombinant proteins and/or by overexpression experiments. Our current data demonstrate that in addition to Ca^{2+} -dependent phospholipid binding, Ca^{2+} -triggered SNARE interactions by synaptotagmin-1 are rate-limiting in stimulating fast neurotransmitter release.

2.2 Materials and Methods

2.2.1 Mouse breedings. All analyses were performed on littermate offspring from heterozygous breedings. For the biochemical experiments and for cultures of cortical neurons, offsprings of matings between standard D232N- or D238N-mutant heterozygotes were used. For the hippocampal neuronal cultures, offspring from D232N/D238N-mutant compound heterozygotes were used. All genotyping was performed as described (Fernandez-Chacon et al., 2002).

2.2.2 Co-immunoprecipitations. One gram of mouse brain was homogenized with a tissue homogenizer (Thomas Scientific, Philadelphia, PA) in 20 ml of 50 mM HEPES-NaOH pH 6.8, 0.1 M NaCl, 4 mM EGTA, 5 $\mu\text{g/ml}$ leupeptin, 2 $\mu\text{g/ml}$ aprotinin, 1 mM PMSF, and 1 mM DTT. 1% Triton X-100 was added, proteins were extracted for 1 hr at 4 °C with rocking, insoluble proteins were removed by centrifugation (150,000 $\times g$ for 1 hr), and the supernatant was used for experiments. Co-immunoprecipitation reactions were performed with polyclonal syntaxin-1 antibodies, U6251 (15 μl serum) or monoclonal

synaptobrevin 2 antibody Cl69.1 (10 μ l ascite) attached to protein A- or G-Sepharose beads (10 μ l; Pharmacia) in a 1 ml volume of immunoprecipitation buffer (50 mM HEPES-NaOH pH 6.8, 0.1 M NaCl, 4 mM EGTA, 2 mM MgCl₂, 0.5% Triton X-100 in the presence of different concentrations of free Ca²⁺). Free Ca²⁺ concentrations were calculated with EqCal software (Biosoft, Ferguson, Missouri). Co-immunoprecipitation reactions were incubated at 4 °C for 2 hr with rocking, beads were washed five times with 1 ml of corresponding immunoprecipitation buffer, and bound proteins were eluted with SDS-PAGE sample buffer. Synaptotagmin-1 (Cl41.1 or V216), SNAP-25 (Cl71.2 or P913), synaptaxin-1 (HPC-1 or U6251), synaptobrevin 2 (Cl69.1 or P939), synaptophysin 1 (Cl43.1), Munc-18 (BD Transduction Laboratories, purified mouse anti-Munc-18 monoclonal antibody, Cat No. 610337), and complexins 1 and 2 (L668 and L669) were quantified by immunoblotting using ¹²⁵I-labeled secondary antibodies.

2.2.3 Phospholipid binding. Total membranes were isolated from mouse brain homogenates (1 gm mouse brain/20 ml 50 mM HEPES-NaOH pH 6.8, 0.1 M NaCl, 4 mM EGTA) after centrifugation at 150,000xg for 1 hr. Samples were re-homogenized in 20 ml of 50 mM HEPES-NaOH pH 6.8, 0.1 M NaCl, 4 mM EGTA, and for partial digestion of synaptotagmin-1, 0.005% trypsin and 0.053 mM EDTA were added, incubated for 1 hr at room temperature with rotation, and 25 μ g/ml leupeptin, 10 μ g/ml aprotinin, 1 mM PMSF, 1 mM DTT, and 2% goat serum were added. The trypsinized membranes were then centrifuged at 150,000xg for 1 hr, and the cytosolic domain of synaptotagmin-1 was recovered in the supernatant and stored at -80 °C. Phospholipid binding assays were performed using heavy liposomes with a synaptic phospholipid

composition and PIP and PIP₂ as indicated (Benfenati et al., 1989; Deutsch and Kelly, 1981; Li et al., 2006; Rhee et al., 2005). After SDS-PAGE, synaptotagmin-1 associated with heavy liposome was quantified by immunoblotting using Cl41.1 and ¹²⁵I-labeled secondary antibody.

2.2.4 Electrophysiological recordings from cortical neurons cultured at high density.

Primary cortical neurons were isolated from P1 mice of wildtype or synaptotagmin-1 D232N mutant mice, dissociated by trypsin digestion, and plated on Poly-D-lysine-coated glass coverslips (Maximov et al., 2007a; Maximov and Sudhof, 2005). Neurons were cultured *in vitro* for 14–18 days in MEM (Gibco) supplemented with B27 (Gibco), glucose, transferrin, fetal bovine serum, and Ara-C (Sigma). Synaptic responses were triggered by 1 ms current injection (900 μ A) through a local extracellular electrode (FHC concentric bipolar electrode, Catalogue No. CBAEC75) with a Model 2100 Isolated Pulse Stimulator (A-M Systems, Inc.), and recorded in whole-cell mode using a Multiclamp 700A amplifier (Axon Instruments, Inc.). Data were digitized at 10 kHz with a 2 kHz low-pass filter. The whole-cell pipette solution contained (in mM): CsCl 135, HEPES 10, EGTA 1, Mg-ATP 4, Na-GTP 0.4, and QX-314 10, pH 7.4. The bath solution contained (in mM): NaCl 140, KCl 5, CaCl₂ 2, MgCl₂ 0.8, HEPES 10, and glucose 10, pH 7.4. IPSCs were pharmacologically isolated by addition of 50 μ M D-AP5 and 20 μ M CNQX to the bath solution. Hypertonic sucrose (0.5 M) solution was applied for 20 s through a perfusion system at a speed of 4 ml/min. Series resistance was compensated to 60-70%, and recordings with series resistances of >15 M Ω were not included. Data were analyzed using Clampfit 9.02 (Axon Instruments, Inc) or Igor 4.0 (Wavemetrics).

Synaptic responses were recorded 2 min after obtaining whole-cell patch before recording of evoked synaptic responses, allowing the internal pipette solution to diffuse into the patched neuron. In almost all cases we obtained robust evoked responses from neurons we recorded. Stimulation intensity of 900 μ A was suprathreshold in most of the cases. We maintained the stimulation at this level for all recordings in order to reduce the variability among cells. Most, if not all, of axons passing in a close vicinity of the stimulation electrode were activated. The major source of variability in our experimental condition was due to the synaptic density. To minimize this variation, we plated wild-type and mutant neurons at similar densities and recorded on the same day between two genotypes.

2.2.5 Electrophysiology from microisland cultures of hippocampal neurons. Cultures of hippocampal neurons from D232N- or D238N-mutant mice were prepared at P0 or P1 on microislands of glia cells (pre-plated in 10% fetal bovine serum) under conditions favouring formation of autapses, and used for experiments after 10-20 days in culture (Li et al., 2006; Rhee et al., 2005). Before seeding neurons in a density of 500 per cm^2 , the medium was exchanged to neurobasal medium A (Gibco) with supplement B27 (Gibco). Only dots containing single neurons were used. Excitatory EPSCs were analyzed in extracellular medium containing (in mM): NaCl 140, KCl 2.4, HEPES 10, glucose 10, CaCl_2 4, MgCl_2 4; pH 7.3, 300 mOsm. Synaptic transmission was recorded in whole-cell configuration under voltage-clamp using 1-2 ms depolarizations from -75 mV to 0 mV to induce action potentials. Hypertonic sucrose solutions contained 0.5 M sucrose in addition to the regular external solution. Patch pipette solutions included (in mM): K-

gluconate 125, NaCl 10, MgCl₂ 4.6, ATP-Na₂ 4, creatine phosphate 15, phosphocreatine kinase (20 U ml⁻¹), EGTA 1; 300 mOsm, and adjusted to pH 7.3. All analyses procedures were performed as described (Fernandez-Chacon et al., 2001).

2.2.6 Statistics. All data presented as means ± SEMs. Unpaired or paired student *t*-tests or two-way ANOVA tests were used as indicated to assess significance.

2.3 Results

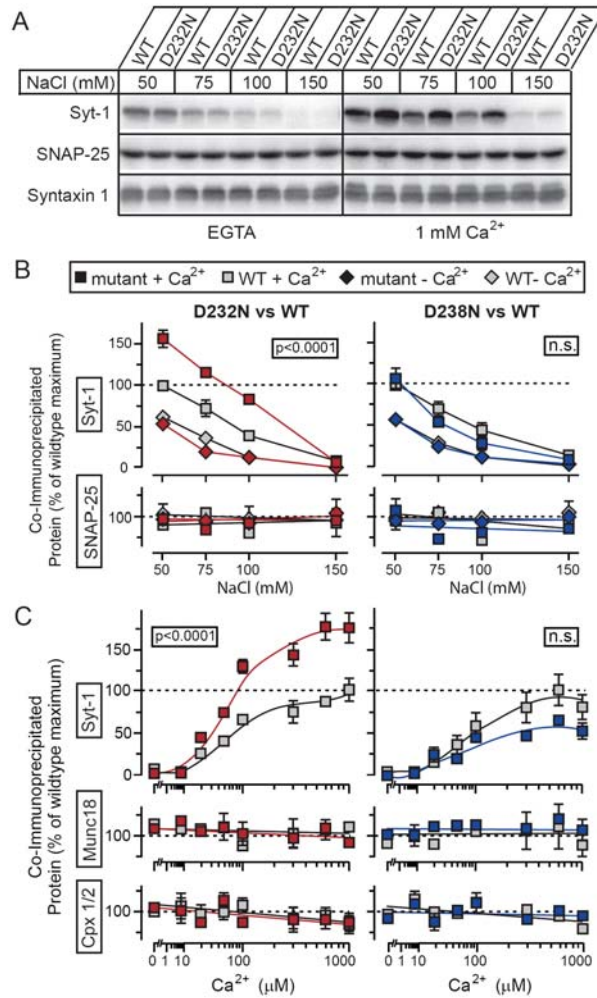
2.3.1 The D232N-mutation increases Ca²⁺-dependent but not Ca²⁺-independent SNARE-binding by synaptotagmin-1

We first examined the effect of the D232N- and D238N-mutations on Ca²⁺-dependent and Ca²⁺-independent interactions of synaptotagmin-1 with SNARE complexes using immunoprecipitations of brain proteins from knockin mice. In initial experiments, we probed these interactions at different ionic strength because the relative degree of Ca²⁺-dependent vs. Ca²⁺-independent binding of wild-type synaptotagmin-1 to SNARE complexes is strongly dependent on the ionic strength (Fig. 2-1A; (Tang et al., 2006)). Unexpectedly, the D232N-mutation strongly increased Ca²⁺-dependent binding of synaptotagmin-1 to SNARE complexes, but had no effect on Ca²⁺-independent binding (Fig. 2-1B). The D238N-mutation, in contrast, did not alter Ca²⁺-dependent SNARE binding by synaptotagmin-1.

We next measured the Ca²⁺-dependence of SNARE binding by synaptotagmin-1 in buffer of approximately physiological ionic strength (100 mM NaCl, 50 mM HEPES-NaOH). The D232N-mutation increased SNARE binding at all Ca²⁺-concentrations tested (Fig. 2-1C). Again, the D238N-mutation had no obvious effect on SNARE-binding. Ca²⁺

did not change the amount of other co-immunoprecipitated proteins (complexins 1/2 and Munc18-1). Quantitations showed that in the absence of Ca^{2+} , ~0.6% of the total synaptotagmin-1 was stably bound to syntaxin-1, while Ca^{2+} increased this to nearly 10% of the total synaptotagmin-1 in D232N-mutant brains. In contrast, approximately 4% of the total Munc18-1, SNAP-25, synaptobrevin 2, and complexin 1/2 are stably bound to syntaxin-1 in the presence or absence of Ca^{2+} . The fact that complexin, a protein that only binds to assembled SNARE complexes (McMahon et al., 1995), is co-immunoprecipitated with the SNARE antibodies in these experiments demonstrates that synaptotagmin-1 binding to SNARE complexes is studied. Nevertheless, to ensure that the effect of the D232N-mutation on the Ca^{2+} -dependent interaction of synaptotagmin-1 with SNARE complexes was not an artifact of the syntaxin-1 immunoprecipitations, we immunoprecipitated SNARE complexes with antibodies to synaptobrevin/VAMP and measured the binding of D232N-mutant synaptotagmin-1 as a function of Ca^{2+} (Fig. 2-2). Again, we observed a ~2-fold increase in binding by the D232N mutation.

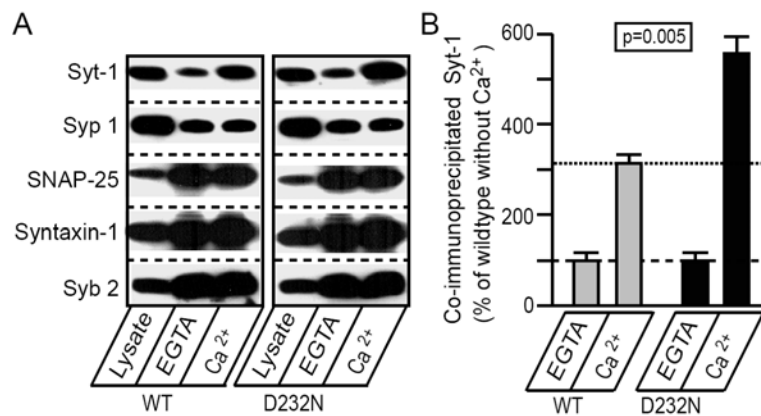
Viewed together, these data demonstrate that the Ca^{2+} -dependent interaction of native synaptotagmin-1 with native SNARE complexes is selectively enhanced by the D232N-mutation, whereas the similar D238N substitution does not significantly alter SNARE-complex binding. Although the lack of an atomic structure of the synaptotagmin-1/SNARE complex makes it difficult to understand the structural basis for the strikingly differential effect of two very similar mutations, it seems likely that Ca^{2+} -dependent binding of SNARE complexes to synaptotagmin-1 involves negatively



By Ok-Ho Shin

Figure 2- 1 Immunoprecipitation analysis of native wild-type and mutant synaptotagmin-1 binding to SNARE complexes using polyclonal syntaxin-1 antibodies.

A, Representative immunoblots of syntaxin-1 immunoprecipitates. Brain proteins from synaptotagmin-1 D232N-mutant and wild-type mice (WT) were solubilized with 1% Triton X-100 to promote SNARE complex formation, and immunoprecipitated with polyclonal syntaxin-1 antibodies at increasing NaCl concentrations, with or without 1 mM free Ca²⁺. Immunoprecipitates were blotted with monoclonal antibodies to synaptotagmin-1 (Syt-1), SNAP-25 (Cl 71.1) and syntaxin-1 (HPC-1); bands were probed with ¹²⁵I-labeled secondary antibodies and visualized in a phosphorImager. **B**, Quantitations of synaptotagmin-1 and SNAP-25 co-immunoprecipitated with syntaxin-1 at increasing NaCl concentrations in the presence or absence of 1 mM Ca²⁺. Quantitations were carried out with ¹²⁵I-labeled secondary antibodies; amounts of co-immunoprecipitated proteins in this and all other immunoprecipitation experiments are normalized for the amount of the immunoprecipitated protein (i.e. syntaxin-1 [Fig. 2-1] or synaptobrevin-2 [Fig.2-2]; n=3). In this and all following figures, gray symbols = WT, red symbols = D232N mutant; blue symbols = D238N mutant; data shown are means ± SEMs. **C**, Quantitations of synaptotagmin-1, Munc18-1, and complexins 1/2 (Cpx 1/2) co-immunoprecipitated with syntaxin-1 in the presence of increasing Ca²⁺-concentrations in 100 mM NaCl (n=3). Statistical analyses in **B** and **C** were performed with a 2-way ANOVA test; n.s. = non-significant.



By Ok-Ho Shin

Figure 2- 2 Immunoprecipitation analysis of synaptotagmin-1 binding to SNARE complexes using monoclonal synaptobrevin-2 antibodies.

A, Representative immunoblots of immunoprecipitations performed in 100 mM NaCl as described in the Fig. 2-1 legend, except that monoclonal synaptobrevin-2 antibodies were employed (Syt-1 = synaptotagmin-1; Syp 1 = synaptophysin-1; Syb 2 = synaptobrevin-2). Bands were visualized by enhanced chemiluminescence. **B**, Quantitations of synaptotagmin-1 co-immunoprecipitated with synaptobrevin-2 in the presence or absence of 1 mM free Ca²⁺. Quantitations were performed with ¹²⁵I-labeled secondary antibodies (means ± SEMs; n=3).

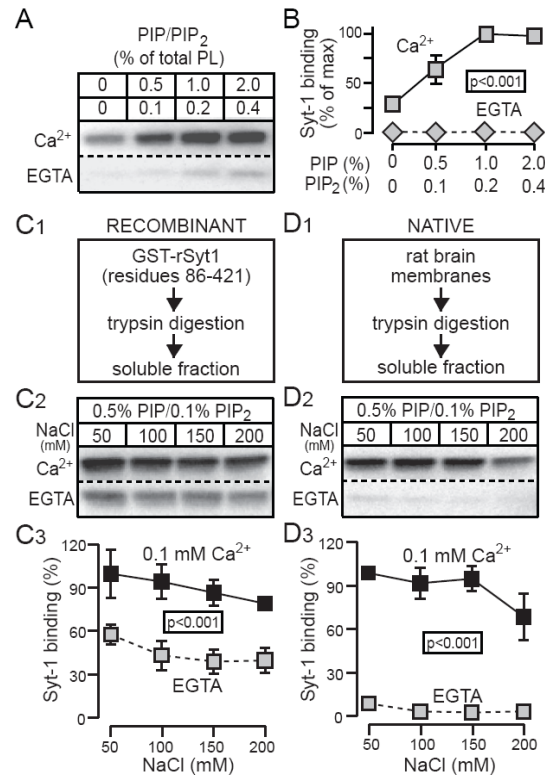
charged SNARE residues that are normally repelled by aspartate 232, thereby increasing the binding strength in the absence of aspartate 232.

Viewed together, these data demonstrate that the Ca²⁺-dependent interaction of native synaptotagmin-1 with native SNARE complexes is selectively enhanced by the D232N-mutation, whereas the similar D238N substitution does not significantly alter SNARE-complex binding. Although the lack of an atomic structure of the synaptotagmin-1/SNARE complex makes it difficult to understand the structural basis for the strikingly differential effect of two very similar mutations, it seems likely that Ca²⁺-dependent binding of SNARE complexes to synaptotagmin-1 involves negatively

charged SNARE residues that are normally repelled by aspartate 232, thereby increasing the binding strength in the absence of aspartate 232.

2.3.2 Effect of the D232N- and D238N-mutations on Ca^{2+} -dependent phospholipid binding

To investigate the effects of the D232N- and D238N-mutations on Ca^{2+} -dependent phospholipid binding by synaptotagmin-1 in greater detail than we had previously done (Fernandez-Chacon et al., 2002), we decided to focus on native synaptotagmin-1 since there may be differences between recombinant and native proteins. To optimize the binding reactions, we first examined the effect of increasing the concentrations of phosphatidylinositols in the phospholipid bilayer on the Ca^{2+} -dependent and Ca^{2+} -independent binding of native synaptotagmin-1 (Figs. 2-3A and 3B). When we measured the binding of native synaptotagmin-1 to vesicles with a lipid composition resembling that of synaptic vesicles but with increasing concentrations of PIP and PIP₂, we found that as expected (Li et al., 2006), phosphatidylinositolphosphates strongly co-activated Ca^{2+} -dependent phospholipid binding by synaptotagmin-1 (Fig. 2-3A and B). Surprisingly, however, we did not observe any Ca^{2+} -independent binding of native synaptotagmin-1 to phospholipids containing even high concentrations of PIP and PIP₂, a result that differs from previous studies using recombinant proteins (Bai et al., 2004; Li et al., 2006). To resolve this discrepancy, we directly compared phospholipid binding by native and recombinant synaptotagmin-1 fragments with identical sequences (Fig. 2-3C and 3D). Binding reactions at different ionic strengths revealed that even at low ionic



By Ok-Ho Shin

Figure 2- 3 Comparison of Ca²⁺-induced phospholipid binding by equivalent fragments of recombinant and native synaptotagmin-1.

A and **B**, Analysis of the effect of incorporating phosphatidylinositides (PIP = phosphatidylinositolphosphate; PIP₂ = phosphatidylinositolbisphosphate) into liposomes on the Ca²⁺-independent and Ca²⁺-dependent binding of native synaptotagmin-1. Panels show representative immunoblots visualized with ¹²⁵I-labeled secondary antibodies (**A**) and quantitations of binding (**B**) in the presence or absence of 0.1 mM Ca²⁺ (means ± SEMs; n=3). Experiments were performed with the cytosolic region of synaptotagmin-1 obtained by mild trypsin digestion of total brain membranes, and with heavy liposome with a 'synaptic' composition (41% phosphatidylcholine, 32% phosphatidylethanolamine, 12% phosphatidylserine, 5% phosphatidylinositol, and 10% cholesterol by weight). Binding was carried out with a centrifugation assay in which synaptotagmin-1 bound to liposomes is measured by immunoblotting. **C** and **D**, Recombinant (**C**) and native (**D**) synaptotagmin-1 fragments were prepared as indicated (**C**₁ and **D**₁). **C**₂ and **D**₂, Representative immunoblots visualized with ¹²⁵I-labeled secondary antibodies of recombinant (**C**₂) and native (**D**₂) synaptotagmin-1. The recombinant GST-rat synaptotagmin-1 (GST-rSyt1, residue 86-421) includes the trypsin-hypersensitive site that is cleaved in native synaptotagmin-1; thus the native and recombinant trypsin-produced fragments contain identical sequences. Fragments were bound at different NaCl concentrations with and without 0.1 mM Ca²⁺ to liposomes with a phospholipid synaptic vesicle composition (PC: 41%, PE: 32%, PS: 12%, PI: 5%, cholesterol: 10%), and with 0.1% PIP and 0.5% PIP₂. **C**₃ and **D**₃, Binding was quantified for both recombinant (**C**₃) and native (**D**₃) synaptotagmin-1 using immunoblotting with ¹²⁵I-labeled secondary antibodies and PhosphorImager detection, and is expressed as percent of the maximum. Data are presented as means ± SEMs (n=3). Statistical analyses were performed with a 2-way ANOVA test.

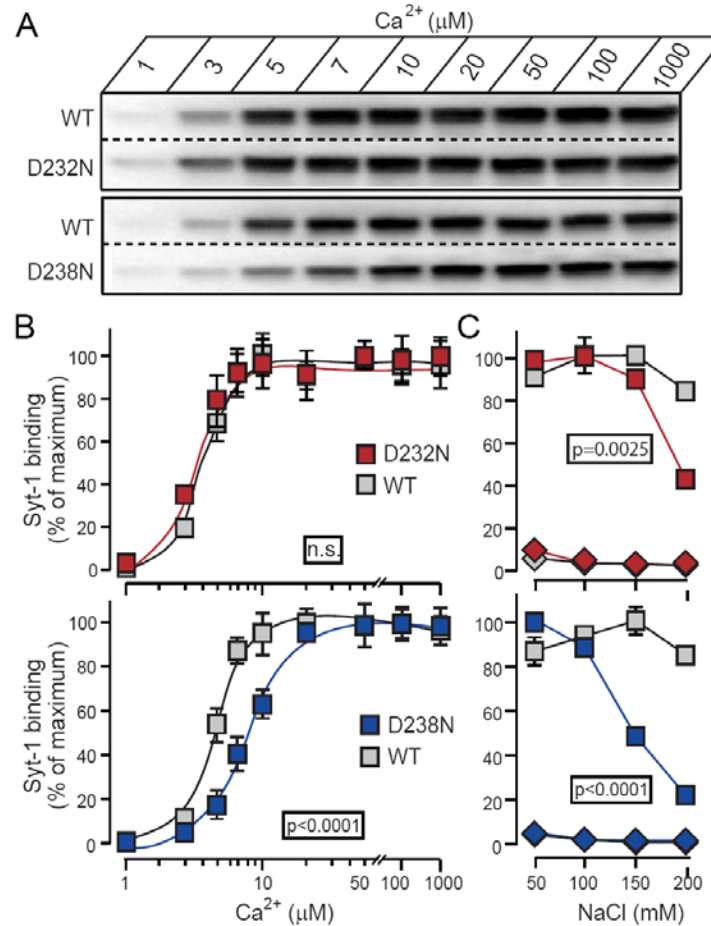
strengths, only recombinant but not native synaptotagmin-1 exhibited Ca^{2+} -independent binding to phospholipid membranes containing 0.5% PIP and 0.1% PIP_2 (Fig. 2-3C and 3D). Thus for native synaptotagmin-1, PIP and PIP_2 are co-activators of Ca^{2+} -dependent phospholipid binding, but are not sufficient to mediate Ca^{2+} -independent binding.

We next tested the effects of the DN-mutations on Ca^{2+} -dependent phospholipid binding. Consistent with previous results (Fernandez-Chacon et al., 2002), the D232N-mutation did not alter the apparent Ca^{2+} -affinity or extent of phospholipid binding by native synaptotagmin-1 (Fig. 2-4A and B). In contrast, the D238N-mutation caused a small but significant decrease in phospholipid binding (Fig. 2-4B). Both mutations destabilized the synaptotagmin-1/ Ca^{2+} /phospholipid complex at high NaCl concentrations (Fig. 2-4C). Viewed together, these experiments establish that two closely spaced mutations in the Ca^{2+} -binding sites of the C_2A -domain have distinct effects on the biochemical properties of synaptotagmin-1 at physiological ionic strengths: whereas the D232N-mutation selectively enhances Ca^{2+} -dependent interactions of synaptotagmin-1 with SNARE complexes without altering phospholipid binding, the D238N-mutation does not alter SNARE binding, but decreases the apparent Ca^{2+} -affinity of phospholipid binding.

2.3.3 The D232N-mutation increases fast synchronous Ca^{2+} -triggered release in inter-neuronal synapses

To test the effect of the aspartate mutations in the Ca^{2+} -binding site on neurotransmitter release, we analyzed synaptic responses in cultured cortical neurons

from littermate wildtype and D232N- or D238N-mutant mice. We studied evoked inhibitory postsynaptic currents (IPSCs) by stimulating presynaptic neurons with a focal electrode (Maximov and Südhof, 2005) (Fig. 2-5A). We found that in absolute terms,



By Ok-Ho Shin

Figure 2- 4 Ca²⁺-dependent binding of native wild-type or mutant synaptotagmin-1 to liposomes.

All experiments were performed as in Fig.2-3A and B. **A** and **B**, Analysis of the Ca²⁺-concentration dependence of the binding of native WT or D232N- and D238N-mutant synaptotagmin-1 to liposomes containing 0.5% PIP/0.1% PIP₂ in 100 mM NaCl. Panels show representative immunoblots (**A**) and quantitations of binding (**B**). **C**, NaCl concentration dependence of the binding of native WT or D232N- and D238N-mutant synaptotagmin-1 to liposomes containing 0.5% PIP/0.1% PIP₂ in the absence or presence of 1 mM free Ca²⁺. Panels **B** and **C** show means ± SEMs (n=3 for D232N, n=4 for D238N); statistical analyses were performed by 2-way ANOVA test.

the D232N-mutation caused a ~1.5-fold increase in the IPSC amplitude, and a ~2.0-fold increase in the synaptic charge transferred per action potential (Fig. 2-5B and C). The D238N-mutation, in contrast, caused moderate, statistically significant decreases in IPSC amplitude and synaptic charge transfer. Thus the two point mutations alter release in a manner that precisely correlates with their effects on the biochemical phospholipid- and SNARE-binding activities of synaptotagmin-1.

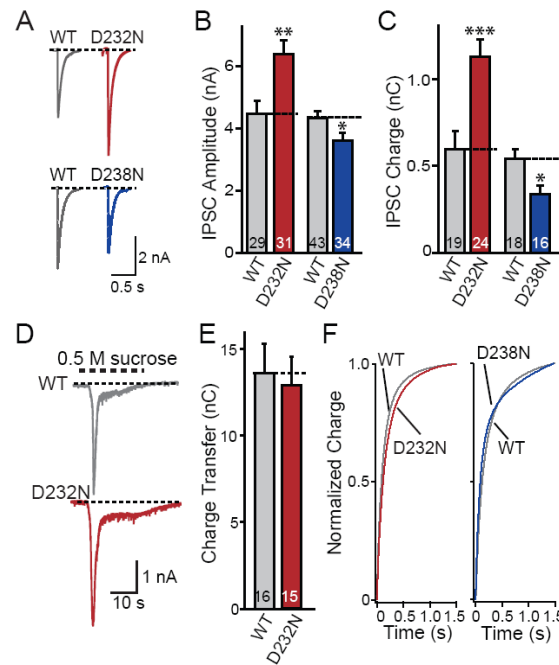


Figure 2- 5 Evoked IPSCs in synapses containing wild-type or mutant synaptotagmin-1. **A**, Representative traces of IPSCs evoked by focal stimulation in cortical neurons cultured from littermate WT and D232N- or D238N-mutant mice. Recordings were made in 2 Ca^{2+} /0.8 Mg^{2+} ; stimulation artifacts were truncated for display purposes. **B** and **C**, Summary graphs of the amplitudes and total charge transfer during IPSCs evoked at low frequency (<1 Hz) in neurons from littermate WT and D232N- (**B**) or D238N-mutant mice (**C**). **D**, Representative traces of IPSCs induced by hypertonic sucrose (0.5 M). **E**, Total synaptic charge transfer integrated over 30 sec in response to a 0.5 M sucrose application for 20 sec. **F**, Time course of synaptic responses to isolated action potentials in cultured cortical neurons from littermate WT and D232N- or D238N-mutant neurons. Graphs show the integrated synaptic charge transfer plotted as a function of time for D232N-mutant (left panel) and D238N-mutant neurons (right panel) compared to their littermate control cultures (D232N WT, n=18; D232N, n=21; D238N WT, n=23; D238N, n=20). Data shown are means \pm SEMs; statistical significance was assessed by unpaired *t*-test (*= p <0.05; **= p <0.01; ***= p <0.001; numbers of recorded neurons are indicated in the bars).

Several potential causes for the large increase in synaptic responses in D232N-mutant synapses can be suggested, for example, changes in the size of the readily-releasable pool (RRP) of vesicles, the mode of release (synchronous vs. asynchronous), or the Ca^{2+} -sensitivity of release. We tested these possibilities by first measuring the size of the RRP using an application of hypertonic sucrose (Rosenmund and Stevens, 1996), but failed to detect a significant change in D232N-mutant synapses in either the size of the RRP (Fig. 2-5D and E) or the kinetic properties (data not shown) of hypertonic sucrose-induced release. We next examined the possibility that the D232N-mutation may have shifted the mode of release from synchronous to asynchronous by measuring the time course of release, but again did not observe a significant difference between wildtype and D232N- or D238N-mutant synapses (Fig. 2-5F). Finally, we assessed the apparent Ca^{2+} -sensitivity of release by titrating the amount of release as a function of the extracellular Ca^{2+} -concentration (Fig. 2-6). We found that the D232N-mutation caused a ~1.5-fold increase in the apparent Ca^{2+} affinity of release, whereas the D238N-mutation had no significant effect (Fig. 2-6C and D; see Table 2-1). Note that in all of these studies, we measure absolute response sizes in multiple independent cultures obtained from littermate knockin and control mice. These data are in agreement with rescue studies in autapses (Stevens and Sullivan, 2003). Interestingly, the apparent Ca^{2+} -affinity of release for extracellular Ca^{2+} in inter-neuronal wildtype synapses measured here closely parallels that observed previously in autapses (Fernandez-Chacon et al., 2001).

These data indicate that the D232N-mutation greatly increases the release probability of synaptic vesicles by enhancing their Ca^{2+} -sensitivity, whereas the D238N-mutation slightly decreases the release probability. To obtain independent evidence for this conclusion, we examined paired-pulse responses in the mutant synapses because a decrease in release probability usually causes an increased paired-pulse ratio (i.e., facilitation), while an increase in release probability causes a decreased paired-pulse ratio (i.e., depression) (Zucker and Regehr, 2002).

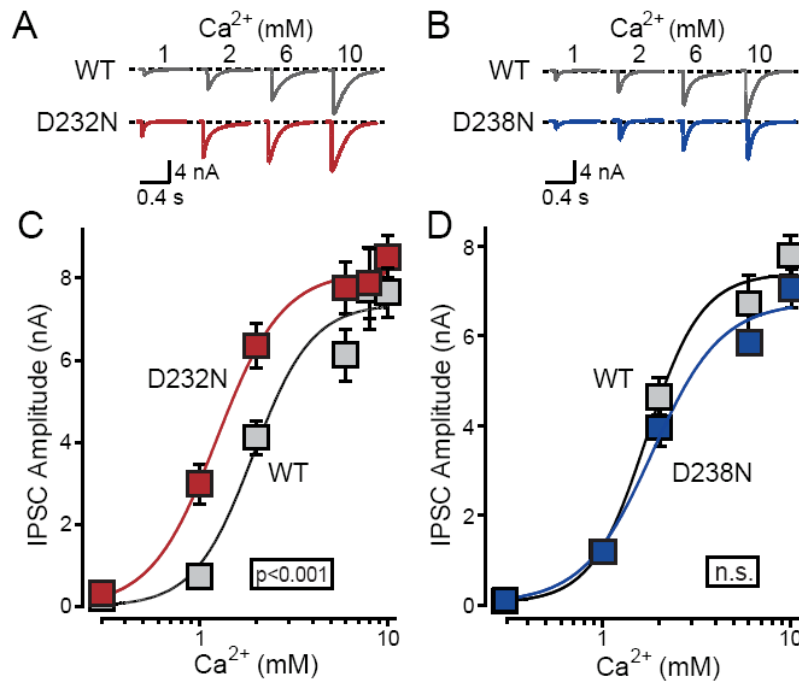


Figure 2- 6 Ca^{2+} dependency of synaptic responses in D232N and D238N mutant synapses. *A* and *B*, Representative traces of evoked IPSCs at the indicated concentrations of free Ca^{2+} . Stimulation artifacts are removed for display purposes. *C* and *D*, Dose-response curves of evoked IPSCs in neurons from littermate WT and D232N- (*C*) or D238N-mutant mice (*D*). Data shown are means \pm SEMs ($n=4-22$ neurons depending on Ca^{2+} -concentration); statistical significance was assessed by a two-way ANOVA test. The curve shown represents the result of a fit of the data to a Hill function that is described in Table 2-1.

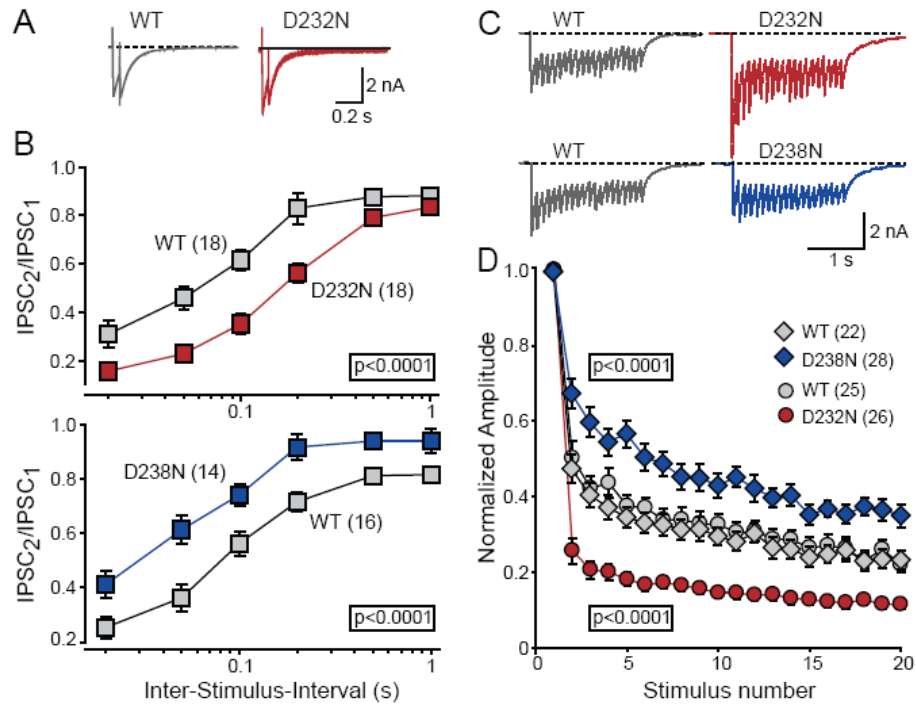


Figure 2- 7 Short-term synaptic plasticity in synapses containing wild-type or mutant synaptotagmin-1.

A and **B**, Representative IPSCs (**A**; interstimulus interval = 50 ms) and summary graphs (**B**) of paired-pulse stimulation experiments. IPSCs were examined in responses to two closely spaced action potentials elicited by focal stimulation in cultured cortical neurons. The summary graph (**B**) displays the ratio of the second to the first IPSC amplitude as a function of the interstimulus interval. **C**, Representative traces of IPSCs during a 2 sec 10 Hz stimulus train. **D**, Summary graphs of IPSC amplitudes during 10 Hz stimulus trains. IPSCs were normalized to the first response. Note that stimulation artifacts are removed for display purposes. In panels **B** and **D**, data shown are means \pm SEMs (number of analyzed neurons are shown in brackets); statistical significance was assessed by a two-way ANOVA test.

Indeed, application of two closely spaced action potentials with different inter-stimulus-intervals revealed that D232N-mutant synapses exhibited increased depression compared to wild-type control neurons, whereas D238N-mutant synapses exhibited decreased depression, i.e. facilitation, relative to wild-type neurons (Fig. 2-7A and B). Moreover, we monitored short-term plasticity during repetitive train stimulation in D232N- and D238N-mutant synapses. Again, we observed increased depression in D232N-mutant and

decreased depression in D238N-mutant neurons (Fig. 2-7C and D). These results are consistent with an increase of release probability in D232N-mutant, and a decrease of release probability in D238N-mutant synapses, and are in agreement to previous data obtained in excitatory autapses (Fernandez-Chacon et al., 2002). In the synaptotagmin-1 mutant synapses examined here, just as in the synaptotagmin-1 deficient synapses we studied previously (Geppert et al., 1994; Maximov and Sudhof, 2005), the effect was restricted to fast synchronous release, and no significant effect on asynchronous release during stimulus trains was observed (Fig. 2-8).

2.3.4 The D232N-mutation increases the apparent Ca^{2+} -sensitivity of release in excitatory autapses

All physiological experiments reported here up to this point were carried out in inhibitory inter-neuronal synapses. To test whether the phenotype observed is applicable to excitatory responses, and to validate the conclusions with a different approach, we monitored synaptic transmission in autapses. In these experiments, we crossed compound heterozygous D232N-/D238N-mutant mice with each other, and cultured neurons from littermate offspring that were homozygous for the D232N- or the D238N-mutation. In this manner, we compared the two mutants directly to each other without a wild-type control. Neurons were cultured under conditions that favor formation of autapses, and were analyzed by whole-cell recordings.

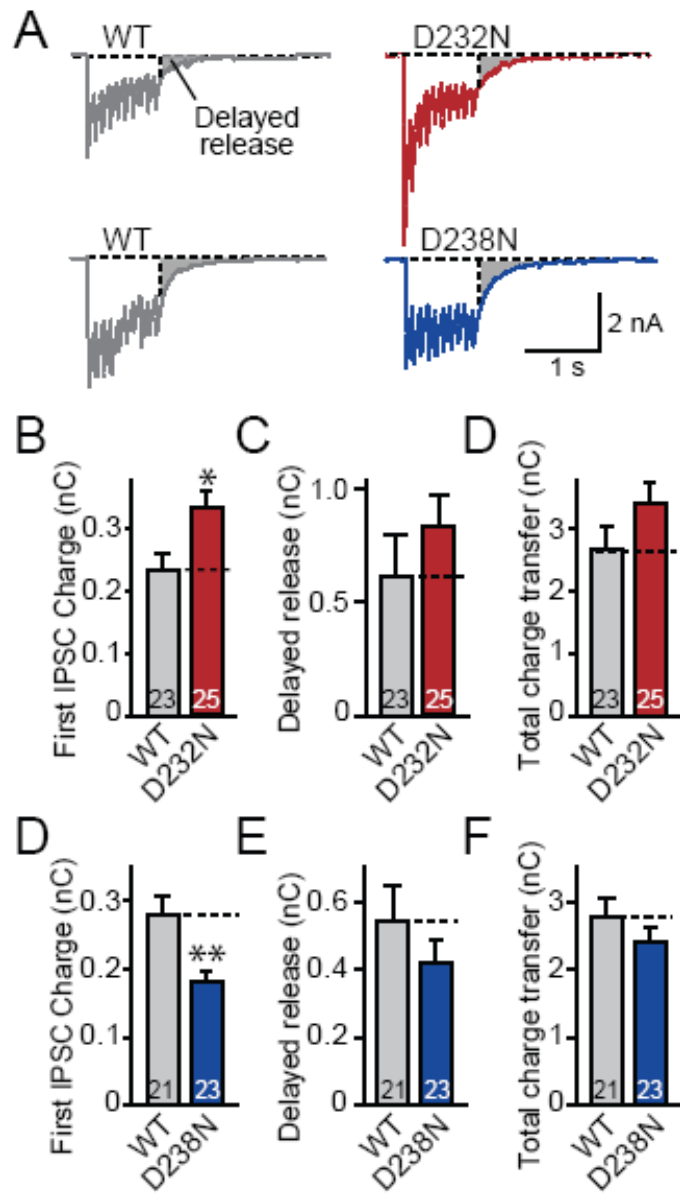
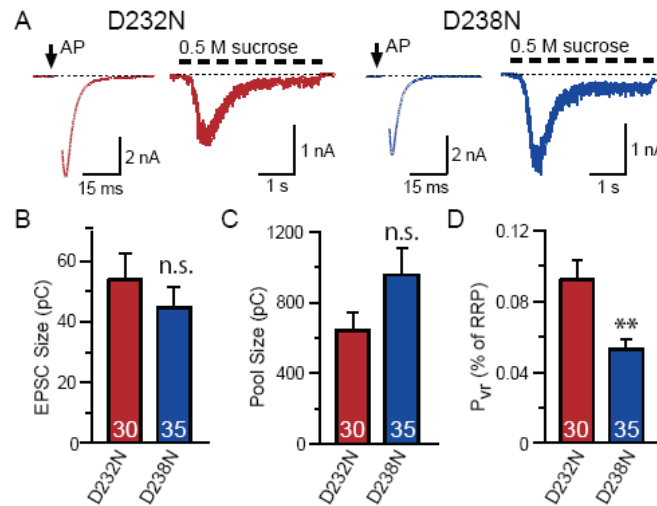


Figure 2- 8 Effect of D232N- and D238N-mutations on asynchronous release during and following a 10 Hz stimulus train.

A, Representative traces of inhibitory synaptic responses in D232N- or D238N-mutant neurons and littermate wildtype control neurons when 10 stimuli at 10 Hz were elicited by focal stimulation. Delayed asynchronous release was defined as the synaptic response observed 100 ms after the last stimulus (shaded area). Recordings were from cortical neurons cultured at high density from littermate wildtype and D232N- or D238N-mutant mice. **B** and **D**, Total charge transfer during the first response; **C** and **E**, total delayed release; **D** and **F**, total amount of release integrated over the entire stimulus train in D232N- and D238N-mutant neurons, respectively. Note that stimulation artifacts are removed for better presentation. Data shown are means \pm SEMs; *, $p < 0.05$; **, $p < 0.01$.

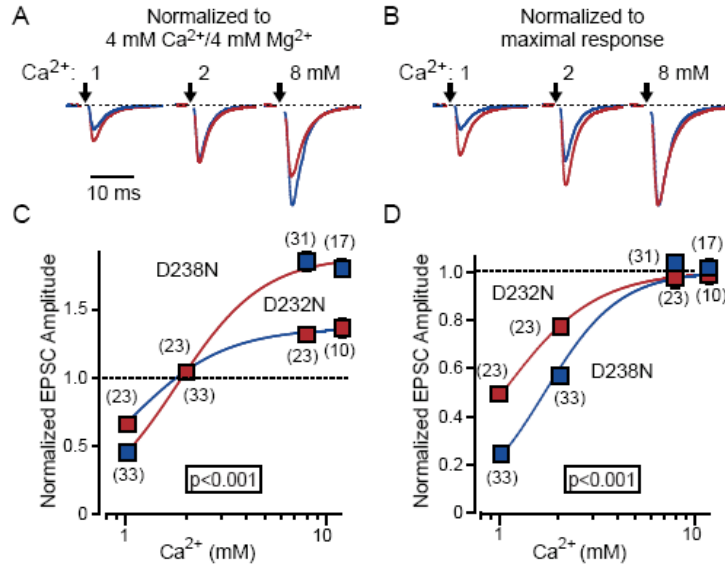
Measurements of synaptic responses evoked by action potentials or by hypertonic sucrose in the same neuron demonstrated that the size of these two types of synaptic responses was not significantly different between the D232N- and D238N-mutant neurons (Fig. 2-9A-C). However, when we determined for each individual neuron the vesicular release probability P_{vr} (calculated as the ratio of action potential- to sucrose-evoked synaptic response in a given neuron), we noted that D232N-mutant neurons displayed an almost 2-fold increase in the P_{vr} compared to D238N-mutant neurons (Fig. 2- 9D).



By A Meyer

Figure 2- 9 Evoked EPSCs in autapses formed by D232N- and D238N-mutant neurons.

A, Representative traces of EPSCs evoked in the same neuron by consecutive stimulation with an action potential (induced by somatic depolarization from -75 mV to 0 mV for 2 ms) and with hypertonic sucrose (0.5 M for 3 sec). EPSCs were recorded in isolated hippocampal neurons cultured on glial microislands where they form hundreds of autapses. Neurons were cultured from littermate D232N- and D238N-mutant mice derived from crossings of compound heterozygous mutant mice. Capacitative and somatic currents are blanked for display purposes. **B** to **D**, Summary graphs of the synaptic charge integrals of action potential-induced EPSCs (**B**) and sucrose-induced EPSCs (**C**, corresponds to the RRP), and of the ratio of the charge integrals of action potential-induced to sucrose-induced EPSCs (**D**, defined as the vesicular release probability P_{vr}). Data shown are means \pm SEMs; statistical significance was assessed by unpaired t-test (**= $p < 0.01$; numbers of recorded neurons are indicated in the bars).



By A Meyer

Figure 2- 10 Determination of the apparent Ca^{2+} -affinity of release from excitatory synapses in autapses from D232N- and D238N-mutant mice.

Recordings were made from autapses in hippocampal neurons cultured from littermate offspring of matings between compound heterozygous mutant mice (i.e., mice carrying one D232N and one D238N mutant allele). Ca^{2+} -titrations were performed by interleaving EPSC-measurements at the indicated test Ca^{2+} -concentration in 1 mM Mg^{2+} with measurements under the standard conditions for autapses (with 4 mM Ca^{2+} and 4 mM Mg^{2+}) in order to control for possible rundown of synaptic responses. **A**, Representative superimposed traces of action potential-evoked EPSCs recorded in D232N- (red) and D238N-mutant neurons (blue) during low-frequency stimulation (0.2 Hz for 30–60 s) at different Ca^{2+} -concentrations as indicated. **B**, Same traces as shown in (A), but normalized to the maximal amplitudes of the EPSCs (i.e., to the responses obtained in 10 mM Ca^{2+} /1 mM Mg^{2+}). Note that stimulus artifacts are removed for display purposes. **C** and **D**, Summary graphs of the Ca^{2+} -dependence of synaptic responses in autapses. EPSC amplitudes were normalized to the EPSC obtained in standard extracellular medium containing 4 mM Ca^{2+} /4 mM Mg^{2+} (**C**), or to the maximal EPSC amplitude (**D**). Data in (**C**) and (**D**) were fitted to a Hill function (see Table 2-1). Data shown are means \pm SEMs (number of analyzed neurons are shown in brackets); statistical significance was assessed by a two-way ANOVA test.

To test whether the difference in P_{vr} between the two synaptotagmin-1 mutants is due to a difference in apparent Ca^{2+} -sensitivity (which might lead to a failure to observe

differences in the absolute synaptic responses if the Ca^{2+} -concentration used for those measurements falls into a range of relative lower sensitivity to external Ca^{2+}), we titrated the magnitude of synaptic responses to isolated action potentials at different ambient Ca^{2+} -concentrations (Fig. 2-10A and B). We plotted the results normalized either for synaptic responses under control conditions (Fig. 2-10C), or for the maximal synaptic response in a titration (Fig. 2-10D). When fitted with a Hill function, the apparent Ca^{2+} affinity of release in D232N-mutant neurons was found to be ~1.8-fold higher than in D238N-mutant neurons (i.e., the apparent K_d value was ~0.6-fold lower; Table 2-1). The data confirm – as described above and consistent with data from rescue experiments (Stevens and Sullivan, 2003) – that the D232N-mutation causes a relative shift to higher apparent Ca^{2+} -sensitivities of release compared to the D238N-mutation. Thus in autapses similar to inter-neuronal synapses, the D232N-mutation induces a relative increase in the apparent Ca^{2+} -sensitivity of release.

Table 2-1 Ca²⁺ affinities in Excitatory and Inhibitory synapses

Genotype	K_d (mM Ca^{2+}) ± SEMs	n	I_{max}	EPSC / IPSC		Normalization	
<u>Inter-neuronal synapses</u>							
Wildtype	1.9 ± 0.3	2.5	7.4 nA	IPSC		none	
Syt-1 D232N	1.2 ± 0.1	2.8	8.2 nA		IPSC		none
Wildtype	1.7 ± 0.2	3.0	7.3 nA	IPSC		none	
Syt-1 D238N	1.8 ± 0.3	2.4	6.7 nA		IPSC		none
<u>Autapses</u>							
Syt-1 D232N EPSC	1.0 ± 0.0	1.8	1.4	EPSC	to 4 Ca^{2+} /4 Mg^{2+}		
Syt-1 D238N EPSC	1.8 ± 0.2	2.0	1.9	EPSC	to 4 Ca^{2+} /4 Mg^{2+}		
Syt-1 D232N	1.0 ± 0.0	1.8	1.0	EPSC	to maximal EPSC		
Syt-1 D238N	1.7 ± 0.1	2.3	1.0	EPSC	to maximal EPSC		
<u>Autapses</u> (Fernandez-Chacon et al., 2001)							
Wildtype EPSC	1.9 ± 0.2	1.7	1.7	EPSC	to 4 Ca^{2+} /4 Mg^{2+}		
Syt-1 R233Q EPSC	3.7 ± 0.8	1.6	1.3	EPSC	to 4 Ca^{2+} /4 Mg^{2+}		

Apparent Ca²⁺-affinities were determined by measuring the amplitudes of synaptic responses as a function of the extracellular Ca²⁺ concentration (all in the presence of 1 mM Mg²⁺ for autapses, and 0.8 mM Mg²⁺ for inter-neuronal synapses). Responses were fitted to a Hill function: $I = I_0 + (I_{\max} - I_0) / (1 + (K_d / [Ca^{2+}])^n)$, where I is the recorded synaptic current plotted as normalized amplitude, I_0 the base value of responses, I_{\max} the maximal current, K_d the apparent dissociation constant for extracellular Ca²⁺, $[Ca^{2+}]$ the extracellular Ca²⁺ concentration, and n the apparent cooperativity. For all fits, I_0 was set to 0. Data shown are from Figs. 2-6 and 2-10, and from Fernandez-Chacon et al. (2001). Wildtype values are always obtained from cultures from littermate mice plated and measured on the same day as the mutant. Syt-1: synaptotagmin-1.

2.4 Discussion

Our data demonstrate that a single amino-acid substitution in synaptotagmin-1 (D232N) selectively increases its Ca^{2+} -dependent binding to SNARE complexes but not to phospholipids, and that the same mutation increases the amount of release triggered by Ca^{2+} -influx into nerve terminals in response to an action potential. Moreover, our results show that a different single amino-acid substitution in a nearby residue (D238N) selectively decreases the apparent Ca^{2+} -affinity of synaptotagmin-1 during phospholipid binding (although its effect is smaller than that of the D232N-mutation on SNARE binding), and decreases the amount of release triggered by Ca^{2+} accordingly. The effects of these substitutions on release were limited to fast synchronous release, as asynchronous release was not significantly altered. Our data thus suggest that synaptotagmin-1 functions by dual Ca^{2+} -dependent activities in triggering fast synchronous release, namely by binding to both phospholipids and SNARE complexes, raising the tantalizing possibility that synaptotagmin-1 triggers fast neurotransmitter release by the Ca^{2+} -dependent coupling of phospholipid membranes to SNARE complexes that were assembled during priming. Upon Ca^{2+} -influx triggered by action potentials, this coupling could occur by simultaneous binding of a single synaptotagmin-1 molecule to both SNAREs and phospholipids, or by separate binding of the two synaptotagmin-1 molecules in a constitutive synaptotagmin-1 dimer (Perin et al., 1991) to SNAREs or phospholipids.

The following evidence supports these conclusions and shows that the effects we observed are specific:

1. Biophysical studies previously demonstrated that the D232N- and D238N-mutations selectively but differentially alter intrinsic Ca^{2+} -binding by the C_2A -domain but have no significant effect on its atomic structure (Fernandez-Chacon et al., 2002). Thus these mutations do not introduce non-specific structural changes into synaptotagmin-1.

2. The D232N and D238N mutations are very similar – both neutralize a negatively charged amino acid in the second Ca^{2+} -binding loop (and the third top loop overall; (Ubach et al., 1998)) of the C_2A -domain of synaptotagmin-1 – and the amino acids involved are only 5 residues apart. Thus these mutations control for each other, and do not mediate their very different biochemical and physiological effects by non-specific electrostatic mechanisms.

3. Although the phospholipid-binding and the synaptic phenotype of the D238N-mutation are subtle, the SNARE complex-binding and the synaptic phenotype of the D232N-mutation are robust, suggesting that these changes are central to the function of synaptotagmin-1.

4. Our experiments were performed with knockin mice in which mutant synaptotagmin-1 is expressed at normal levels, and analyzed native synaptotagmin-1 from knockin mice instead of recombinant proteins. The former avoids artifacts induced by overexpression in rescue experiments (or worse, by overexpression experiments in cells such as PC12 cells containing endogenous synaptotagmin-1), whereas the latter prevents the problems with recombinant proteins that may lack crucial modifications. The potential problems with recombinant proteins are illustrated in the Ca^{2+} -independent

binding of recombinant synaptotagmin-1 to membranes containing phosphatidylinositolphosphates, binding that is not observed for native synaptotagmin-1 (Fig. 2-3B to D). Thus we are studying native proteins in a physiological context.

5. Finally, we analyzed the D232N- and D238N-mutant synapses with two different electrophysiological approaches, inter-neuronal inhibitory and autaptic excitatory synapses. The central finding that the D232N-mutation increases the apparent Ca^{2+} -affinity of release was confirmed for both preparations, and the changes of short-term plasticity during stimulation trains (a faster depression in D232N-mutant synapses) are essentially the same in both preparations. Thus the phenotype is not dependent on a particular type of synapse or a particular experimental approach, although the effects of the mutations are more pronounced in inter-neuronal synapses, possibly because inter-neuronal synapses allow more sensitive monitoring of changes in synaptic transmission.

Our current results add to previous studies that had demonstrated that Ca^{2+} -dependent binding of synaptotagmin-1 to phospholipid membranes is a crucial step in neurotransmitter release *in vivo*. Specifically, it was shown that mutations which selectively decrease phospholipid-binding by synaptotagmin-1 cause a corresponding decrease of release (Fernandez-Chacon et al., 2001), whereas mutations that enhance phospholipid binding produce an increase of release (Rhee et al., 2005). In addition, a large number of prior studies supported the notion that SNARE binding by synaptotagmin-1 is important, but these results were largely obtained with transfected cells and/or recombinant proteins, and often presented contradictory conclusions (Banerjee et al., 1996; Bennett et al., 1992; Bowen et al., 2005; Chapman et al., 1995;

Chapman and Jahn, 1994; Davletov and Sudhof, 1993; Fernandez et al., 2001; Lee et al., 2004; Li et al., 1995b; Rickman et al., 2004; Rickman and Davletov, 2003; Schiavo et al., 1997; Yoshida et al., 1992). These previous studies had two limitations. First and most importantly, no synaptotagmin-1 mutation was known that selectively alters SNARE binding, whereas such mutations are available for phospholipid binding. In the absence of such a selectively acting mutation, no *in vivo* analysis of SNARE binding by synaptotagmin-1 was possible. Second, these studies largely relied on transfected neuroendocrine cells that represent an artificial and potentially misleading methods to study neurotransmitter release. This problem is illustrated by the controversy regarding the role of synaptotagmin-1 (and other proteins) in fusion pores. Overexpression experiments suggested that the synaptotagmin-1/SNARE interaction shapes the fusion pore (Bai et al., 2004; Wang et al., 2001). However, knockin experiments that alter synaptotagmin-1 function without changing its expression levels do not reveal a role in fusion pores (Sorensen et al., 2003). Moreover, overexpression of many other proteins also alters fusion pore dynamics in transfected cells, suggesting that sheer overexpression of a protein can change the membrane tension and thereby secondarily affect fusion pores (reviewed in (Jahn et al., 2003)). We tried in a previous study to circumvent the difficulty associated with testing the importance of synaptotagmin-1/SNARE interactions using an alternative approach that employs Sr^{2+} instead of Ca^{2+} to trigger release, because Sr^{2+} is relatively ineffective in stimulating the interaction of synaptotagmin-1 with SNARE complexes (Shin et al., 2003). However, Sr^{2+} -triggered release is also largely asynchronous, limiting its use in probing synaptotagmin-1/SNARE interactions in release

(Xu-Friedman and Regehr, 2000). Given the previous difficulty in directly testing the importance of the SNARE/synaptotagmin-1 interaction, the finding reported here that a single amino-acid substitution in synaptotagmin-1 selectively alters this interaction may provide a useful general tool for future studies.

Why did we not observe in our initial study (Fernandez-Chacon et al., 2002) the large increase of synaptotagmin-1/SNARE interactions that we report here? Several potential explanations can be advanced. Only recent results uncovered the extreme sensitivity of the synaptotagmin/SNARE interaction to ionic strength (Tang et al., 2006), and thus we were not previously able to analyze the mutant mice properly for changes in SNARE binding. Moreover, we were misled by the problems inherent with recombinant proteins, as opposed to analyzing native synaptotagmin-1. The differences between the native and recombinant proteins are probably not due to a modification of native synaptotagmin-1, but rather caused by the contamination of recombinant synaptotagmin-1 with bacterial acidic small molecules that is extremely difficult to remove (Ubach et al., 2001).

A major remaining question regards the atomic mechanism by which synaptotagmin-1 binds to both phospholipids and SNARE complexes via its top Ca^{2+} -binding loops. It is unexpected that two similar mutations – D232N and D238N – with comparable although not identical effects on intrinsic Ca^{2+} -binding (Fernandez-Chacon et al., 2002) have dramatically different effects on the Ca^{2+} -dependent interactions of synaptotagmin-1 with SNARE complexes and phospholipids. This observation implies that although these interactions involve the same Ca^{2+} -binding sites of synaptotagmin-1,

their precise atomic constraints differ. Functionally, this observation suggests that SNARE complex and phospholipid binding are indeed tightly coupled in synaptotagmin-1, consistent with the notion that pulling these two components of the membrane fusion machinery together represents the mechanism of action of synaptotagmin-1. A better biophysical description of these interactions will be required to clarify this hypothesis.

CHAPTER III: GENETIC ANALYSIS OF SYNAPTOTAGMIN-2 IN SPONTANEOUS AND Ca^{2+} -TRIGGERED NEUROTRANSMITTER RELEASE

3.1 Introductions

Synaptotagmin-1 is a synaptic vesicle protein that binds Ca^{2+} via its two C_2 -domains and functions as a Ca^{2+} -sensor for fast neurotransmitter release (Fernandez-Chacon et al., 2001; Fernandez et al., 2001; Geppert et al., 1994; Perin et al., 1990). The Ca^{2+} -affinities of the synaptotagmin C_2 -domains are unphysiologically low ($>0.1 \text{ mM}$) in the absence of phospholipids, but are boosted to physiological levels ($\sim 1\text{-}20 \text{ }\mu\text{M}$ Ca^{2+}) in the presence of phospholipids (Fernandez et al., 2001; Ubach et al., 1998; Zhang et al., 1998). In hippocampal synapses and in chromaffin cells, Ca^{2+} -binding to synaptotagmin-1 determines the Ca^{2+} -affinity of fast exocytosis (Fernandez-Chacon et al., 2001; Sorensen et al., 2003).

In addition to synaptotagmin-1, 14 other synaptotagmins exist that share the same overall domain structure, but differ in expression patterns and biochemical properties. Among the 'other' synaptotagmins, synaptotagmin-2 most closely resembles synaptotagmin-1 (76% sequence identity in mice), and is the only synaptotagmin besides synaptotagmin-1 that was unequivocally localized to synaptic vesicles (Geppert et al., 1991). Synaptotagmins 1 and 2 both bind to SNARE proteins and phospholipids in a Ca^{2+} -dependent manner, although with distinct apparent Ca^{2+} -affinities (Geppert et al., 1991; Hui et al., 2005; Li et al., 1995a; Li et al., 1995b; Rickman et al., 2004; Sugita et al., 2001; Sugita et al., 2002). These data suggest that synaptotagmins 1 and 2 perform

similar functions. Consistent with this hypothesis, synaptotagmin-2 rescues the synaptotagmin-1 deficiency phenotype in neurons and chromaffin cells (Nagy et al., 2006; Sorensen et al., 2003). However, synaptotagmin-2 has only been studied in overexpression experiments, and it remains unclear whether synaptotagmins 1 and 2 really perform equivalent functions. One reason for this uncertainty is that although synaptotagmins 1 and 2 share many properties, they also exhibit differences. For example, synaptotagmin-1 is primarily present in forebrain which contains almost no synaptotagmin-2, whereas synaptotagmin-2 is more abundant in caudal brain areas (Berton et al., 1997; Geppert et al., 1991; Marqueze et al., 1995; Ullrich et al., 1994). Moreover, synaptotagmin-2 but not synaptotagmin-1 selectively binds inositolpolyphosphates (Fukuda et al., 1994; Mehrotra et al., 2000).

Although synaptotagmin-1 has been studied more extensively than synaptotagmin-2, even its functional definition remains incomplete. Loss-of-function mutants of synaptotagmin-1 cause a decrease in fast Ca^{2+} -triggered synchronous release in all preparations tested (Geppert et al., 1994; Littleton et al., 1993b; Mackler et al., 2002; Nishiki and Augustine, 2004; Nonet et al., 1993; Sorensen et al., 2003; Yoshihara and Littleton, 2002), but the additional role of synaptotagmin-1 in other forms of release is unclear. Among others, this is illustrated by results with *Drosophila* synaptotagmin-1 mutants in which an increase of spontaneous release was observed at late larval stages (Broadie et al., 1994; DiAntonio and Schwarz, 1994; Littleton et al., 1993b; Mackler et al., 2002), but not at embryonic synapses (Yoshihara and Littleton, 2002), or in larval synapses after acute inactivation of synaptotagmin-1 (Marek and Davis, 2002).

In the present study, we describe mice that contain a point mutation in the synaptotagmin-2 gene. Analysis of synaptic transmission in the Calyx of Held of the mutant mice revealed that Ca^{2+} -triggered synchronous neurotransmitter release is decreased, but spontaneous release is enhanced. We show that synaptotagmin-1-deficient cortical neurons also displayed a similar phenotype. Our data, the first functional analysis of synaptotagmin-2 in neurons and of any synaptotagmin in a central synapse in situ, reveal that synaptotagmin-1 and 2 generally act in triggering evoked release and in limiting spontaneous release. This result is consistent with the notion that in different types of synapses, synaptotagmin-1 and 2 perform analogous functions in ‘release slots’ at the active zone (Maximov and Sudhof, 2005) where they, possibly in a Ca^{2+} -independent complex with SNARE proteins, simultaneously stabilize primed vesicles in the absence of Ca^{2+} , and trigger the exocytosis of these vesicles in the presence of Ca^{2+} .

3.2 Materials and methods

3.2.1 Generation, breeding and analysis of Synaptotagmin-2I377N mutant mice.

Synaptotagmin-2^{I377N} mutant mice were generated by Ingenium Pharmaceuticals in a screen of chemically mutagenized mice (Russ et al., 2002; Stumm et al., 2002). All analyses described were performed on littermate offspring of heterozygous matings to control for background effects.

3.2.2 Behavioral Assays. Force-plate actometry (Fowler et al., 2001) was performed with 3-month old mice on a force plate (28 cm x 28 cm) for 6 min. The ataxia index was

calculated from the area:distance ratio measured from the movement traces monitored over 6 min (normal range: 0.26-060).

3.2.3 Expression and purification of recombinant proteins. Wildtype and I377N-mutant synaptotagmin-2 and PKC C₂-domain expression vectors in pGEX-KG were described previously (Sugita et al., 2001) or generated by mutagenesis. Recombinant C₂B-domain proteins were stripped of their bacterial contaminants by treatment with benzonase and extensive washing as described (Ubach et al., 2001).

3.2.4 Centrifugation pospholipid binding assays. Ca²⁺-dependent phospholipid binding assays were carried out with purified soluble GST fusion proteins in 50 mM HEPES-NaOH, pH 6.8, 0.1 M NaCl, and 4 mM Na₂EGTA using a centrifugation assay (Fernandez et al., 2001; Shin et al., 2003; Shin et al., 2002).

3.2.5 Circular Dichroism Spectra were recorded on an Aviv model 62 DS spectropolarimeter at 200 to 260 nm using a 1 mm path-length cell. Thermal denaturation curves were collected by monitoring the absorption at 217 nm, with or without 5 mM Ca²⁺. The fraction of unfolded protein at each temperature was calculated by using the formula $(I_{\text{obs}} - I_f) / (I_u - I_f)$, where I_{obs} is the observed signal intensity, and I_u and I_f are the signal intensities of the unfolded and folded states, respectively. I_u and I_f as a function of temperature were calculated by extrapolation of the linear regions at the extremes of the unfolding curves.

3.2.6 Immunoprecipitations were performed from brain homogenates using synaptotagmin-2 polyclonal (A320) or syntaxin monoclonal (HPC-1) antibodies essentially as described (Shin et al., 2003).

3.2.7 Immunofluorescence labeling of brainstem cryostat sections was performed with antibodies to synaptotagmins 1 or 2 and to synapsins (syt1: 41.1, 1:5 000; syt2: A320, 1:500; Synapsin: C110.22, 1:1 000 or E028, 1:1 000) essentially as described (Ullrich et al., 1994).

3.2.8 Brain slicing and whole-cell recordings from MNTB neurons. Preparation of slices (200 μ m thickness), simultaneous whole-cell recordings of the nerve terminal and the postsynaptic neuron were performed mostly as described (Borst et al., 1995; Wu and Borst, 1999). Presynaptic whole-cell recordings were made with an EPC-9 amplifier (HEKA, Lambrecht, Germany) and postsynaptic recordings with an Axopatch 200B amplifier (Axon Instruments Inc., Foster City, CA). The pre- and postsynaptic series resistances (<15 M Ω) were compensated by 60% and 98% (lag 10 μ s), respectively. Both pre- and postsynaptic currents were low-pass filtered at 5 KHz and digitized at 20 KHz. mEPSCs were analyzed by a home-made program in Igor which automatically recognizes individual single mini events in the trace.

3.2.9 Neuromuscular junction recordings. Intracellular recordings from isolated whole diaphragm were made using an Axoclamp 2B amplifier in normal Ringer's solution (for Fig. 3-8A: 136.8 mM NaCl, 5 mM KCl, 1 mM MgCl₂, 1 mM NaH₂PO₄, 12 mM NaHCO₃, 11 mM D-glucose and 2 mM CaCl₂) or in HEPES buffer for the Ca²⁺ titrations (Fig. 3-8B: 140 mM NaCl, 5 mM KCl, 1mM MgCl₂, 10 mM HEPES, 10 mM glucose, pH 7.4) with a sharp electrode containing 3 M KCl. mEPPs were analyzed by mini analysis software (Synptosoftware Inc, NJ).

3.2.10 Neuronal cortical cultures. from E18 or P1 pups of WT or synaptotagmin-1-deficient mice were obtained and used for recordings as described (Maximov et al., 2007a; Maximov and Sudhof, 2005).

3.2.11 Statistical analysis. All data are presented as means \pm SEMs, and were analyzed using the two-tailed paired Student's *t*-test.

3.3 Results

3.3.1 An ataxic mouse harboring a point mutation in synaptotagmin-2.

Synaptotagmin-2^{I377N} mutant mice were identified in a screen of chemically mutagenized mice by Ingenium Pharmaceuticals, and shown by standard procedures (Russ et al., 2002; Stumm et al., 2002) to carry a single basepair substitution in exon 8 of the synaptotagmin-2 gene. This basepair change causes a non-conservative substitution (I377N) in the seventh β -strand of the C₂B-domain (Figs. 1A and 1B). Homozygous synaptotagmin-2^{I377N} mutant mice were viable but infertile, weighed less, and were severely uncoordinated (Figs. 1C-1E). On a force actometer (Fowler et al., 2001), wildtype (WT) mice walked along the edges of the plate, exploring all four sides with even, smooth movements. In contrast, synaptotagmin-2^{I377N} mutant mice stayed in a small sector of the force plate, and moved abruptly with sudden shifts of the head and tail, often appearing to shoot out of the perimeter of the force plate (Fig. 1E). Quantitation of the cumulative movements of mice on the force plate showed that the ataxia index was increased >2-fold in synaptotagmin-2^{I377N} mutant mice compared to littermate WT controls (Fig. 3-1F). Heterozygous mutant mice exhibited no change in weight (Fig. 3-1D)

or force-plate behavior (data not shown), indicating that the synaptotagmin-2^{I377N} mutation acts recessively.

As a first test of how the I377N-mutation might alter synaptotagmin-2 function, we measured the levels of synaptotagmin-2 and a series of control proteins in the forebrain, cerebellum, and spinal cord from littermate WT and synaptotagmin-2^{I377N} mutant mice (Fig. 3-1G). Consistent with earlier studies (Marqueze et al., 1995; Ullrich et al., 1994), synaptotagmin-2 was not detectable in forebrain, but abundant in caudal brain regions. In cerebellum and spinal cord from mutant mice, we observed a large decrease in synaptotagmin-2 (to 20-30% of WT levels) but an increase in synaptotagmin-1 (to 130-140% of WT levels; Fig. 3-1G). No other significant changes were found.

3.3.2 The synaptotagmin-2I377N mutant C2B-domain is unstable but functional.

To test the effect of the synaptotagmin-2^{I377N} substitution on the structural and functional properties of the C₂B-domain, we examined recombinant WT and I377N-mutant C₂B-domains biophysically. The circular dichroism (CD) spectra of WT and mutant C₂B-domains were indistinguishable, suggesting that the mutant domain folded correctly (Fig. 3-2A). Thermal denaturation curves in the absence or presence of 5 mM Ca²⁺ showed that the mutant C₂B-domain exhibited a sharp melting point that is shifted by Ca²⁺ to higher temperatures, consistent with Ca²⁺-binding to the properly folded mutant C₂B-domain (Fig. 3-2B). However, both in the absence and presence of Ca²⁺, the I377N-mutant C₂B-domain was denatured at lower temperatures than the WT C₂B-domain (Fig. 3-2C).

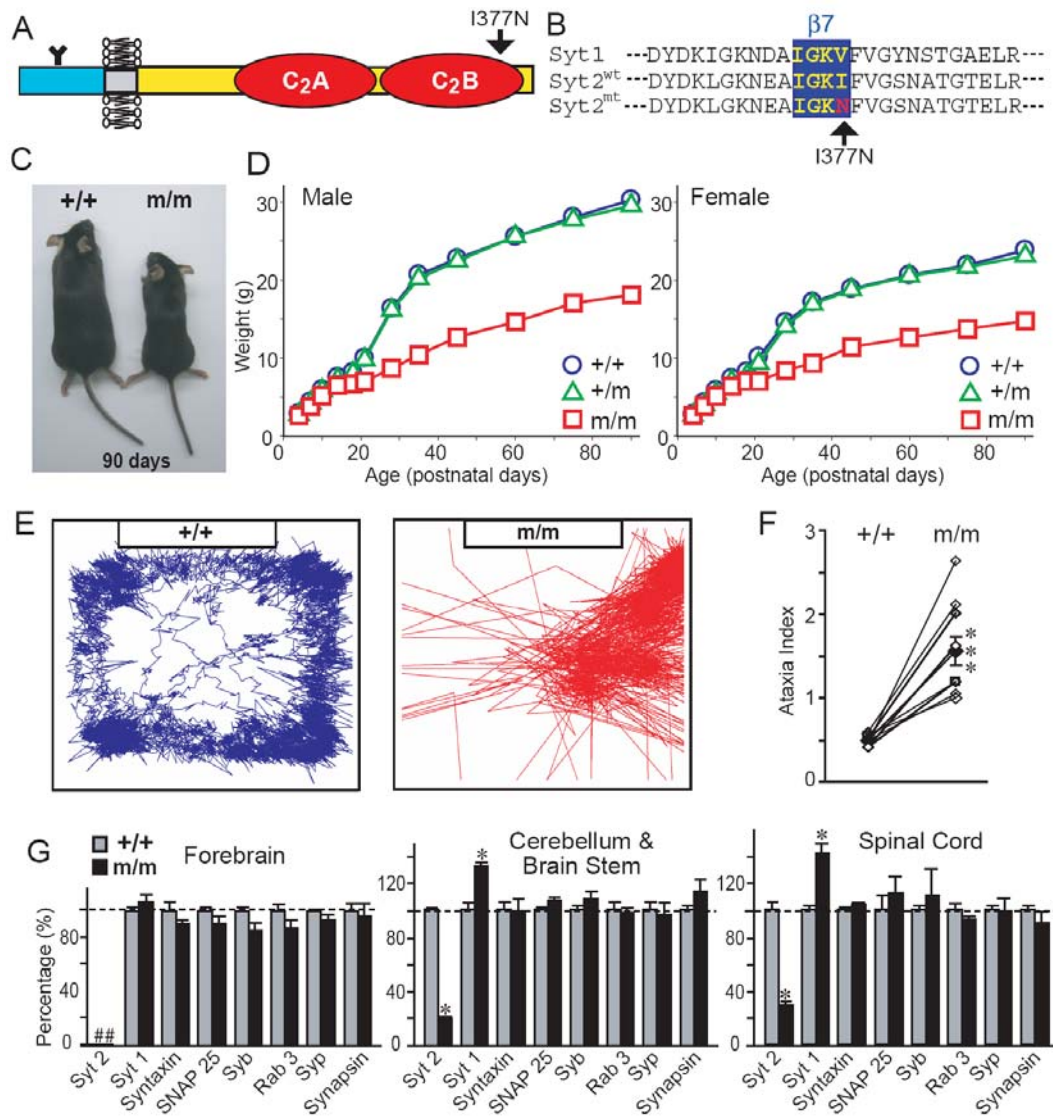


Figure 3-1 Characterization of synaptotagmin-2^{I377N} mutant mice.

A. Domain structure of synaptotagmin-2; arrow points to position of the I377N substitution. **B.** Sequence alignment of WT synaptotagmin-1 and 2 and mutant synaptotagmin-2^{I377N}. **C.** Pictures of littermate WT (+/+) and synaptotagmin-2^{I377N} homozygous mutant mice (m/m). **D.** Body weights of WT and hetero- and homozygous mutant male and female mice as a function of age (n=10-33). **E.** Representative traces of the movements of littermate WT and synaptotagmin-2^{I377N} mutant mice monitored on a force plate. **F.** Ataxia indices of eight independent pairs of littermate WT and synaptotagmin-2^{I377N} mutant mice calculated from force-plate traces (*** p<0.001). **G.** Protein levels in synaptotagmin-2^{I377N} mutant mice (m/m; black) expressed as percent of WT levels (+/+; gray). Protein levels were determined in three independent pairs of littermate WT and synaptotagmin-2^{I377N} mutant mice using quantitative immunoblotting with ¹²⁵I-labeled secondary antibodies and phosphorImager detection. Abbreviations used: Syt 1 and syt 2, synaptotagmin-1 and 2; Syb = synaptobrevin (*p<0.05). In these and all subsequent figures, data shown are means ± SEMs; statistical significance is assessed with the Student's t-test.

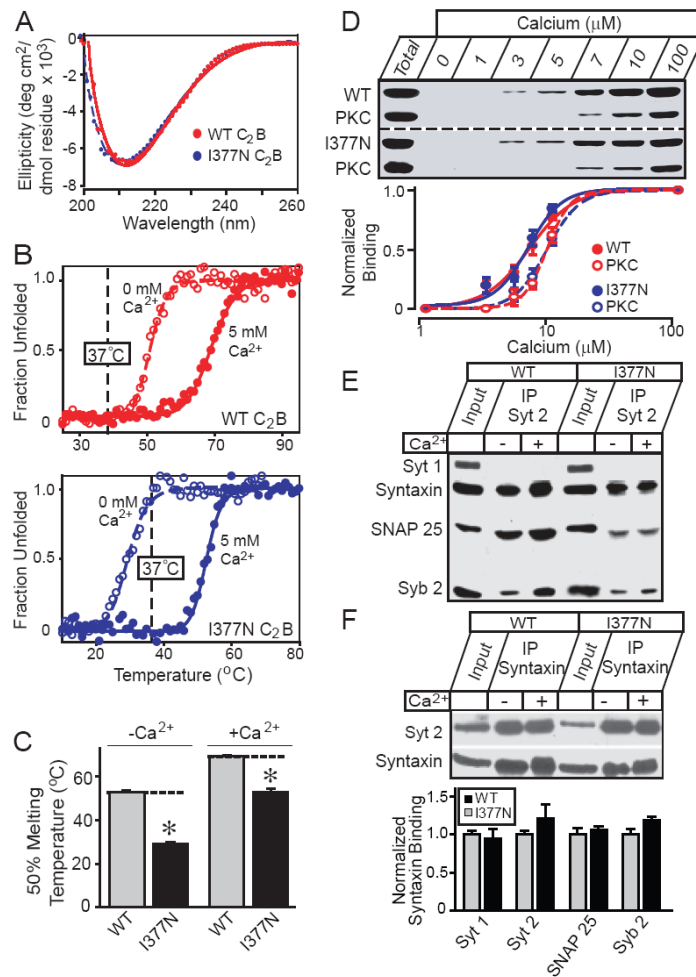


Figure 3- 2 Biochemical characterization of synaptotagmin-2^{I377N} mutant protein.

A and **B**. Circular dichroism spectra (**A**) and thermal denaturation curves (**B**) of WT and I377N-mutant synaptotagmin-2 C₂B domains. Denaturation was monitored by CD at 217 nm without or with 5 mM Ca²⁺. **C**. Mean 50% melting temperature of WT and I377N mutant C₂B-domain without or with 5 mM Ca²⁺ (* = p<0.05). **D**. Ca²⁺-dependent phospholipid binding by the double C₂AB-domain fragment from WT and I377N-mutant synaptotagmin-2 (tested as purified GST-fusion proteins). Liposomes (25% PS/75% PC) were incubated at the indicated free Ca²⁺-concentrations with the C₂AB-domain fragment of synaptotagmin-2 and the C₂-domain of PKCβ (as an internal control); bound C₂-domains were measured by SDS-PAGE and Coomassie staining. Upper panel shows a representative Coomassie stained gel; binding was quantified in multiple independent experiments by scanning of Coomassie-stained gels as shown in lower panel. **E**. and **F**. Binding of WT and I377N-mutant synaptotagmin-2 to SNARE complexes analyzed by immunoprecipitations. Synaptotagmin-2 (**E**) or syntaxin-1 (**F**) were immunoprecipitated from detergent-solubilized brain extracts from control and synaptotagmin-2^{I377N} mutant mice without or with Ca²⁺; co-precipitated proteins were examined by immunoblotting (Syt1 and 2 = synaptotagmins 1 and 2; Syb2 = synaptobrevin 2). In **F**, the amount of synaptotagmins 1 and 2, SNAP-25, and synaptobrevin 2 present in the syntaxin-1 immunoprecipitates in the absence of Ca²⁺ were quantified using ¹²⁵I-labeled secondary antibodies and phosphorImager detection.

We next investigated whether the I377N mutation alters phospholipid- or SNARE-binding by the C₂B-domain. We measured phospholipid binding with a centrifugation assay that monitors Ca²⁺-dependent binding of recombinant C₂-domains to liposomes (Fernandez et al., 2001), using the double C₂A/B-domain fragment instead of the single C₂B-domain because the properties of the normally occurring double C₂A/B-domain fragment differ from those of the single domains (Fernandez-Chacon et al., 2001). To ensure that we did not miss subtle shifts in apparent Ca²⁺-affinity, we included the PKC β C₂-domain as an internal standard (Fig. 3-2D). We found that the apparent Ca²⁺-affinities of WT and mutant C₂-domains were indistinguishable (WT C₂B: $EC_{50} = 7.0 \pm 0.1 \mu\text{M Ca}^{2+}$; I377N-mutant C₂B: $EC_{50} = 6.7 \pm 0.1 \mu\text{M Ca}^{2+}$), but higher than that of the PKC C₂-domain ($10.0 \pm 0.0 \mu\text{M Ca}^{2+}$ [n=5]).

We next examined binding of SNARE proteins to WT and mutant synaptotagmin-2 (Figs. 2E and 2F). We prepared homogenates of the cerebellum and brainstem from WT and synaptotagmin-2^{I377N} mutant mice under conditions favoring SNARE complex assembly, immunoprecipitated synaptotagmin-2 or syntaxin-1, and analyzed the immunoprecipitates by immunoblotting. We found that both WT and I377N-mutant synaptotagmin-2 co-immunoprecipitated with syntaxin-1, SNAP-25 and synaptobrevin-2 (Figs. 2E and 2F). The immunoprecipitations were specific because control antibodies were inactive, and control proteins were not co-immunoprecipitated (data not shown), and because synaptotagmin-1 was not brought down by the synaptotagmin-2 antibodies (Fig. 3-2E). To test whether SNARE proteins bind less well

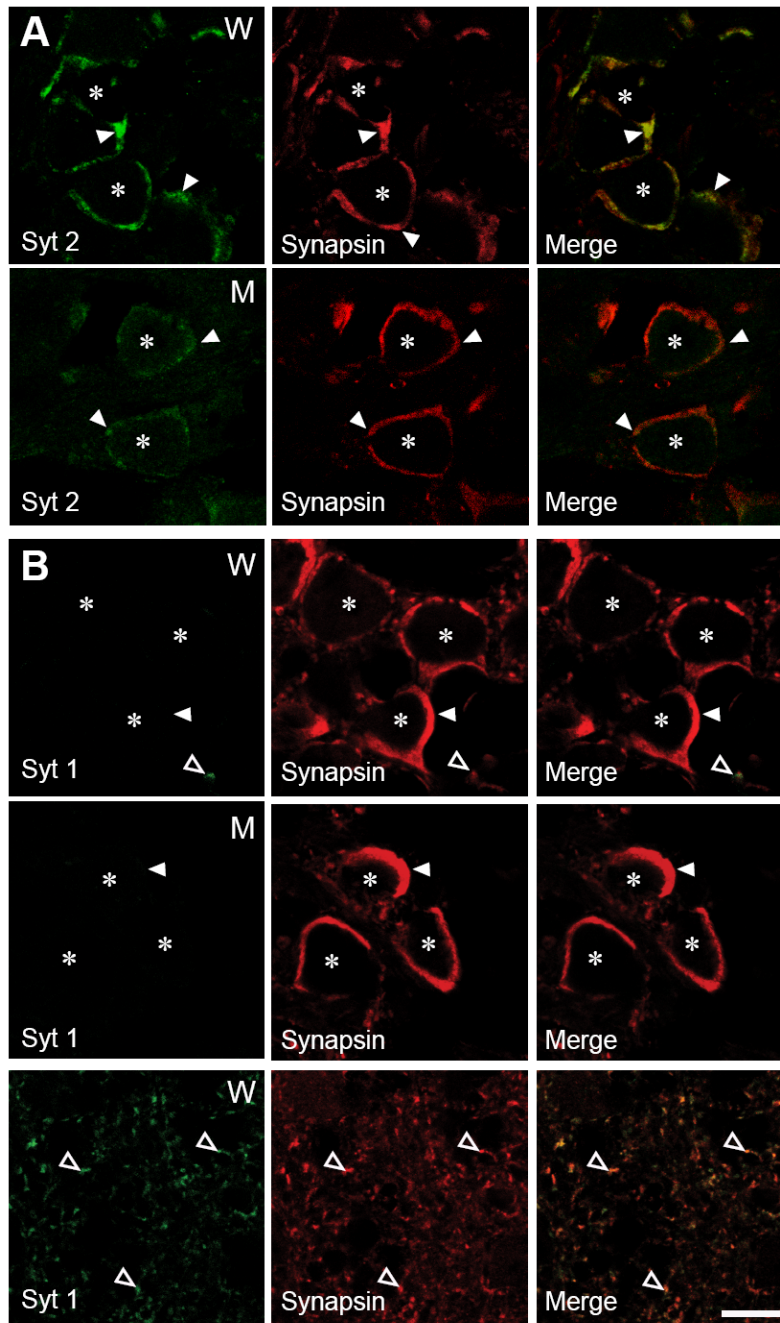


Figure 3- 3 Synaptotagmin-2 but not synaptotagmin-1 is present in Calyx terminals.

Panels show double immunofluorescence labeling experiments of brainstem sections from wildtype and synaptotagmin-2^{I377N} mutant mice with antibodies to synaptotagmin-2 (Syt 2) and synapsins (A) or to synaptotagmin-1 and synapsins (B). Note that although no synaptotagmin-1 can be detected in wildtype (W) or mutant Calyx terminals (M) in the ventral brainstem, synaptotagmin-1 is abundantly expressed in smaller terminals in the dorsal brainstem (bottom panels in B). Closed arrowheads identify Calyx presynaptic terminals; open arrowheads non-Calyx terminals; * = soma of postsynaptic MNTB neurons. Bar=10 μ m.

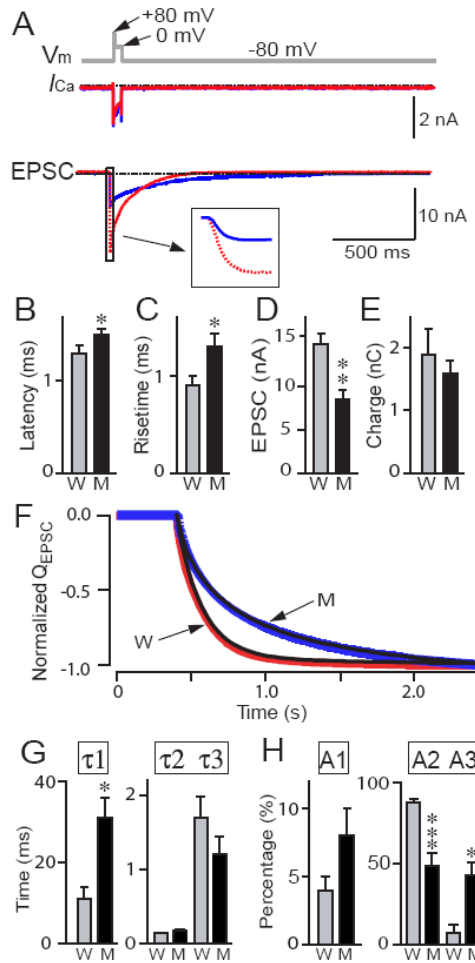
to mutant synaptotagmin-2, or whether binding of synaptotagmin-1 to SNARE proteins is upregulated in mutant synapses, we quantitated the amount of co-immunoprecipitated synaptotagmin-1 and 2 as well as co-immunoprecipitated SNAP-25 and synaptobrevin 2 in syntaxin 1 immunoprecipitates (Fig. 3-2F). However, we found that synaptotagmin-2 mutation did not impair binding of synaptotagmin-2 to immunoprecipitated SNARE complexes, nor did the mutation lead to a compensatory increase in synaptotagmin-1 binding to SNARE complexes. Viewed together, these experiments establish that the synaptotagmin-2^{I377N} mutation impairs the motor behavior of the mutant mice by destabilizing synaptotagmin-2 and depressing synaptotagmin-2 levels without altering the known functional properties of synaptotagmin-2.

3.3.3 Neurotransmitter release in WT and synaptotagmin-2I377N mutant neurons.

To measure whether neurotransmitter release is altered in the mutant mice, we examined synaptic transmission in the Calyx of Held synapse, using whole-cell recordings in the MNTB (medial nucleus of the trapezoid body) in acute brainstem slices. Immunofluorescence labeling showed that the Calyx terminals only contain synaptotagmin-2, but no detectable synaptotagmin-1 (Fig. 3-3). In synaptotagmin-2^{I377N} mutant Calyx synapses, staining for synaptotagmin-2 is significantly decreased (Fig. 3-3A) as expected from the decrease in synaptotagmin-2 protein levels in the mutant mice (Fig. 3-1), but no upregulation of synaptotagmin-1 was observed (Fig. 3-3B).

We first patched presynaptic Calyx terminals and postsynaptic MNTB neurons simultaneously to monitor both presynaptic Ca^{2+} -currents and postsynaptic EPSCs, and stimulated release with a presynaptic depletion protocol (Sakaba and Neher, 2001). According to this protocol, we depolarized the terminals from -80 mV to +80 mV for 4 ms, partly repolarized them to 0 mV for 50 ms, and then returned them to the holding potential of -80 mV (Fig. 3-4A). These experiments were performed with tetrodotoxin (1 μM), kynurenic acid (1 mM), cyclothiazide (0.1 mM), and D-AP-5 (50 μM) in the bath solution.

We found that synaptotagmin-2^{I377N} mutant synapses exhibited no major change in presynaptic Ca^{2+} currents (Fig. 3-4A), but that the EPSCs displayed a significantly longer latency, slower risetimes, and decreased EPSC amplitudes, consistent with a role for synaptotagmin-2 in Ca^{2+} -triggering of release (Figs. 4B-4D). The total charge transfer, when integrated over 2 sec, was not significantly different between WT and mutant synapses (Fig. 3-4E), whereas the kinetics of release was dramatically altered. Plotting the normalized charge transfer as a function of time and fitting it with a three-exponential function (Fig. 3-4F) revealed that the time constant for the first component of release was >2-fold longer for mutant than for WT synapses, while the time constants for the second and third components were unchanged (Fig. 3-4G). Moreover, the relative contributions of the three components to total release changed significantly: in WT synapses, the second component accounted for almost 90% of the total charge transfer; whereas in mutant synapses, the contribution of the second component was halved, but the contribution of the third component increased 5-fold (Fig. 3-4H).



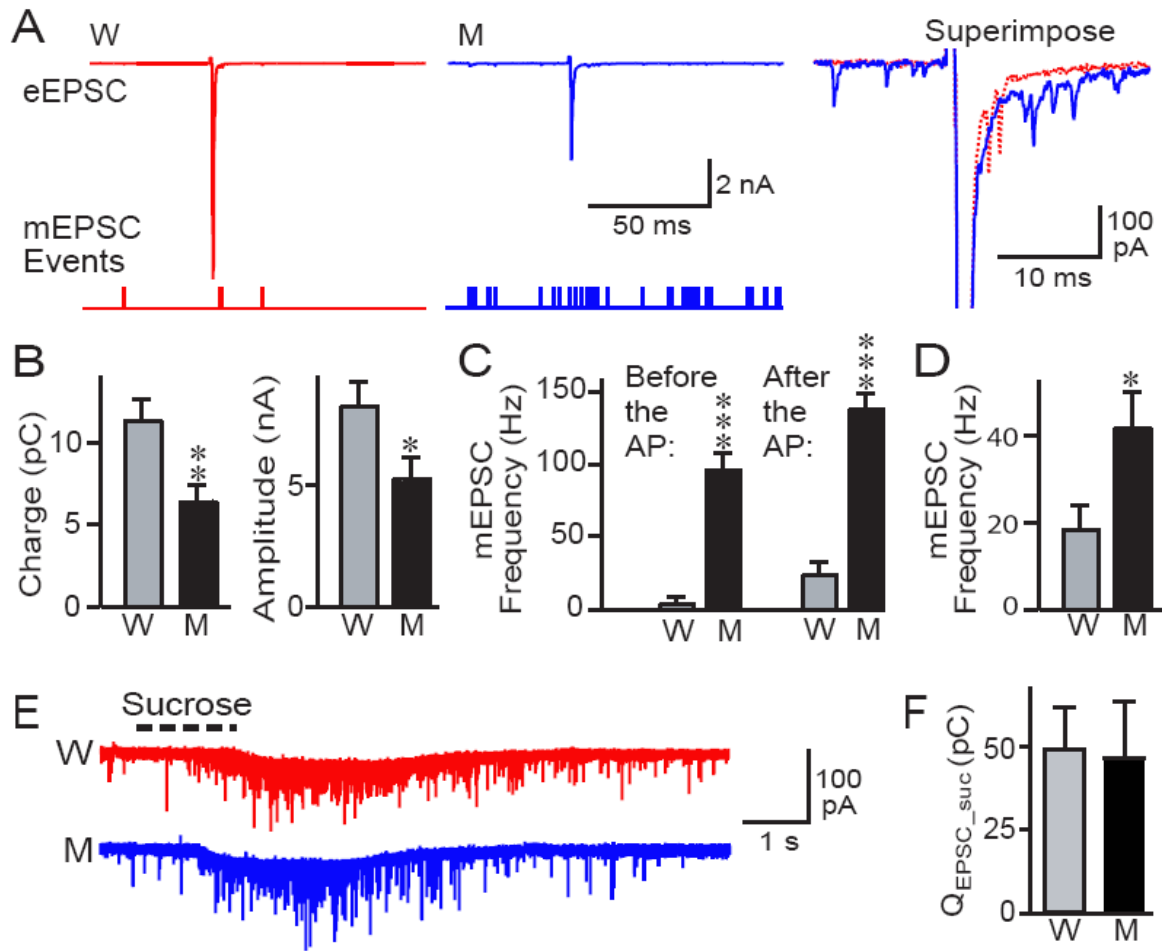
Jianyuan Sun

Figure 3- 4 Kinetics of release in Calyx synapses in response to a 50 ms presynaptic depolarization.

Simultaneous pre- and postsynaptic voltage-clamp recordings were obtained in brainstem slices from WT and synaptotagmin-2^{I377N} mutant mice at P7-P9 in the presence of 0.1 mM CTZ, 1 mM kynurenic acid, and 50 μ M D-AP5. **A.** Experimental protocol (top gray line) and representative traces of presynaptic Ca^{2+} -currents (I_{Ca}) and postsynaptic EPSCs in WT (W; red) and mutant mice (M; blue). In the bottom panels, representative WT and mutant I_{Ca} and EPSCs traces are superimposed; inset shows an enlargement of the initial phase of the EPSCs. **B.-E.** Quantitative comparison of EPSCs from WT and synaptotagmin-2^{I377N} mutant synapses: latencies from onset of the Ca^{2+} current to 10% of the EPSC (**B**), 20-80% rise times (**C**), amplitudes (**D**) and synaptic charge transfer integrated over 2 sec (**E**; W: n=12; M: n=14 for B-D; W: n=6; M: n=8 for E). **F.** Normalized integrals of EPSC charge transfer over 2 sec from littermate WT (W; red) and mutant mice (M; blue). The integration traces are fitted by three-exponential functions (black line, $r^2 > 0.9999$). **G.** and **H.** Time constants (**G**) and fraction (**H**) of each component from a three-exponential function fitting for each trace of the integral of EPSCs from WT (n=6) and synaptotagmin-2 mutants (n=8).

To examine release triggered by action potentials (APs), we induced APs by afferent fiber stimulation, and measured postsynaptic responses by whole-cell recordings. The amplitude and charge of the AP-induced EPSCs were significantly smaller in synaptotagmin-2^{I377N} mutant than in WT synapses (Figs. 5A and 5B). In addition, we unexpectedly found that the frequency of unitary release events was dramatically enhanced in synaptotagmin-2^{I377N} mutant synapses (Fig. 3-5C). In the following discussion, we refer to all unitary release events as ‘minis’, independent of whether they are recorded from resting synapses, or from synapses stimulated by APs. At rest, the mini frequency was potentiated almost 5-fold in mutant synapses (Fig. 3-5C). After an AP, the mini frequency was increased in both WT and mutant synapses, but the absolute increase was ~2-fold higher in mutant than in WT synapses (Fig. 3-5D). The augmentation in mini frequency in synaptotagmin-2^{I377N} mutant synapses, however, was insufficient to compensate for their decrease in synchronous release, because the total charge of the AP-induced EPSC (the sum of synchronous and spontaneous release) when integrated over 100 ms was significantly reduced in synaptotagmin-2^{I377N} mutant synapses (Fig. 3-5B; please note that this result refers to an AP-induced EPSC as opposed to the presynaptic depletion protocol applied in Fig. 3-4E).

The decrease in evoked release and the increase in spontaneous release could reflect abnormal synaptic vesicle priming that establishes the readily-releasable pool of vesicles (RRP). One operational definition of the RRP is the amount of release triggered by application of hypertonic sucrose which provokes Ca²⁺-independent release of vesicles (Rosenmund and Stevens, 1996). To measure the RRP, we puffed 2 M sucrose onto



Jianyuan Sun

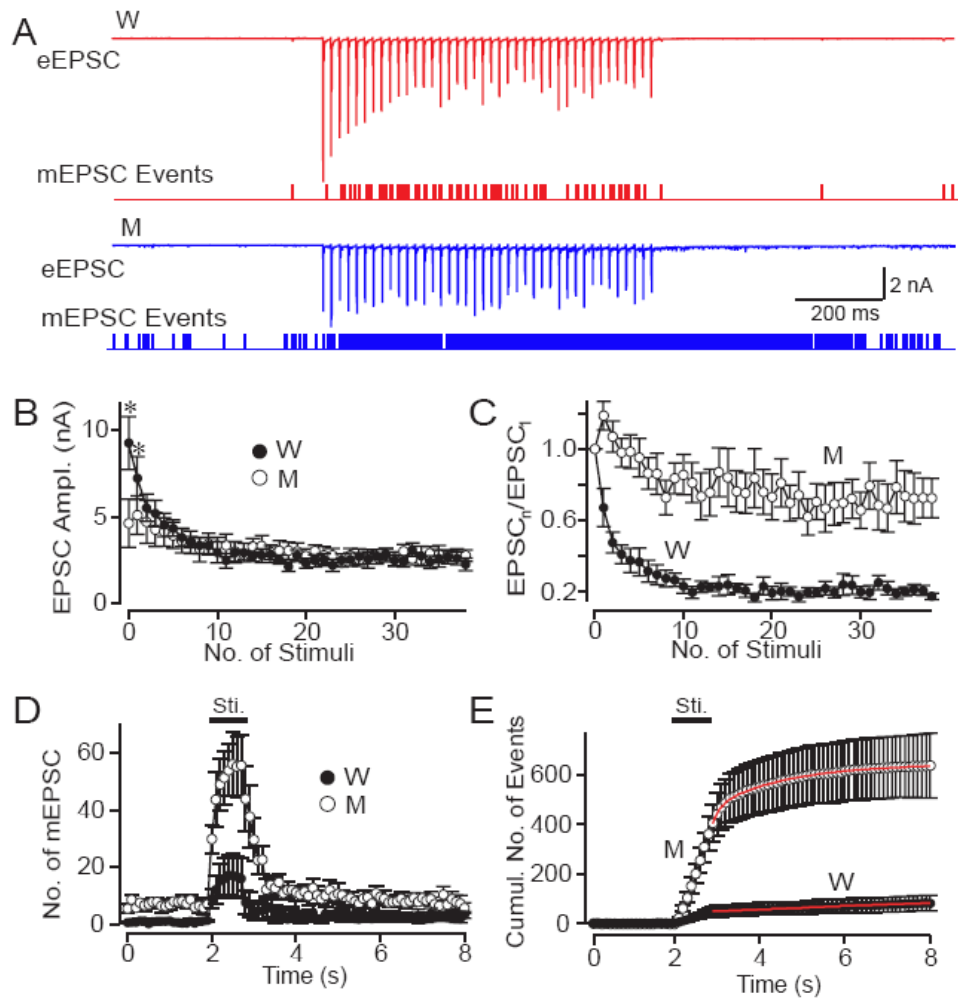
Figure 3- 5 Release evoked by single APs or hypertonic sucrose in Calyx synapses at postnatal day P14.

A. Representative EPSC traces monitored in the presence of bicuculline (10 μ M), strychnine (10 μ M) and D-AP-5 (50 μ M) in response to isolated APs evoked by fiber stimulation (WT = W; red; synaptotagmin-2^{I377N} mutants = M; blue); traces are scaled and superimposed on the right. Below the traces, mEPSC events are indicated as notches. **B.** Mean electrical charge transfer (integrated over 100 ms) and amplitude of evoked EPSCs. **C.** Frequency of mEPSCs in the 100 ms periods before and after stimulation. **D.** Absolute increases in mEPSCs frequency in 100 ms after stimulation (W: n=12; M: n=9). **E.** Representative recordings of mEPSCs induced by a 1s puff of hypertonic sucrose (a glass pipette containing 2 M sucrose positioned \sim 5 μ m from the Calyx, and puffed the sucrose solution onto the terminal using a 1 sec pressure pulse as indicated by the dashed line above the traces) from WT (W; red) and mutant (M; blue). **F.** Average charge transfer during hypertonic sucrose-induced mEPSCs from WT (n=4) and mutant (n=4) integrated over 5 s (* p<0.05; **p<0.01; ***p<0.001).

the terminal for 1 sec using a glass pipette that was positioned close to the Calyx (<5 μm). Hypertonic sucrose induced a train of mEPSCs; integration of the charge transfer revealed that the WT and synaptotagmin-2^{I377N} mutant synapses produced similar amounts of sucrose-induced release (Fig. 3-5E and 5F).

3.3.4 Release evoked by AP stimulus trains.

We next monitored synaptic responses induced by 40 APs applied at 50 Hz, a physiological stimulation frequency for this synapse (Sommer et al., 1993). In WT synapses, the EPSC amplitudes initially depressed during the stimulus train to stabilize at a steady-state level, but the EPSC timecourse remained completely synchronous (Fig. 3-6A). Although the initial EPSCs were decreased in synaptotagmin-2^{I377N} mutant synapses, no use-dependent depression was observed, and EPSCs stabilized after ~5 APs in mutant synapses at the same average amplitude as in WT synapses (Fig. 3-6B). When plotted as normalized data, this behavior manifests as moderate facilitation (Fig. 3-6C). Thus the increase in residual Ca^{2+} that presumably accumulates during the high-frequency train 'rescues' the decrease in synchronous release in synaptotagmin-2^{I377N} mutant synapses; as a result, the mutant synapses exhibit the same amount of neurotransmitter release as WT synapses after ~5 APs (Fig. 3-6B).



Jianyuan Sun

Figure 3- 6 EPSCs evoked by a 50 Hz AP train.

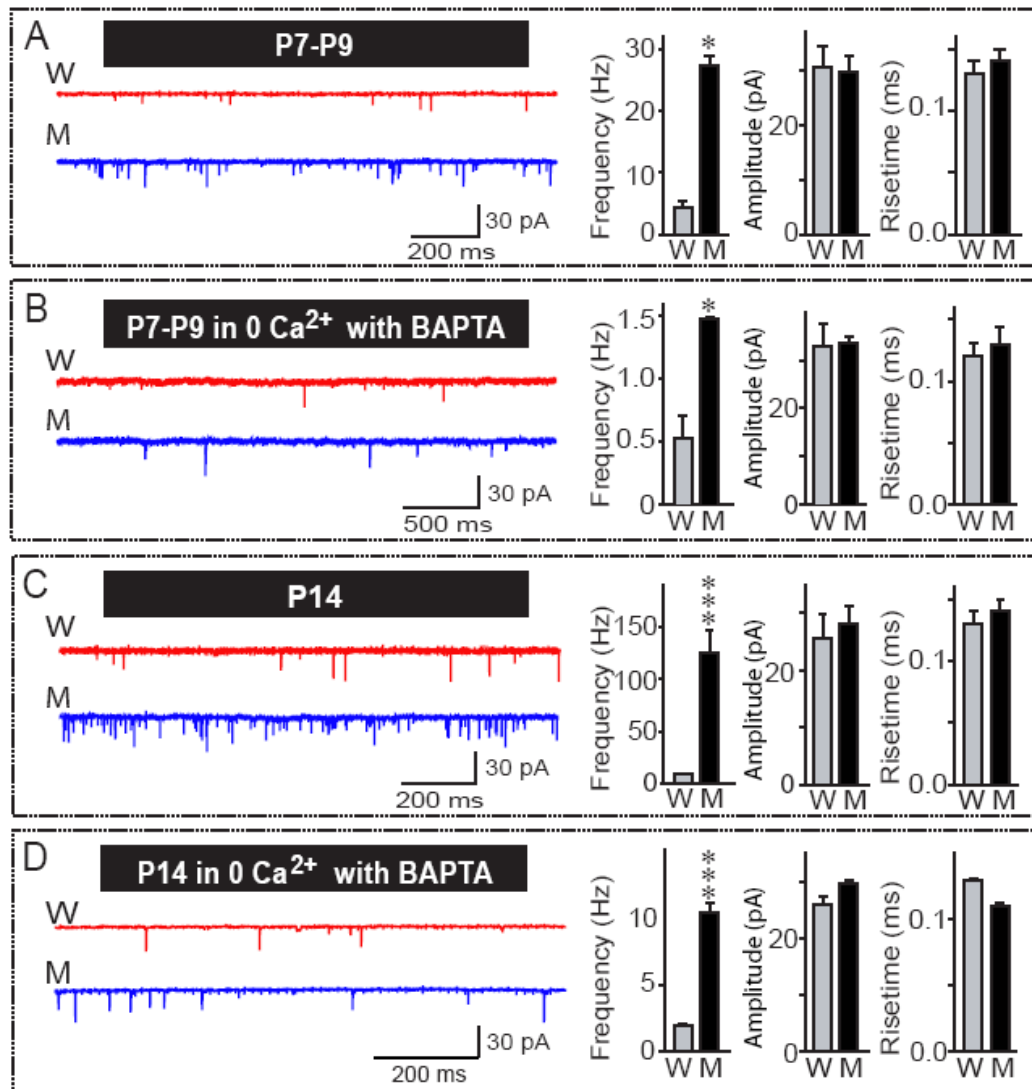
A. Representative traces of EPSCs evoked by 40 APs at 50 Hz (WT, red; synaptotagmin-2^{I377N} mutant, blue). Below the traces, mini events are indicated as notches. **B.** and **C.** Absolute (**B**) and normalized (**C**) EPSC amplitudes of 40 stimuli at 50 Hz. **D.** and **E.** Mini event frequency before, during, and after the 50 Hz stimulus train plotted as a function of time as the number of events per 0.1 sec interval (**D**) or as the cumulative number of events after normalization for basal mini release (**E**; see text for detail). The time of stimulation is indicated by the horizontal bar above the plot (WT, W: n=6, filled symbols; synaptotagmin-2^{I377N} mutant, M: n=5, open symbols).

As observed in response to a single AP, synaptotagmin-2^{I377N} mutant synapses exhibited a massive stimulation-dependent increase in mini frequency during AP trains

(Fig. 3-6D). We plotted the cumulative number of minis as a function of time during the stimulus train, and corrected for the increase in mini frequency in mutant synapses by adjusting the slope of cumulative mini events before stimulation to zero (Fig. 3-6E). The corrected plot thus represents the accumulated mini release during and after the stimulus train. According to the slope of the accumulative mini release, the average rate of mini release during stimulation (indicated by the horizontal bar in Figs. 6D and 6E) was estimated as 0.45 vesicle/ms for synaptotagmin-2 mutant synapses and 0.06 vesicle/ms for WT synapses. In synaptotagmin-2 mutant synapses, the latter part of the trace (after 2.8 s) could be fitted with a double exponential function [$\tau_1=0.21$ s (37%), $\tau_2=1.79$ s (63%); Fig. 3-6E]. In contrast, the WT trace could only be fitted by a single exponential function with a long time constant (33 s), implying the negligible amount of mini release after stimulation.

3.3.5 Spontaneous neurotransmitter release in WT and synaptotagmin-2^{I377N} mutant neurons.

To test whether the increase in mini frequency in synaptotagmin-2^{I377N} mutant synapses reflects an intrinsic alteration of the release machinery, or is due to residual bulk Ca^{2+} remaining after an AP, we systematically examined spontaneous minis in MNTB neurons at rest, both from P7-P9 and from P14 mice, and both in the presence or absence of Ca^{2+} (Fig. 3-7). We found that at P7-P9 and at P14, the resting mini frequency was dramatically increased in synaptotagmin-2^{I377N} mutant synapses (>6 times at P7-P9; >12



Jianyuan Sun

Figure 3- 7 Spontaneous neurotransmitter release in WT and synaptotagmin-2^{I377N} mutant neurons (mEPSCs).

In all panels, representative traces are shown on the left, and summary diagrams for the mini frequency, amplitude, and risetimes (20%-80% for the calyx; 10%-90% for NMJ) on the right. **A.** and **B.** Recordings from the calyx at P7-9 in regular extracellular medium (**A**; W: n=7; M: n=8) or medium containing 0 mM Ca²⁺ and 0.1 mM BAPTA/AM (**B**; W and M: n=6 for both). **C.** and **D.** Recordings from the calyx at P14 in regular extracellular medium (**C**; W: n=8; M: n=9) or medium containing 0 mM Ca²⁺ and 0.1 mM BAPTA/AM (**D**; W and M: n=9 and 6, respectively)(*p<0.05; ***p<0.001).

times at P14), whereas the mini amplitudes and rise times were unchanged (Fig. 3-7). Removal of Ca^{2+} by application of 0.1 mM BAPTA-AM in a Ca^{2+} -free bath solution had no effect on the amplitudes and risetimes of minis, but reduced the frequency of minis in both WT and mutant synapses ~ 10 fold (Fig. 3-7B and 7D). Even under Ca^{2+} -free condition, synaptotagmin-2^{I377N} mutant synapses exhibited an increased mini frequency (~ 3 times at P7-P9; ~ 5 times at P14). Quantitatively, Ca^{2+} removal caused a relatively larger decrease in mini frequency in mutant synapses (~ 18 fold at P7-P9, ~ 12 -fold at P14) than in WT synapses (~ 5 -fold at both P7-P9 and at P14), indicating that although the mini frequency in mutant synapses is enhanced in the absence of Ca^{2+} , it is increased more strongly than in WT synapses by the low levels of Ca^{2+} present in resting synapses.

To ensure that the changes observed are not specific to the Calyx synapse, we additionally monitored minis as miniature endplate potentials (mEPPs) in neuromuscular junctions (NMJs) of diaphragm muscle in WT and synaptotagmin-2^{I377N} mutant mice at P16. Again, we detected a massive increase in mini frequency in mutant synapses (Fig. 3-8A), but no changes of mini amplitudes and risetimes. Next, to confirm the generality of the observed effect of Ca^{2+} on spontaneous release in the calyx (Fig. 3-7), we tested the effect of Ca^{2+} on mini frequency in NMJs by recording mEPPs either in Ca^{2+} -free external solution with BAPTA-AM (to ensure that the conditions are totally Ca^{2+} -free), or in external solutions containing 2, 5, or 10 mM Ca^{2+} (Fig. 3-8C). These recordings were performed at P22 when NMJ development is more mature. As in the Calyx synapse, significant spontaneous release was observed even in the total absence of Ca^{2+} , but was dramatically enhanced with increasing concentrations of Ca^{2+} . At all Ca^{2+} -concentrations

examined – both in the complete absence of Ca^{2+} and in the presence of high extracellular Ca^{2+} concentrations - the frequency of mEPPs was several fold higher in mutant NMJs than in NMJs from littermate control mice (Fig. 3-8D).

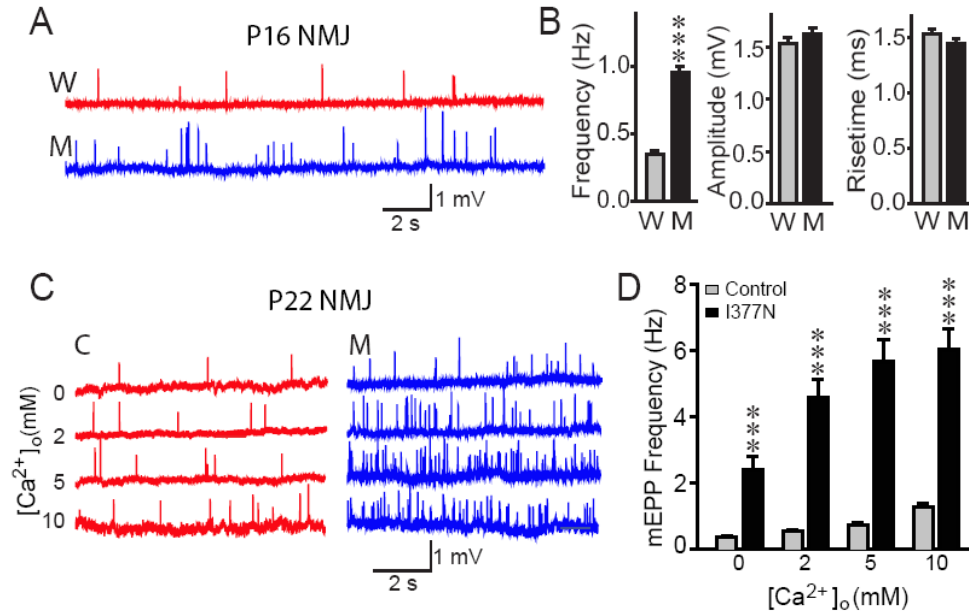


Figure 3- 8 Spontaneous neurotransmitter release at the NMJ.

A. and **B.** Representative traces of mEPPs (**A**) and summary diagrams of mEPP frequency, amplitude, and risetimes (**B**) in diaphragm NMJs from wildtype (W) and synaptotagmin-2^{I377N} mutant mice at P16, recorded in normal *Ringer's* solution (W: n=57, 3 mice; M: n=68, 3 mice). **C.** and **D.** Representative traces of mEPPs (**C**) and summary diagrams of the mEPP frequencies (**D**) recorded at the indicated Ca^{2+} -concentrations in NMJs from control (C) and synaptotagmin-2^{I377N} mutant mice (M) at P22. Note that the 0 Ca^{2+} condition included BAPTA-AM to remove nerve terminal Ca^{2+} . (n=25~30, two animals each genotype)(***p<0.001 in B and D).

3.3.6 Deletion of synaptotagmin-1 also increases mini-frequency.

The properties we describe here for synaptotagmin-2^{I377N} mutant synapses resemble those of the synaptotagmin-1-deficient synapses in mice with one exception: no increase in mini frequency was detected in autapses from such mice(Geppert et al., 1994; Nishiki and Augustine, 2004), although recent analyses of cortical inhibitory synapses

from synaptotagmin-1-deficient mice suggested that such an increase may in fact occur (Maximov and Sudhof, 2005). To examine this question, we measured the mini frequency in synapses formed by cultured cortical neurons from synaptotagmin-1-deficient mice. We monitored both excitatory and inhibitory synapses, and examined the effects of either lowering or raising the Ca^{2+} -concentration (Figs. 9A-9D). In resting excitatory and inhibitory synapses, deletion of synaptotagmin-1 enhanced the mini frequency ~5-fold. Decreasing Ca^{2+} in the bath depressed, whereas increasing Ca^{2+} augmented the mini-frequency both in WT and mutant synapses; however, under both conditions the large difference between the mutant and WT synapses was retained (Fig. 3-9D). Addition of EGTA-AM to remove intracellular Ca^{2+} had little further effect on mini frequency in WT and mutant synapses. Thus, synaptotagmin-1-deficient cortical synapses behave very similar to synaptotagmin-2^{I377N} mutant synapses in that an intrinsic difference in mini-frequency is present. In synaptotagmin-1-deficient synapses, this difference is not a compensatory change in response to the decrease in release because it persisted even after prolonged treatment of the cultures with TTX which should abolish all network activity in WT and mutant synapses (Fig. 3-9D).

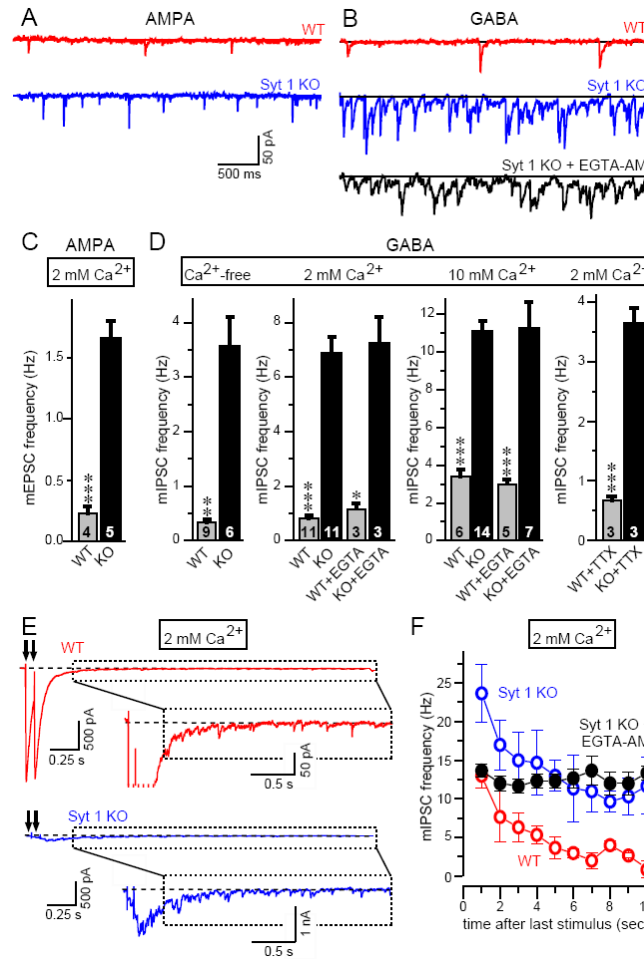
We next applied two closely spaced APs to examine whether stimulation of release increases mini frequency in synaptotagmin-1-deficient neurons. We found that after the APs, the mini frequency was enhanced in both WT and mutant synapses, again with mutant synapses exhibiting a higher frequency (Figs. 3-9E and -9F). The stimulation-dependent increase in mini frequency in mutant synapses was abolished by

EGTA-AM, demonstrating that it is due to the increase in intracellular Ca^{2+} produced by the APs (Fig. 3-9F).

3.4 Discussion

Using mutant mice that carry a single amino acid substitution (I377N) in synaptotagmin-2, we demonstrate that synaptotagmin-2 is an essential component of the Ca^{2+} -triggering machinery for release in the Calyx of Held synapse. Moreover, we show that impairment of synaptotagmin-2 enhances the rate of spontaneous synaptic vesicle exocytosis, as does deletion of synaptotagmin-1. Our study demonstrates that the normal function of synaptotagmin-2 is analogous to that of synaptotagmin-1, although performed in different neurons, thereby extending the synaptotagmin-1 paradigm to synaptotagmin-2. In addition, our data reveal that synaptotagmin-1 and 2 generally limit spontaneous release at a synapse. These results show that synaptotagmin-1 and 2, as integral components of the release machinery, control initiation of fusion pore opening of synaptic vesicles at the active zone.

Effect of the I377N substitution on synaptotagmin-2. Three observations show that the I377N-mutation does not change known functional properties of synaptotagmin-2, but destabilizes synaptotagmin-2 in brain. First, the I377N-mutant C₂B-domain was normally folded (Fig. 3-2A) but exhibited decreased thermal stability (Figs. 3-2B and 2C). Second, mutant synaptotagmin-2^{I377N} exhibited apparently normal Ca^{2+} -dependent phospholipid binding and Ca^{2+} -dependent and Ca^{2+} -independent SNARE



Anton Maximov

Figure 3- 9 Spontaneous release in synaptotagmin-1-deficient cortical neurons.

A. and **B.** Representative spontaneous mEPSCs (**A**) and mIPSCs (**B**) recorded in the presence of acutely added TTX (1 μ M) from WT (red) and synaptotagmin-1-deficient neurons (blue). In **B**, mIPSCs were also recorded from synaptotagmin-1-deficient neurons preincubated for 5 min in 0.1 mM EGTA-AM (black; holding potential = -70 mV; scale bars apply to all traces). **C.** and **D.** Average mEPSC (**C**) and mIPSC (**D**) frequencies in WT and synaptotagmin-1-deficient neurons. Extracellular Ca^{2+} concentrations are indicated on the top; number of cells analysed are shown in the bars. The 2 and 10 mM Ca^{2+} experiments were also carried out after a 5 min preincubation of neurons in 0.1 mM EGTA-AM. The 2 mM Ca^{2+} data on the right were obtained in neurons that were incubated with 1 μ M TTX for 4 days prior to the recordings. **E.** Representative IPSCs evoked by two closely spaced (0.1 s interval) APs in the presence of AP5 and CNQX. Insets illustrate individual mini events observed at the ends of evoked responses. **F.** Plot of the average mIPSC frequency in WT and synaptotagmin-1-deficient neurons after the neurons were stimulated by two APs separated by 0.1 s. Frequencies were calculated in 1 s bins starting 0.5 s after the second AP in train. Data are from three different WT, synaptotagmin-1-deficient neurons and synaptotagmin-1-deficient neurons preincubated with 0.1 mM EGTA-AM (* p <0.05; ** p <0.01; *** p <0.001).

binding (Figs. 3-2D-2F). Finally, the levels of mutant synaptotagmin-2^{I377N} were selectively decreased ~5-fold in the brainstem and spinal cord of the mutant mice (Fig. 3-1G). Hence, the phenotypes observed in the I377N-mutant mice likely arise from a reduction in the amount of synaptotagmin-2 protein.

Synaptotagmin-2 functions in the fast Ca²⁺-triggering of neurotransmitter release. In Calyx synapses, the synaptotagmin-2^{I377N} mutation slowed the time course of release and decreased the EPSC amplitude (Figs. 3-4 and 3-5). Both the latency and risetime of EPSCs were increased (Figs. 3-4B and 3-4C). The size of the RRP, as defined by the amount of release that can be triggered with hypertonic sucrose, was unchanged (Figs. 3-5E and -5F). Overall, this phenotype resembles that of the synaptotagmin-1 deletion in hippocampal (Geppert et al., 1994) and cortical synapses (Maximov and Sudhof, 2005), suggesting that synaptotagmin-1 and 2 perform analogous functions, although in different synapses.

The I377N mutation impairs release in the Calyx synapse less severely than the synaptotagmin-1 deletion in hippocampal or cortical synapses (Geppert et al., 1994; Maximov and Sudhof, 2005). This difference is most likely due to the fact that the I377N mutation does not delete synaptotagmin-2, but only decreases its levels (Fig. 3-1). Thus residual synaptotagmin-2 may mediate the remaining Ca²⁺-triggered fast release.

Synaptotagmin function in asynchronous release. Synaptotagmin-1-deficient synapses exhibit no significant change in asynchronous release in response to single APs, but display a selective increase in asynchronous delayed release triggered by trains of

action potentials (Maximov and Sudhof, 2005). The delay in the EPSC time course after a 50 ms depolarization in synaptotagmin-2^{I377N} mutant synapses suggests that a similar increase in asynchronous delayed release may be present in the synaptotagmin-2 mutant (Fig. 3-4H). Alternative explanations for this delay are that it is caused by a change in the properties of postsynaptic receptors, such that the receptors remain active longer, or by a decrease in the clearance of glutamate from the synaptic cleft, such that 'lingering' glutamate continues to activate receptors. The fact that the shape of spontaneous minis and of EPSCs triggered by isolated APs is not altered in synaptotagmin-2^{I377N} mutant neurons makes the two alternative explanations implausible. Moreover, it is difficult to imagine a postsynaptic mechanism for synaptotagmin-2 because synaptotagmin-2 is highly enriched in presynaptic vesicles. This indicates that, as previously demonstrated for synaptotagmin-1 mutants (Maximov and Sudhof, 2005), the synaptotagmin-2 mutants may exhibit an increase in delayed release.

Synaptotagmin-1 and 2 function in spontaneous 'mini' release. In synaptotagmin-2^{I377N} mutant mice, Calyx and NMJ synapses exhibited large increases in mini frequency at rest, after removal of Ca²⁺, and after stimulation by AP's (Figs. 3-5 to 3-8). Thus the synaptotagmin-2 mutation increases both spontaneous Ca²⁺-independent fusion and fusion induced by residual Ca²⁺ after an AP. The increase in spontaneous fusion is not a peculiar effect of the I377N mutation but reflects a general participation of synaptotagmins in spontaneous exocytosis because we observed a comparable increase in mini-frequency in both excitatory and inhibitory synapses in cortical neurons from synaptotagmin-1-deficient mice (Fig. 3-9). This increase again was Ca²⁺-independent,

and was not due to a homeostatic effect because the difference was retained after chronic treatment with TTX. Furthermore, in synaptotagmin-1-deficient cortical neurons, minis were also increased after AP stimulation (Figs. 3-9E and 9F).

Previous studies obtained conflicting data on minis in synaptotagmin mutants. In autapses formed by cultured hippocampal neurons, deletion of synaptotagmin-1 consistently does not increase spontaneous release (e.g., see (Geppert et al., 1994; Nishiki and Augustine, 2004; Shin et al., 2003)). However, in the neuromuscular junction of *Drosophila*, deletion of synaptotagmin-1 increased mini frequency at least under certain conditions (Broadie et al., 1994; DiAntonio and Schwarz, 1994; Littleton et al., 1993b) (see discussion in the Introduction), and overexpression of synaptotagmin-1 or 2 in frog neuromuscular junctions inhibited spontaneous release (Morimoto et al., 1998). We observed an increase in mini-frequency for mutations in two different synaptotagmins (synaptotagmin-1 and 2) and four different synapses (the Calyx of Held synapse, the NMJ, and excitatory and inhibitory cortical synapses), suggesting that the lack of this phenotype in autapses is peculiar to that system, and that synaptotagmin-1 and 2 mutations truly alter spontaneous fusion. Moreover, in cultured neurons this phenotype was not abolished by activity blockade (Fig. 3-9D), demonstrating that the mini-frequency increase is not a secondary phenomenon of decreased synaptic activity.

Implications for the mechanism of Ca^{2+} -triggering of fast release by synaptotagmin-1 and 2. Together with earlier data, our results demonstrate that synaptotagmin-1 and 2 are not passive inhibitors of fusion that block a constitutive fusion reaction because the total amount of Ca^{2+} -dependent fusion is dramatically decreased in

the absence of synaptotagmins. Conversely, synaptotagmin-1 and 2 do not simply act separately from the fusion machinery but are intrinsic components of this machinery because in their absence, spontaneous fusion, even under totally Ca^{2+} -free conditions, is enhanced. Previous observations showed that synaptotagmin-1 is unlikely to be a component of the fusion pore (Sorensen et al., 2003). Consistent with these observations, we thus propose that synaptotagmin-1 and 2 bind to assembled SNARE complexes during priming (Rickman et al., 2004; Shin et al., 2003) to achieve two effects: First, to inhibit spontaneous fusion and evoked fusion triggered by low Ca^{2+} -concentrations that are unable to activate synaptotagmin-1 and 2. Second, to position synaptotagmin-1 and 2 close to where the fusion pore will form, presumably by SNARE proteins. This model suggests Ca^{2+} flowing into the terminal during an action potential triggers fusion pore opening by binding to the synaptotagmin C₂-domains, which in turn causes these C₂-domains to bind to the phospholipid membrane, thereby inducing a mechanical stress on the membrane that is instrumental in catalysing fusion pore opening.

Although this hypothesis accounts for all currently available data, it raises questions that need to be addressed before it can be considered plausible. A key question relates to SNARE binding: if Ca^{2+} -independent binding of SNAREs by synaptotagmin-1 and 2 is crucial, why do synaptotagmins additionally bind to SNAREs in a Ca^{2+} -dependent manner? Another question regards the role of complexins that bind to SNARE complexes and are essential for normal Ca^{2+} -triggering of release, but whose action is obscure (McMahon et al., 1995; Reim et al., 2001). A third question concerns the nature of asynchronous release during and after action potentials. Clearly, additional Ca^{2+} -

sensors must exist, but do these trigger release analogous to, but slower than synaptotagmin-1 and 2, or do these Ca^{2+} -sensors simply act indirectly by accelerating reactions upstream of the final fusion step? Future experiments using additional tools that need to be developed will have to address these issues.

CHAPTER IV: SYNAPTOTAGMIN-2 IS ESSENTIAL FOR SURVIVAL AND CONTRIBUTES TO Ca^{2+} -TRIGGERING OF NEUROTRANSMITTER RELEASE IN CENTRAL AND NEUROMUSCULAR SYNAPSES

4.1. Introductions

Neurotransmitter release from presynaptic nerve terminals is triggered when an action potential gates Ca^{2+} influx into the terminal, and Ca^{2+} induces exocytosis of synaptic vesicles (Katz and Miledi, 1967b). Neurotransmitter release occurs in two modes: fast synchronous release that is induced by brief transients of high Ca^{2+} -concentrations, and slow asynchronous release that is induced at a slower rate by lower Ca^{2+} -concentrations (Atluri and Regehr, 1998; Barrett and Stevens, 1972; Cummings et al., 1996; Hagler and Goda, 2001; Lu and Trussell, 2000; Otsu et al., 2004). In forebrain, synaptotagmin-1 functions as the Ca^{2+} -sensor for fast synchronous release (Fernandez-Chacon et al., 2001; Geppert et al., 1994). Synaptotagmin-1 belongs to a large family of proteins (15 members in mouse) that contain similar domain structures, with an N-terminal transmembrane region, a linker sequence, and two C-terminal C_2 domains that bind Ca^{2+} in most but not all synaptotagmins (Sudhof, 2002). Among synaptotagmins, synaptotagmin-2 shares the highest homology with synaptotagmin-1, has similar biochemical characteristics, and can functionally replace synaptotagmin-1 in neurons and chromaffin cells that lack synaptotagmin-1 (Nagy et al., 2006; Stevens and Sullivan, 2003). These experiments suggested that synaptotagmin-1 and -2 have similar functions. However, synaptotagmin-1 and -2 are not entirely functionally redundant because synaptotagmin-1 knockout (KO) mice express normal levels of synaptotagmin-2 but

nevertheless exhibit a severe phenotype that in hippocampal and cortical neurons manifests as a loss of fast synchronous release and perinatal lethality (Geppert et al., 1994; Maximov and Sudhof, 2005; Nishiki and Augustine, 2004). A possible explanation for this finding is based on the differential expression of synaptotagmin-1 and -2, with the former being present primarily in forebrain and the latter in caudal brain regions (Geppert et al., 1994; Marqueze et al., 1995; Ullrich et al., 1994). These expression patterns suggested that synaptotagmin-1 and -2 may have similar functions in different types of neurons, thereby making each essential in the type of neuron in which they are expressed.

Recent studies on a mutant mouse carrying a point mutation in synaptotagmin-2 confirmed the importance of synaptotagmin-2 in neurotransmitter release in brainstem synapses and in NMJs (Pang et al., 2006b). However, in these mice, the mutant synaptotagmin-2 was functional, and the mice survived, raising the question whether synaptotagmin-2 normally functions as an essential Ca^{2+} -sensor similar to synaptotagmin-1, or performs a more ancillary, possibly regulatory role. To address this question, we have generated and analyzed synaptotagmin-2 KO mice that also allowed us to characterize synaptotagmin-2 expression by means of a knocked-in lacZ sequence. We find that synaptotagmin-2 is abundantly expressed in caudal brain neurons and in restricted populations of forebrain neurons. Using electrophysiological studies, we demonstrate that Ca^{2+} -triggered neurotransmitter release is impaired in synaptotagmin-2 deficient striatal neurons and NMJs. However, this impairment was less severe than that of cortical and hippocampal neurons lacking synaptotagmin-1. Consistent with this unexpectedly limited release phenotype, we observed co-expression of synaptotagmin-1

with synaptotagmin-2 in NMJs, suggesting that at least in NMJs, Ca^{2+} -triggering of release is driven by both synaptotagmin-1 and -2.

4.2 Materials and Methods

4.2.1 Generation and maintenance of synaptotagmin-2 knockout mice

The targeting vector (Fig. 4-1A) was constructed employing routine techniques.

The homology arms were obtained from a genomic clone containing the entire synaptotagmin-2 gene (GenBank AF257303) isolated from a 129 SVJ genomic library (Lambda Fix II, Stratagene) using the cDNA for synaptotagmin-2 as template for the probe (Baram et al., 1999). The 5' arm is a 3.8 kb Bgl II – Nco I fragment that contains exon 1 and part of exon 2 and the 3' arm is a 3.1 kb BamH I – Sac II fragment that includes exon 8. The poliovirus internal ribosomal entry site (IRES) was cloned from pSBC-1 (Dirks et al., 1993), lacZ with a nuclear localization signal from pPD 46.21 (Goldhamer et al., 1992) and PGK-Neo and MC1-TK from NTKV 1907 (pKO Scrambler, Lexicon). The construct was electroporated into R1 embryonic stem (ES) cells.

Homologous recombination events were enriched under Geneticin (Invitrogen) and FIAU selection and confirmed by Southern blot of Sal I-digested genomic DNA using as template for the probe a fragment upstream of the 5' arm obtained from a Bgl II digest.

Chimeric males were generated by injection of selected ES cell clones into C57BL/6 blastocysts and then used to found mutant lines. PCR with primers P1:

AGAAGACATGTTCGTCCAAGC, P2: TCATGTTTCATGGCGTTCTTC, and P3:

ACGGACACCCAAAGTAGTCG was used to detect the wildtype (P1 + P2 product ~ 1 kb) and mutant (P1 + P3 product ~ 1.5 kb) synaptotagmin-2 allele and to genotype

wildtype, heterozygous and homozygous mice. Mutant animals were propagated as heterozygous colonies in a barrier facility while being backcrossed for nine generations into a C57BL/6 background before generating homozygous animals by heterozygous crossings.

4.2.2 *X-gal* (β -Galactosidase) staining

Wildtype and synaptotagmin-2 KO mice at ages of post natal day 14-16 were deeply anesthetized with halothane and transcardially perfused with 15 ml of 2% paraformaldehyde and 0.25% glutaraldehyde followed by 5 ml of phosphate buffered saline (PBS). Brains, spinal cords and eyeballs were dissected out and post-fixed in the same fixative for 30 min at 4 °C. For experiments with brain sections, tissues were submerged in 30% sucrose overnight at 4 °C for cryoprotection and then embedded in Tissue-Tek O.C.T. (Ted Pella, Inc.) on dry ice. Brain sections at 20 μ m were obtained using a Leica cryostat (Leica CM3050S) and were mounted onto slides. Slides with sections were rinsed in buffer A (100 mM PBS pH 7.4; 2 mM MgCl₂; 5 mM EGTA) and buffer B (100 mM PBS pH 7.4; 2 mM MgCl₂; 0.01% Na-deoxycholate; 0.02 % NP-40) twice, each for 5 min. Sections were then developed in buffer C (buffer B containing 5 mM K-ferricyanide, 5 mM K-ferrocyanide; and 0.5 mg/ml X-Gal) at 37 °C for 6 hours in the dark. Samples were twice rinsed with distilled water, counter-stained with neutral red (1% neutral red, in pH 4.8 acetate buffer) for 1 min and washed in distilled water. Finally, sections were air-dried, dehydrated with gradients of ethanol, cleared with xylene, and mounted with coverslips using Permount (SP15-100, Fisher Scientific). Microscopy was performed after 24 hours. In the case of whole-mount tissues (brain and spinal cord),

tissues were rinsed twice for 15 min each in buffer A and buffer B, and developed in buffer C overnight at 37 °C in the dark.

4.2.3 Electrophysiological analyses of cultured striatal neurons

Primary striatal neurons were cultured as described (Mao and Wang, 2001) with modifications. Briefly, dorsal striatum was isolated from 1 day-old pups of wildtype or synaptotagmin-2 KO mice, dissociated by trypsin digestion, and plated on matrigel-coated glass coverslips. Neurons were cultured in Modified Eagle Medium (MEM, Gibco) supplemented with B27 (Gibco), glucose, transferrin, fetal bovine serum, and Ara-C (Sigma). To monitor synaptic responses, whole-cell patch-clamp recordings were made with neurons at 14 to 16 days in vitro. Synaptic responses were triggered by a 1 ms current pulse (900 μ A) through a local extracellular electrode (FHC, Inc.), and recorded in whole-cell voltage-clamp mode using a Multiclamp 700A amplifier (Axon Instruments, Inc.). Data were digitized at 10 kHz with a 2 kHz low-pass filter. The pipette solution contained 135 mM CsCl₂, 10 mM HEPES, 1 mM EGTA, 4 mM Mg-ATP, 0.4 mM Na-GTP, and 10 mM QX-314 (pH 7.4). The bath solution contained 140 mM NaCl, 5 mM KCl, 2 mM or 10 mM CaCl₂, 0.8 mM MgCl₂, 10 mM HEPES, and 10 mM glucose (pH 7.4). Inhibitory postsynaptic currents (IPSCs) were isolated pharmacologically by including 50 μ M D-AP5 and 20 μ M CNQX in the bath solution. Series resistances were compensated 60-70%, and recordings with series resistances higher than 15 M Ω were excluded. Data were analyzed using Clampfit 9.02 (Axon Instruments, Inc) or Igor 4.0 (Wavemetrics).

4.2.4 Electrophysiological analysis of the neuromuscular junction

Neuromuscular junction (NMJ) recordings were carried out at room temperature using intracellular recordings on acutely isolated phrenic nerve/diaphragm preparations at P14-16. Muscles were dissected in oxygenated normal Ringer's solution containing 136.8 mM NaCl, 5 mM KCl, 12 mM NaHCO₃, 1 mM NaH₂PO₄, 1 mM MgCl₂, 2 mM CaCl₂, and 11 mM glucose pH 7.4 (Liley, 1956), pinned onto Sylgard coated dishes, and continuously superfused with oxygenated Ringer's solution. Sharp glass microelectrodes were filled with 3 M KCl. Spontaneous synaptic responses were recorded in normal Ringer's solution or with Ringer's solution containing 10 μ M EGTA-AM. For experiments with EGTA-AM, phrenic nerve-muscle preparations were treated with EGTA-AM for at least 20 min before recordings. Evoked endplate potentials were elicited by suprathreshold stimulation (2-6 V, 1 ms) of the phrenic nerve via a suction electrode. In order to prevent muscle contractions, which would destabilize the recordings, 2 μ M ω -conotoxin were added to the bath solution to block the muscle specific sodium channel (Cruz et al., 1985). The number of acetylcholine (Ach) vesicles release upon one single nerve impulse (i.e. the quantal content) was calculated as the mean evoked endplate potential (EPP) amplitude divided by the mean amplitude of miniature endplate potential (mEPP). Data were collected with an AxonClamp 2B amplifier, digitized at 10k Hz, and analyzed using Clampfit 9.02 (Axon Instruments, Inc.) and MiniAnalysis (Synaptosoft, Inc.).

4.2.5 Immunohistochemistry

Whole-mounts of diaphragmatic muscle were dissected and fixed with 2% paraformaldehyde overnight at 4 °C. Samples were rinsed thoroughly in PBS, and incubated in 0.1 M glycine/PBS pH 7.3 at room temperature for 30 min. Coronal 20 µm sections of diaphragmatic muscle were made after overnight immersion of tissues in PBS containing 30% sucrose. Sections were directly mounted onto slides. Slides with muscle sections were incubated with 0.1 mg/l Alexa 594-conjugated α -bungarotoxin (Molecular Probes) in antibody dilution buffer (0.5 M NaCl, 10 mM phosphate buffer pH 7.3, 3% bovine serum albumin, 0.1% sodium azide, 0.3% Triton-X 100) for 1 hr at room temperature. Sections were permeabilized in 100% methanol at -20 °C for 7 min, and washed with 0.5% Triton-X 100 in PBS. Samples were incubated with primary antibodies (for synaptotagmin-2, A320, 1:500; synaptotagmin-1, Cl41.1, 1:3 000 dilution) overnight at 4 °C. Sections were washed in 0.5% Triton X-100 3 times, and incubated with secondary antibodies (Alexa fluor 488-conjugated anti-rabbit or-mouse IgG) at 4 °C overnight. Samples were then washed in PBS, mounted with VectaShield mounting medium (H-1000, Vector) and examined by confocal microscopy.

4.2.6 Miscellaneous procedures

For immunoblotting analyses, forebrains, cerebellums and spinal cords of P15 wildtype and mutant mice were homogenized in PBS. Protein concentrations were determined using the BCA assay (Pierce). Equivalent amounts of brain proteins from wildtype and synaptotagmin-2 KO mice were analyzed by SDS-PAGE and immunoblotting using antibodies as follows: synaptotagmin-2 (A320), synaptotagmin-1 (Cl41.1); syntaxin 1(I6251); SNAP-25 (P913); synaptobrevin 2 (Cl69.1); Rab3A (42.2);

secretory carrier membrane proteins (SCAMP, R806); synptophysin (7.2); synapsin (E028); PSD95 (L667); complexins (L668); Munc18 (J371); calmodulin-associated serine/threonine kinase (CASK, N3927); synuclein (U1126); cysteine-string protein (CSP, R807); GDP-dissociation inhibitor (GDI, 81.2); and vasolin-containing protein (VCP, K330; used as an internal control). For quantitations, ¹²⁵I-labeled secondary antibodies and PhosphoImager detection (Molecular Dynamics) were used. GDI and VCP were employed as internal standards.

4.2.7 Statistical analysis

Data are presented as means \pm SEMs. Unpaired Student's t-tests were used. Differences were considered significant at $p < 0.05$.

4.3 Results

4.3.1 Generation of synaptotagmin-2 knockout (KO) mice

We generated synaptotagmin-2 KO mice by homologous recombination in ES cells using the strategy depicted in Fig. 3-1A. In the mutant allele, the synaptotagmin-2 gene sequence containing exons 2 to 7 was replaced by three termination codons, the poliovirus IRES element followed by the cDNA for LacZ with a nuclear localization signal, and by PGK-Neo. Southern blots with a probe outside the targeting construct and PCR were used to demonstrate successful homologous recombination. We maintained two independent lines (S2KO-D, S2KO-K) originating from two different ES cell electroporations, and backcrossed them into a C57BL/6 background. The phenotype of both lines is identical, confirming that it is the result of the synaptotagmin-2 deletion and not of another mutation introduced by ES cell

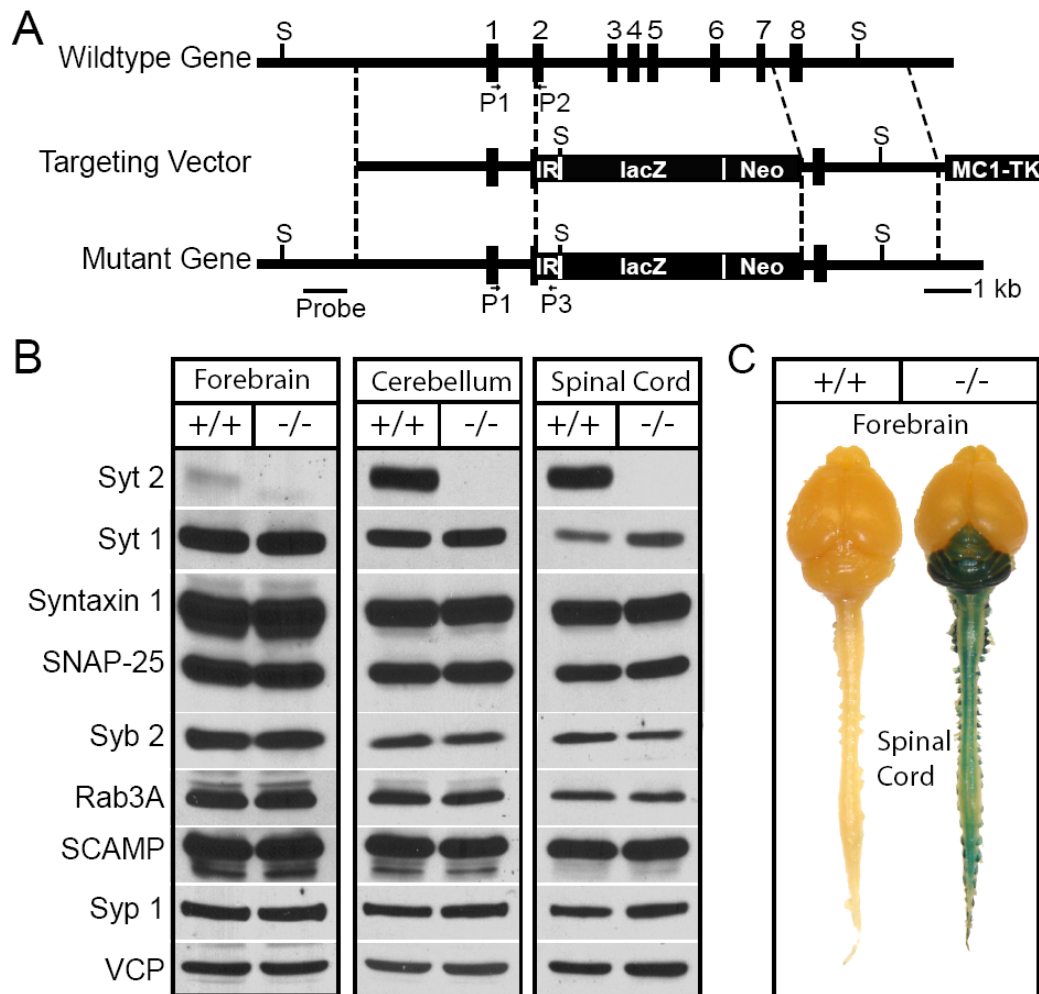


Figure 4- 1 Generation of synaptotagmin-2 KO mice by homologous recombination.

A, Strategy for mutating synaptotagmin-2 in the mouse. The diagrams depict the structures of the wildtype synaptotagmin-2 gene which contains all 8 exons for synaptotagmin-2 (top), the targeting vector constructed for the mutation of the synaptotagmin-2 gene (middle), and the mutant gene resulting from homologous recombination (bottom). In the final product part of exon 2 through exon 7 were replaced by the poliovirus IRES (IR), the cDNA for lacZ with a nuclear localization signal (lacZ) and PGK-Neo (Neo). This last gene was used for positive selection, while the MC1 thymidine kinase gene (TK) at the 3' end of the construct was used for negative selection. The positions of the oligonucleotide primers used to identify the wildtype and mutant alleles are indicated by arrows (P1, P2 and P3). The Sal I recognition sites (S) and template for the probe used for Southern blotting are also indicated. **B**, Western blots indicate the lacking of synaptotagmin-2 in mutant mouse brain and spinal cord. Other synaptic proteins that were quantified (Table3-1) in homogenate of brain, cerebellum/brain stem and spinal cord homogenates are also showed in the figure. **C**, X-gal staining of whole-mount mouse central nervous system in WT and synaptotagmin-2 KO. Note that dorsal root ganglia attached to the spinal cord also show positive staining. Abbreviations: SCAMP: secretory carrier membrane protein; Syt 2: synaptotagmin-2; Syt 1: synaptotagmin-1; Syb 2: synaptobrevin-2; Syp 1, synaptophysin-1; VCP: vasolin-containing protein.

manipulation. For this study we used mice from the S2KO-D line. To confirm that the homologous recombination created a null allele for synaptotagmin-2, we performed immunoblotting analyses on forebrain, cerebellum, and spinal cord samples from littermate wildtype and homozygous mutant mice (Fig. 4-1B). As expected, in wildtype mice synaptotagmin-2 was almost undetectable in forebrain, but abundantly present in cerebellum and spinal cord. In homozygous mutant mice, no synaptotagmin-2 was detectable in any brain region (Fig. 3-1B). Although the coding region for the first 69 amino acids of synaptotagmin-2 was not deleted, we did not detect expression of the predicted 7.6 kD band in our immunoblots using an antibody raised against the N terminus the protein (data not shown). We also analyzed the levels of fourteen other synaptic proteins in the same brain samples, using quantitative immunoblotting with ¹²⁵I-labeled secondary antibodies (Table 4-1). We detected no significant changes in any synaptic protein tested except for synaptotagmin-1, which exhibited a moderate increase in spinal cord but not in forebrain (Fig.4-1B and Table 4-1). These data suggest that absence of synaptotagmin-2 does not induce a massive increase of synaptotagmin-1 expression or a restructuring of the protein composition of rostral or caudal brain regions.

4.3.2 Synaptotagmin-2 KO mice are postnatally lethal and have motor defects

To test the effect of the synaptotagmin-2 deletion on mouse development and survival, we systematically examined the offspring from heterozygous matings. At birth, synaptotagmin-2 homozygous and heterozygous mutant and wildtype control mice were present at close to Mendelian ratio (wildtype/ heterozygous/homozygous ratio =

1.10/2.00/1.05 [n=447]). However, homozygous synaptotagmin-2 KO mice began to display severe motor dysfunction in the second postnatal week, and were almost unable to move at postnatal day 15. Whereas wildtype and heterozygous mice grew vigorously in the first four weeks of life, KO mice stopped growing in the second postnatal week (Figs. 4-2A and 2B). At postnatal day 19, synaptotagmin-2 KO mice started to die, and all mice perished by postnatal day 24 (Fig. 4-2C). However, we observed no seizures, different for example from SV2 KO mice which also die at a similar age (Janz et al., 1999). These data indicate that synaptotagmin-2 is essential to the well-being and survival of mice.

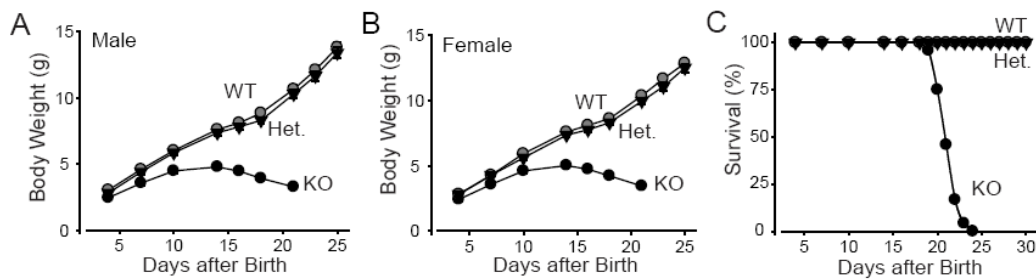


Figure 4- 2 Weight and survival of synaptotagmin-2 KO mice.

A and B, Body weight of littermate male (**A**) and female (**B**) wildtype and mutant mice as a function of age. Homozygous wildtype (WT), heterozygous mutant (Het) and homozygous mutant (KO) mice were examined (n=10-21 for male and 10-41 for female animals in each genotype group; $p < 0.05$ at all ages for the KO mice compared to wildtype or heterozygous mice which are not significantly different from each other). **C,** Survival of wildtype, synaptotagmin-2 heterozygous and synaptotagmin-2 KO mice. All synaptotagmin-2 KO mice die between ages of postnatal days 19 to 24 (n=35, 60, 24 for wildtype, heterozygous and KO, respectively).

4.3.3 Expression pattern of synaptotagmin-2 in mice

The insertion of lacZ after the IRES element into the synaptotagmin-2 gene placed the expression of β -galactosidase encoded by the lacZ sequences under the

transcriptional control of the synaptotagmin-2 gene regulatory elements (Fig. 4-1A). We used the β -galactosidase activity to follow the precise expression pattern of synaptotagmin-2 in the mutant mice (Figs. 1C, 3 and 4). Consistent with previous studies (Geppert et al., 1991; Marqueze et al., 1995; Ullrich et al., 1994), examination of the entire nervous system from mutant mice revealed that synaptotagmin-2 was primarily expressed in the hindbrain, cerebellum and spinal cord (Fig. 4-1C). Although on a macroscopic level synaptotagmin-2 was absent from forebrain, coronal sections revealed considerable expression of synaptotagmin-2 in selected forebrain neurons (Figs. 3A and 3F). Unexpectedly, the majority of neurons in the striatum and the zona incerta appear to express synaptotagmin-2 (Figs. 3C and 3F). Moreover, considerable synaptotagmin-2 expression was observed in the reticular nucleus of the thalamus (Fig. 4-3I) and the ventromedial nucleus of the hypothalamus (Fig. 4-3J). In contrast, the major thalamic nuclei, the cortex (Fig. 4-3B), and the hippocampal formation (Fig. 4-3G and H) expressed little synaptotagmin-2. In the latter structures, a few isolated synaptotagmin-2 positive neurons were observed as exemplified in the image of the CA3 region of the hippocampus in Fig. 4-3H, but the vast majority of neurons did not express synaptotagmin-2. Although it is not possible to determine the nature of the synaptotagmin-2 expressing neurons from these analyses, most of these neurons appear to be inhibitory based on their location. This is suggested by the fact that the majority of neostriatal neurons are inhibitory and express synaptotagmin-2, that the reticular nucleus of the thalamus is largely composed of inhibitory neurons, and that the location of the scattered synaptotagmin-2 positive cells in the cortex (Fig. 4-3B) hippocampus

corresponds to those of inhibitory interneurons, especially in the hippocampal hilus region (Figs. 3G-3H). Some of the synaptotagmin-2 positive neurons found here may correspond to recently discovered hippocampal parvalbumin-expressing basket cells that are still capable of mediating fast synchronous inhibitory synaptic responses even in the absence of synaptotagmin-1 (Kerr et al., 2006).

The pattern of inhibitory neurons expressing synaptotagmin-2 is also present in the cerebellum where all Purkinje neurons and the majority of the neurons of deep cerebellar nuclei express synaptotagmin-2 (Figs. 4A and 4B). In contrast, few neurons in the granule cell layer (which primarily contains excitatory granule cells) contain synaptotagmin-2, and scattered synaptotagmin-2 positive cells are observed in the molecular layer (which contains scattered inhibitory interneurons).

A different expression pattern for synaptotagmin-2 emerges in the brainstem and spinal cord where a majority of neurons appears to express synaptotagmin-2. In the brainstem, abundant expression of synaptotagmin-2 is observed for example in the inferior colliculus, the pontine reticular nuclei, the nuclei of the 5th and 7th cranial nerves, and the nucleus of the trapezoid body (Figs. 4C-4F). Similarly, in the spinal cord most neurons appear to express synaptotagmin-2, including all motoneurons (Figs. 4G and 4H). Most of the neurons that express synaptotagmin-2 in the brainstem and spinal cord correspond by location to excitatory neurons, either glutamatergic or cholinergic, suggesting that different from the forebrain where synaptotagmin-2 appears to be concentrated in inhibitory neurons, synaptotagmin-2 is more widely expressed in all classes of neurons in the brainstem and spinal cord.

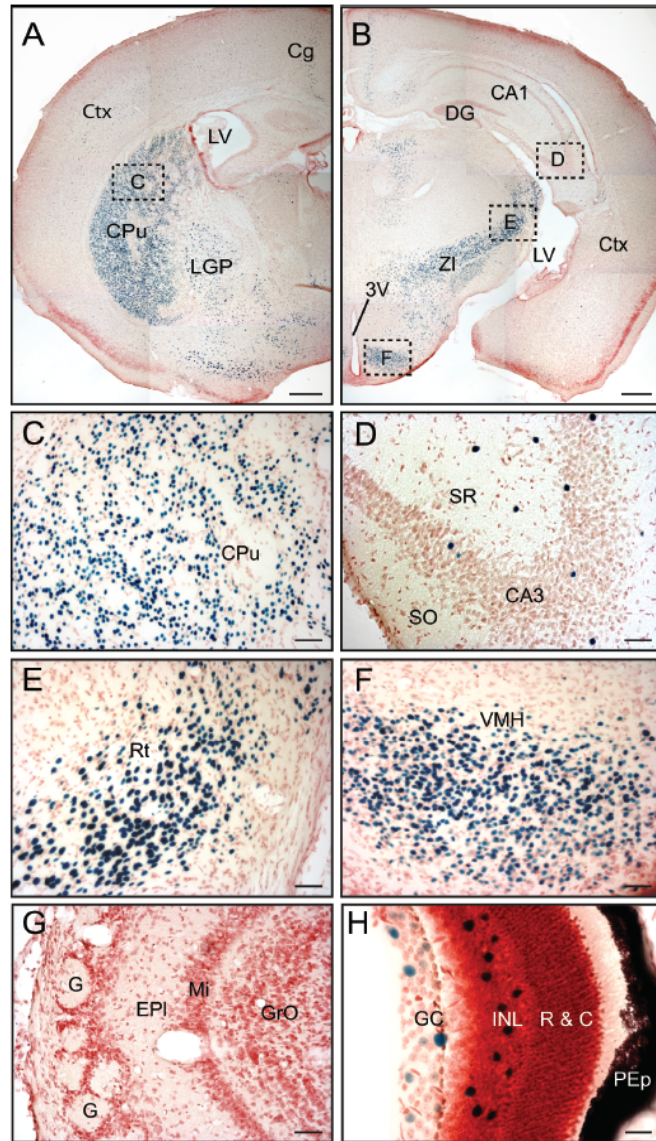


Figure 4- 3 Expression pattern of synaptotagmin-2 in forebrain.

β -galactosidase activity is revealed by X-gal staining in synaptotagmin-2 KO homozygous mice. **A**, The majority of striatal neurons show β -galactosidase activity. **B & C**, Higher magnifications of brain areas indicated by dashed squares in (**A**). **D**, No synaptotagmin-2 expression is found in olfactory bulb. **E**, scattered neurons in retina showing β -galactosidase positivity. **F**. Very few neurons in cortex and hippocampus are β -galactosidase positive. **G-J**, Higher magnifications of brain areas indicated by dashed squares in (**F**). Abbreviations: 3V: 3rd ventricle; Cg: cingulate cortex; Ctx: cortex; CPu: caudate putamen (striatum); DG: dentate gyrus; EPI: external plexiform layer of olfactory bulb; G: glomeruli; GC: Ganglion cell layer; GrO: granular cell layer of olfactory bulb; INL: inner nuclear layer; LGP: lateral globus pallidus; LV: lateral ventricle; Mi: mitral cell layer of olfactory bulb; PEp: Pigment epithelium; SO: stratum oriens; SR: stratum radiatum; R & C: Layer of rods and cones; Rt: reticular thalamic nucleus; VMH: ventromedial hypothalamic nucleus; ZI: zona incerta. Bars in **A & F**=50 μ m; Bar in **B-D & G-J**=5 μ m; Bar in **E**=2.5 μ m.

4.3.4 Synaptotagmin-2 expression in the NMJ

The X-gal staining showed that synaptotagmin-2 is expressed in motoneurons, consistent with the NMJ phenotype in hypomorphic synaptotagmin-2^{I377N} mutant mice (Pang et al., 2006b). To determine whether synaptotagmin-2 is indeed present in NMJs and whether it is co-expressed with synaptotagmin-1, we performed an immunofluorescence localization study of synaptotagmin-1 and -2 in NMJs in the diaphragmatic muscle from wildtype and KO mice at postnatal days P14-16 (Fig. 4-5). Conjugated fluorescent α -bungarotoxin was used to label postsynaptic acetylcholine receptors. The diaphragmatic muscle is innervated by phrenic nerves that branch upon reaching the muscle to form discrete NMJ synapses that are distributed in a characteristic branching pattern in the middle of the diaphragm; this pattern is controlled by synaptic activity, and becomes abnormal when synaptic activity is altered (Buffelli et al., 2003). However, the distribution of NMJs, as revealed by staining with fluorescent α -bungarotoxin, was not significantly altered in synaptotagmin-2 KO mice. We next examined individual NMJs for the presence of synaptotagmin-1 and -2. Synaptotagmin-2 was present in every endplate in wildtype diaphragmatic muscle but absent from KO NMJs (Figs. 5A and 5B). Three-dimensional reconstructions by confocal microscopy revealed that individual NMJ endplates in synaptotagmin-2 deficient mice were structurally similar to those from wildtype mice. A subpopulation of wildtype NMJs expressed synaptotagmin-1 (~40%), whereas an appreciably higher percentage of synaptotagmin-2 deficient NMJs (~90%) contained synaptotagmin-1 (Figs. 5C and 5D).

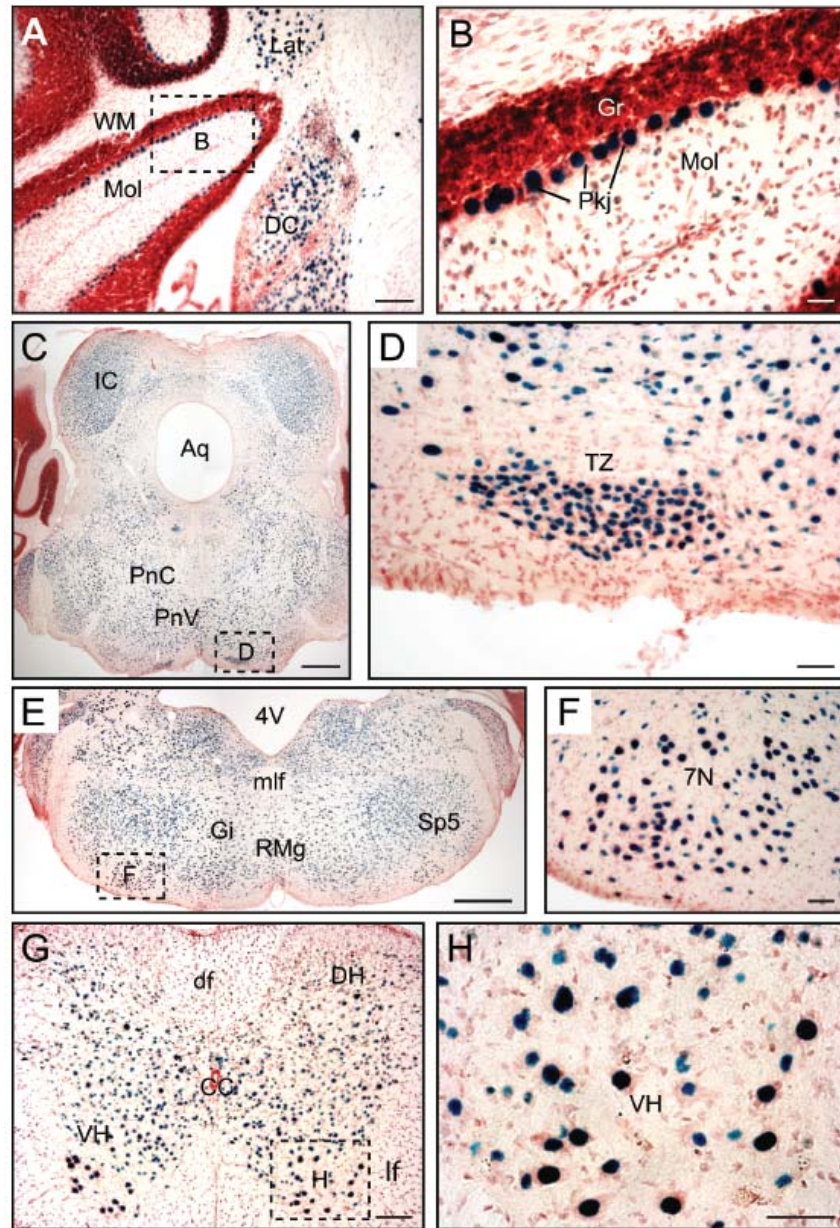


Figure 4- 4 Expression pattern of synaptotagmin-2 in caudal brain.

X-gal staining in synaptotagmin-2 KO homozygotes **A**, cerebellum; **C** and **E**, brain stem; **G**, spinal cord. **B**, **D**, **F** and **H**, Higher magnifications of brain areas as indicated by dashed squares in (**A**, **C**, **E** & **G**). Abbreviations: 4V: 4th ventricle; 7N: facial nucleus; Aq: aqueduct; CC: Central canal; DC: dorsal cochlear nucleus; df: dorsal fasciculus; DH: Dorsal horn; Gi: gigantocellular reticular nucleus; Gr: granular layer; Lat: lateral cerebellar nucleus; lf: lateral fasciculus; IC: inferior colliculus; mlf: medial longitudinal fasciculus; Mol: Molecular layer; PnC: caudal pontine reticular nucleus; PnV: ventral pontine reticular nucleus; Pkj: Purkinje cells; RMg: raphe magnus nucleus; Sp5: interpolar subnucleus of the spinal trigeminal nucleus. Tz: nucleus of trapezoid body; VH: Ventral horn; WM: White matter. Bars in **A** & **G**=10 μm; Bar in **B**=2.5 μm; Bars in **C** & **E**=50 μm; Bars in **D**, **E** & **H**=5 μm.

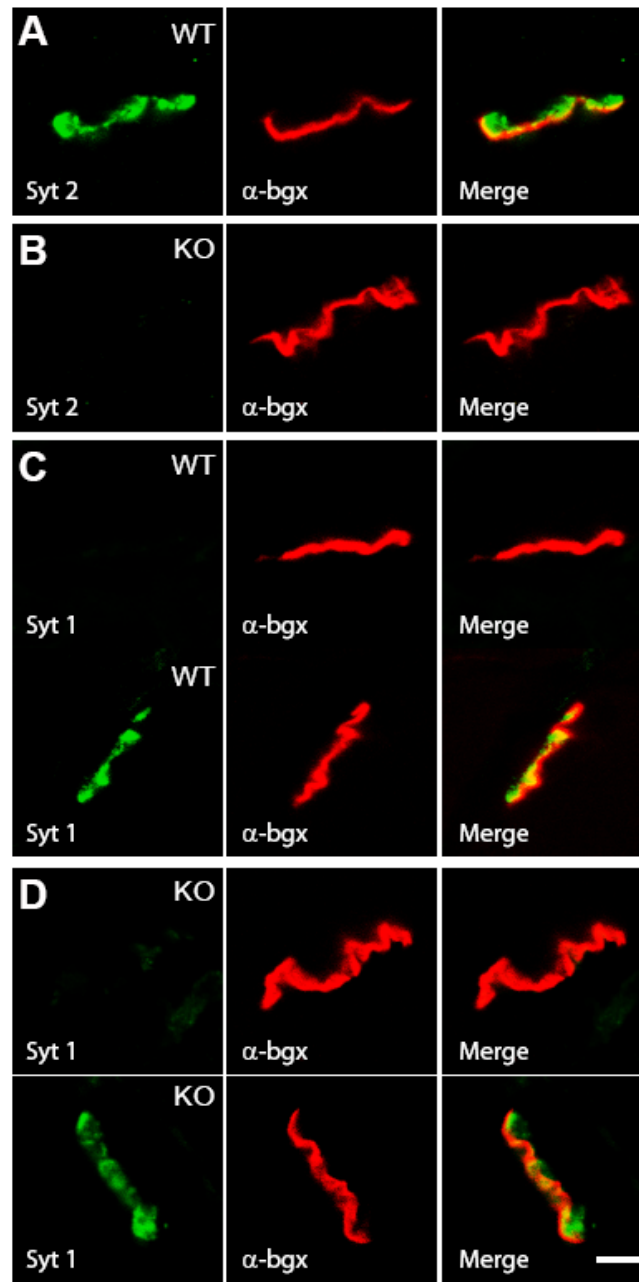


Figure 4- 5 Immunostaining of synaptotagmin-1 and-2 in NMJ.

A, All end plates express synaptotagmin-2 in wildtype (WT) NMJ. *B*, No synaptotagmin-2 was detected in synaptotagmin-2 KO NMJ. *C* and *D*, Synaptotagmin-1 was detected in some (lower panel) but not other endplates (upper panel) in both wildtype and synaptotagmin-2 KO. Bar=10 μ m, applies to all sub-panels.

This finding agrees well with the modest but significant increase in the overall levels of synaptotagmin-1 in spinal cord (Table 4-1).

4.3.5 Evoked synaptic release in cultured neurons from the neostriatum

To examine the functional consequences of the deletion of synaptotagmin-2 on synaptic transmission, we performed electrophysiological recordings in cultured neurons from the dorsal neostriatum of newborn mice (Fig. 4-6), and in NMJs in the phrenic nerve/diaphragm preparation from adolescent mice (P14-16; Figs. 7-11). In the neostriatal neurons, we analyzed inhibitory postsynaptic currents (IPSCs) as an example of inhibitory synaptic transmission effected by forebrain neurons that express synaptotagmin-2 (Fig. 4-3C), and NMJs as an example of excitatory synaptic transmission in a caudal synapse that expresses synaptotagmin-2 (Fig. 4-5). As with all other experiments performed in the present study, all recordings were made with samples from littermate wildtype and mutant mice, with the genotype 'blinded' to the experimentalist. IPSCs could be efficiently induced by focal stimulation in cultured neostriatal neurons from both wildtype and KO mice. We observed no significant decrease in the amplitude or total synaptic charge transfer per stimulus as integrated over 1.5 sec (Figs. 4-6A and 4-6B). However, we found that the synaptic charge transfer exhibited a significantly slower time-course in synaptotagmin-2 deficient striatal neurons than in wildtype control neurons (Fig. 4-6D). The integrated charge transfer can be fitted by a two-exponential function. The mean decay time constants for both the fast and slow constituent (called 'constituent' in order to avoid confusion of these different kinetic

Table 4-1. Levels of synaptic proteins in synaptotagmin-2 knock-out mice

Protein		Cortex		Cerebellum		Spinal Cord	
		wildtype	knockout	wildtype	knockout	wildtype	knockout
Syt 1	(n=4)	100±2.1	94.2±3.8	100±4.8	112.8±7.4	100±7.2	132.3±2.9*
Syntaxin	(n=4)	100±3.2	102.6±4.5	100±10.6	100.5±10.7	100±6.7	83.6±11.5
SNAP 25	(n=4)	100±2.2	100.3±2.3	100±9.6	90.0±8.5	100±9.1	83.4±10.4
Syb	(n=4)	100±5.0	111.3±3.9	100±8.2	92.8±3.8	100±10.9	106.9±6.5
Rab 3	(n=4)	100±6.2	101.2±9.9	100±12.2	80.7±7.1	100±7.7	86.0±8.7
Syp 1	(n=4)	100±2.7	105.6±3.4	100±8.5	85.7±3.1	100±5.1	91.1±8.1
Synapsin	(n=4)	100±1.8	87.9±1.0	100±5.9	91.3±4.4	100±6.0	86.2±6.3
PSD95	(n=3)	100±2.4	103.8±4.2	100±3.1	97.9±6.0	100±2.3	98.8±0.5
Cpx	(n=3)	100±3.7	95.5±10.2	100±4.4	89.3±0.8	100±4.2	103.0±6.2
Munc18	(n=3)	100±6.2	98.3±2.9	100±2.0	102.4±1.3	100±3.7	109.3±3.7
CASK	(n=3)	100±4.3	89.8±0.3	100±0.6	101.2±3.7	100±8.5	93.3±5.6
SCAMP	(n=3)	100±1.6	100.8±3.0	100±2.4	98.0±7.5	100±2.1	98.3±0.8
Synuclein	(n=3)	100±6.6	95.7±5.6	100±2.7	95.5±8.5	100±3.6	99.5±14.2
CSP	(n=3)	100±4.6	104.5±0.8	100±1.3	112.3±7.8	100±5.1	93.2±7.4

Total proteins in brain homogenates were analyzed by SDS-PAGE and western blots. ¹²⁵I-conjugated secondary antibodies were used and analyzed by a PhosphorImager. CASK: calmodulin-associated serine/threonine kinase; CSP: cysteine-string protein; Cpx: complexin; SCAMP: secretory carrier membrane proteins; Syb: synaptobrevin 2; Syp: synaptophysin; Syt1: synaptotagmin-1. Numbers of samples were listed in the parenthesis. * indicates p<0.05.

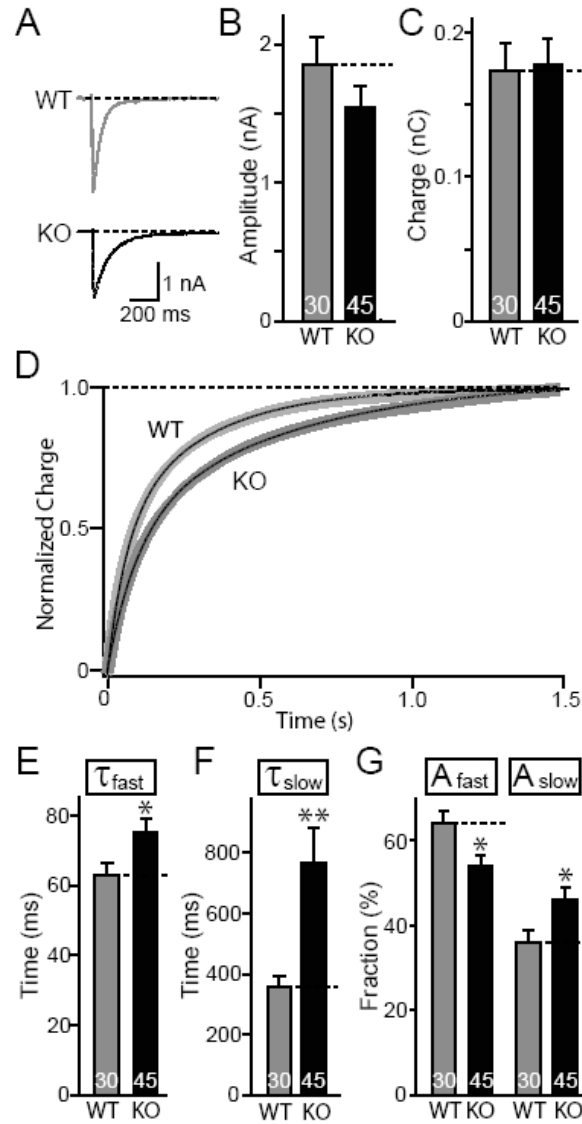


Figure 4- 6 Synaptic release in striatal neuronal cultures.

A, Representative traces of evoked IPSC in both wildtype (WT) and synaptotagmin-2 KO. Pooled data for both amplitude (**B**) and charge transfer over a time period of 1.5 s (**C**). **D**, Normalized average charge integration as a function of time over 1.5 s. WT: n=16; KO: n=17. The integrated charge transfer can be well fitted by a double exponential function (black solid line superimposed on to the integrated lines). The fitting gave out a fast decay (τ_{fast}) and slow decay (τ_{slow}). **E & F**, pooled data indicate both τ_{fast} and τ_{slow} increased in synaptotagmin-2 KO striatal synapses. **G**, The fraction of the slow constituent (A_{slow}) increased in KO synapses and fast constituent (A_{fast}) decreased accordingly. Numbers of neurons recorded are indicated by numbers within each bar. **H**, Representative traces of spontaneous miniature IPSC (sIPSC) in both wildtype (WT) and synaptotagmin-2 KO mice. There is no significant differences in average sIPSC amplitudes (**I**), 20-80% rise time (**J**) and 80-20% decay time (**K**). Events with amplitudes higher than 150 pA, possibly due to spontaneous firing of presynaptic neurons, are excluded from analyses. * p<0.05; ** p<0.01.

components with the slow and fast component of release that are differentially affected in synaptotagmin-1 KO neurons (Geppert et al., 1994) were significantly increased in synaptotagmin-2 deficient neurons. This effect is relatively small for the fast decay constant (~20%), but very large for the slow time constant (>100%; Figs. 6E and 6F).

Moreover, consistent with a shift to a slower time course of release, the relative contributions of the fast and slow processes to the overall release are significantly shifted in favor of the slow process (Fig. 4-6G). Please note that in these calculations the two time constants of the integrated IPSCs are purely descriptive tools to characterize the changes in release time course observed in synaptotagmin-2 deficient striatal neurons. We noticed in a subpopulation of neurons (7 out of 45) that release was largely desynchronized similar to synaptotagmin-1 deficient cortical neurons (Maximov and Sudhof, 2005), but the majority of neurons did not exhibit this phenotype, presumably because other synaptotagmins are also expressed in these neurons and functionally compensate (Marqueze et al., 1995; Ullrich et al., 1994; Xu et al., 2007). In order to eliminate the possibility that the change in IPSC kinetics induced by the synaptotagmin-2 deletion is due to an alteration in the properties of postsynaptic GABA receptors, we analyzed the kinetics of spontaneous miniature IPSCs (sIPSCs) in cultured striatal neurons. Spontaneous events with amplitude exceeded 150 pA were excluded from this analysis, due to the possibility that bigger responses resulted from spontaneous firing of presynaptic neurons. We found no changes in the average amplitude, rise time, or decay

time of sIPSCs (Fig. 4-6 H-K). Thus the changes in the delayed release time course are most likely caused by a presynaptic defect due to the elimination of synaptotagmin-2.

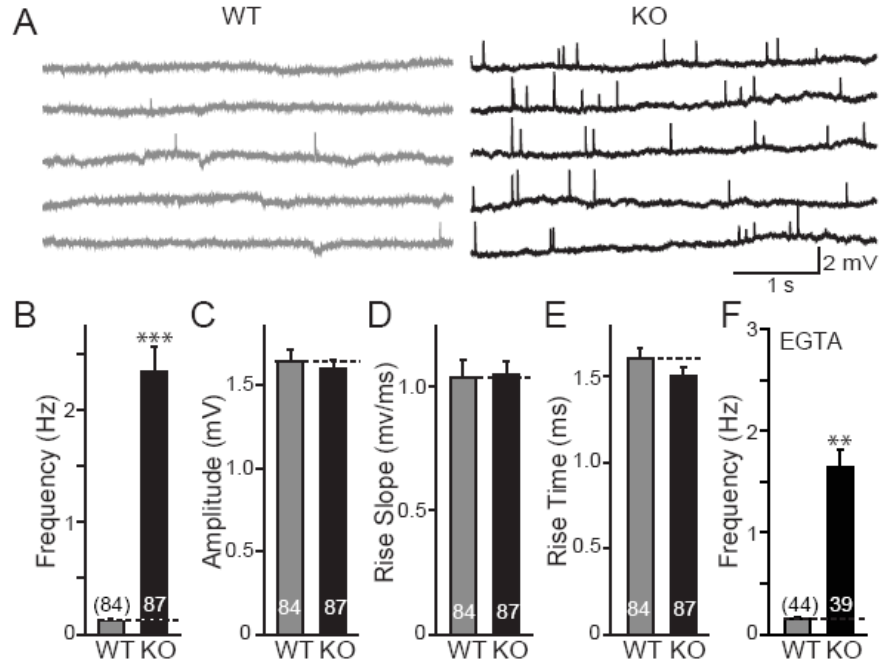


Figure 4- 7 Spontaneous miniature synaptic responses in NMJ.

A, Representative traces of spontaneous miniature endplate potential (mEPPs) of wildtype (WT) and synaptotagmin-2 KO; **B**, Pooled data indicate a significant increase in the frequency of miniature synaptic release, while amplitude (**C**), rise slope (**D**) and rise time (**E**) show no differences in both wildtype and synaptotagmin-2 KO. **F**, In the presence of EGTA-AM (10 μ M), a significant reduction of mEPP frequency is found in synaptotagmin-2 KO but not in WT NMJ. Frequency of mEPPs is still significantly higher compared to wildtype control in the presence of EGTA. Numbers of neurons recorded as indicated by the numbers above or within each bar. ** $p < 0.01$; *** $p < 0.001$.

4.3.6 Spontaneous neurotransmitter release in NMJs

To examine synaptic transmission in the NMJ, we performed sharp-electrode intracellular recordings from diaphragmatic muscle. We first studied spontaneous release events (mEPPs for miniature endplate potentials) in normal Ringer solution. The

frequency of mEPPs was almost 10-fold higher in synaptotagmin-2 KO mice than in littermate wildtype control mice at an age of post natal day 14-16 (Fig. 4-7B), whereas the average amplitude, the rise slope, and rise time of the mEPPs were the same in wildtype and KO mice (Figs. 7C-7E). In order to determine whether the increased mEPP frequency is due to residual Ca^{2+} in nerve terminals, we applied 10 μM EGTA-AM for >20 min in the bath solution before recording mEPPs (Fig. 4-7F). The EGTA slightly decreased the mEPP frequency in both wildtype and synaptotagmin-2 mutant NMJs, but the difference between the two synapses remained the same (Fig. 4-6 F), demonstrating that the increase in mEPPs frequency in the mutant NMJs is Ca^{2+} -independent.

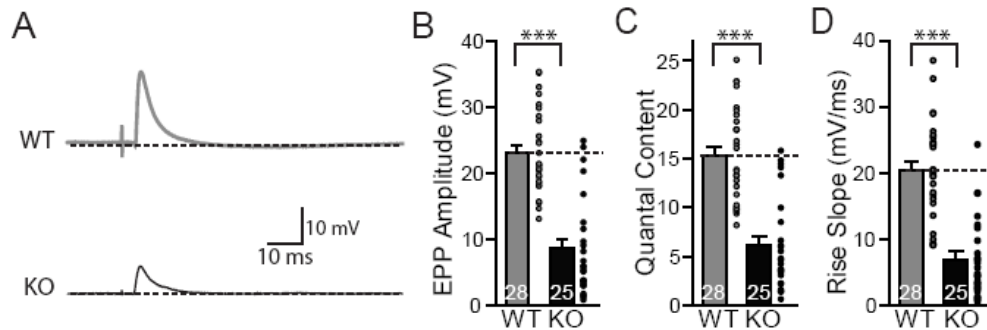


Figure 4- 8 Evoked synaptic responses in NMJ.

A, Representative traces of phrenic nerve evoked endplate potential (EPP) by a suction electrode in wildtype (WT) and synaptotagmin-2 KO. Maximum stimulus (2-6 V) intensities were used to evoke synaptic responses. **B –D**, Pooled data of the amplitude (**B**), quantal content (**C**) and speed of the EPP increase (**D**) in wildtype and synaptotagmin-2 deficient NMJs. Gray and black circles indicate individual evoked responses of each recording. Numbers of recordings are indicated in each bar. ** $P < 0.01$; *** $P < 0.001$.

4.3.7 Evoked synaptic responses in synaptotagmin-2 deficient NMJs

We stimulated the phrenic nerve with a suction electrode using a maximal stimulus intensity (2-6 V), and recorded evoked endplate potentials (EPPs) in the muscle

(Fig. 4-8A). In these recordings, we applied 2 μ M ω -conotoxin in order to prevent muscle contractions that interfere with stable recordings (Cruz et al., 1985). The amplitude and the quantal content of the EPPs were decreased \sim 2-fold in synaptotagmin-2 deficient NMJs when compared to wildtype littermate controls (Figs. 4-8B and 8C, amplitude: KO = 8.6 ± 1.5 mV, n=25; WT = 23.0 ± 1.4 , n=28, $p < 0.001$; quantal content [evoked EPP amplitude/mEPP amplitude]: WT = 15.3 ± 0.9 , n=28; KO = 7.0 ± 1.2 , n=25, $p < 0.001$). Thus less acetylcholine is released per action potential in NMJs from mutant mice than from control mice. At the same time, the speed with which the EPPs increases when an action potential is triggered was decreased \sim 3-fold in synaptotagmin-2 deficient NMJs compared to wildtype control NMJs (Fig. 4-8C; KO = 6.2 ± 1.0 mV/ms, n=25; WT = 20.4 ± 1.4 mV/ms, n=28, $p < 0.01$). Since the amplitudes and the rise kinetics of mEPPs were not altered in the synaptotagmin-2 KO mice (Fig. 4-7), these data demonstrate that the Ca^{2+} -triggered stimulation of vesicle release but not the filling or fusion of individual vesicles are impaired in the synaptotagmin-2 deficient NMJs.

A plausible explanation for the changes in evoked EPPs in synaptotagmin-2 deficient NMJs is that the release probability is decreased. To test this hypothesis with an independent method, we made use of the fact that a decreased release probability induces increased facilitation in response to either two closely spaced action potentials (paired-pulse facilitation) or action potential trains (Zucker and Regehr, 2002). When two or more action potentials invade a nerve terminal in rapid succession, residual Ca^{2+} in the vicinity of presynaptic Ca^{2+} channels builds up and enhances the probability of vesicle release within this local Ca^{2+} -domain for each subsequent action potential (Katz and

Miledi, 1968). The lower the initial release probability, the more facilitation can be achieved.

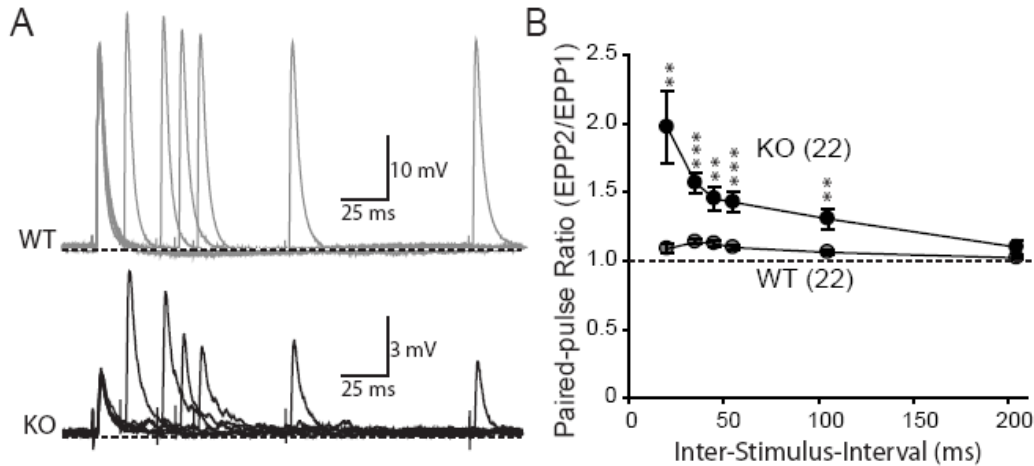


Figure 4-9 Paired-pulse facilitation.

A, Representative traces of paired-pulse stimuli induced synaptic responses in wildtype (WT) and synaptotagmin-2 KO NMJ. **B**, Paired-pulse ratio of evoked endplate potential (EPP) when given two stimuli at different inter-stimulus-intervals ranging from 20-100 ms. Numbers of recordings are indicated in parentheses. ** P<0.01; *** P<0.001.

We first examined paired-pulse facilitation with inter-stimulus-intervals ranging from 20 - 200 ms (Fig. 4-9A). Under the conditions used, we observed little facilitation in wildtype control NMJs, but a large degree of paired-pulse facilitation in synaptotagmin-2 deficient NMJs than in control NMJs at all intervals tested except for the 200 ms interval (Fig. 4-9B).

We next monitored EPPs that were evoked by 10 Hz – 50 Hz stimulus trains (Fig. 4-10). At 20 Hz, wildtype NMJs exhibited a small amount of initial facilitation followed by moderate depression that leads to a steady-state response. Both the facilitation and depression are evident in plots of either the absolute or the normalized

EPP amplitudes (Figs. 4-10A-10C). At 10 Hz and 20 Hz stimulation frequencies, synaptotagmin-2 deficient NMJs different from control NMJs exhibited continued facilitation without depression. The facilitation in the mutant NMJs was much larger than the initial facilitation observed in wildtype NMJs, (Fig. 4-10D). The initial EPP amplitude in synaptotagmin-2 deficient NMJs was ~2-fold lower than in wildtype control NMJs (see also Fig. 4-8B), but the facilitation increased the steady-state EPP amplitudes in the mutant NMJs to a level that was almost the same as that in the wildtype NMJs (Fig. 4-10B). These results strongly support the notion of a decreased release probability, a conclusion that is further supported by the finding that synaptotagmin-2 deficient NMJs exhibited a failure rate at 10 Hz and 20 Hz of $6.0 \pm 1.6\%$ and $1.5 \pm 0.7\%$, respectively, whereas no failures were detected in wildtype control synapses. The relative decrease in the failure rate at 20 Hz was probably due to the facilitation during repetitive stimulations. Note that during 50 Hz stimulus trains, however, we observed no facilitation in the mutant NMJs and could not determine the failure rate, probably because release becomes largely desynchronized at 50 Hz (see below).

4.3.8 Desynchronization of evoked vesicle release during repetitive stimulation

During studies of EPPs in response to high-frequency stimulus trains, we observed that release became highly desynchronized in mutant but not wildtype NMJs (Fig. 4-11A). Desynchronization became evident already at 10 Hz stimulation frequencies, resulting in an increasing number of sub-maximal release events during the

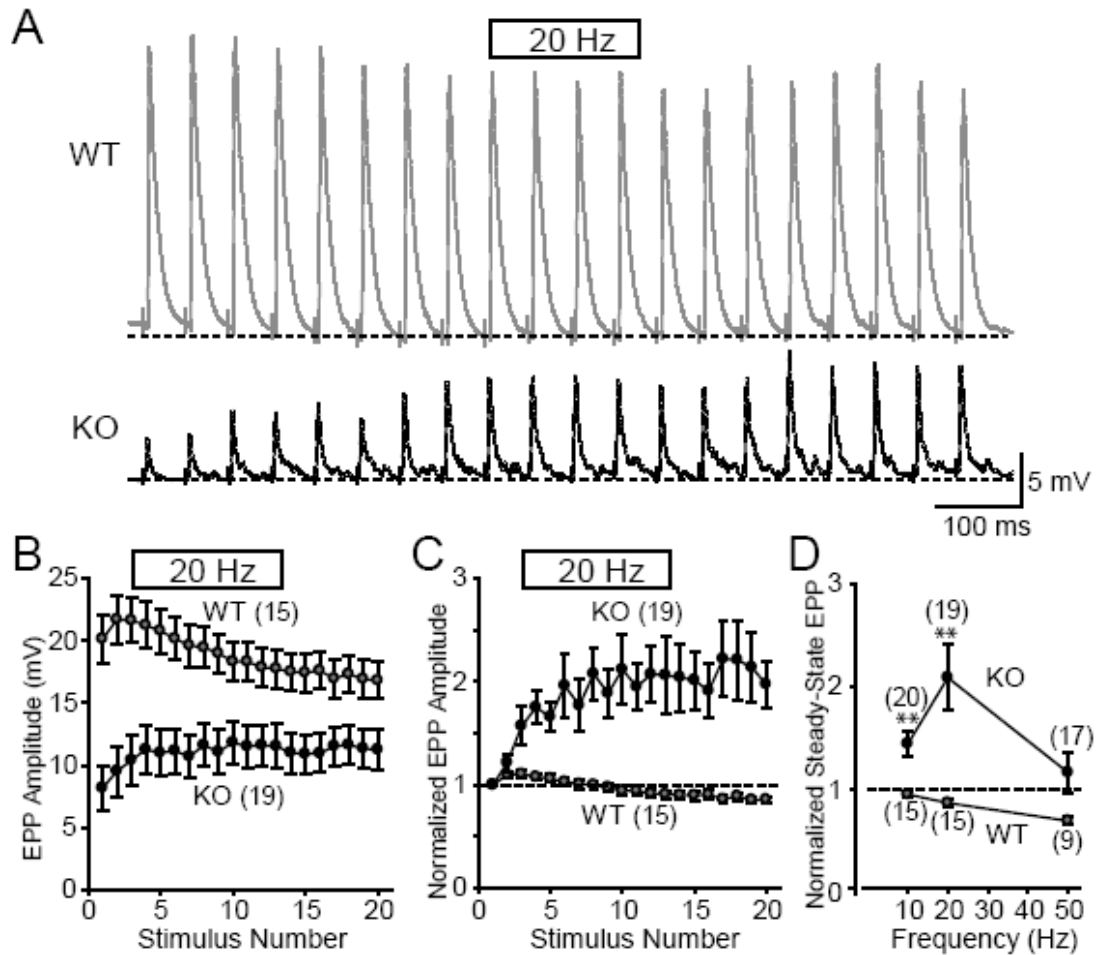


Figure 4-10 Short-term plasticity of evoked endplate potentials (EPP) in NMJ.

A, Representative traces of EPPs evoked by a 20 Hz stimulus train in wildtype (WT) and synaptotagmin-2 KO NMJs. **B** and **C**, Pooled data showing the absolute (**B**) and normalized amplitudes (**C**) of EPPs evoked at 20 Hz. Wildtype EPPs are larger (see Fig. 4-8B), and exhibit a moderate initial facilitation followed by depression. KO EPPs show facilitation. **D**, Normalized amplitudes of the steady-state EPPs as a function of stimulation frequency. Steady-state EPP amplitudes are the average of the last five responses during 1s of train stimulation at 10, 20 and 50 Hz. Steady-state EPP values are the averages of the last 5 responses during the train of stimulation. Numbers of recordings are indicated in parentheses. ** p<0.01.

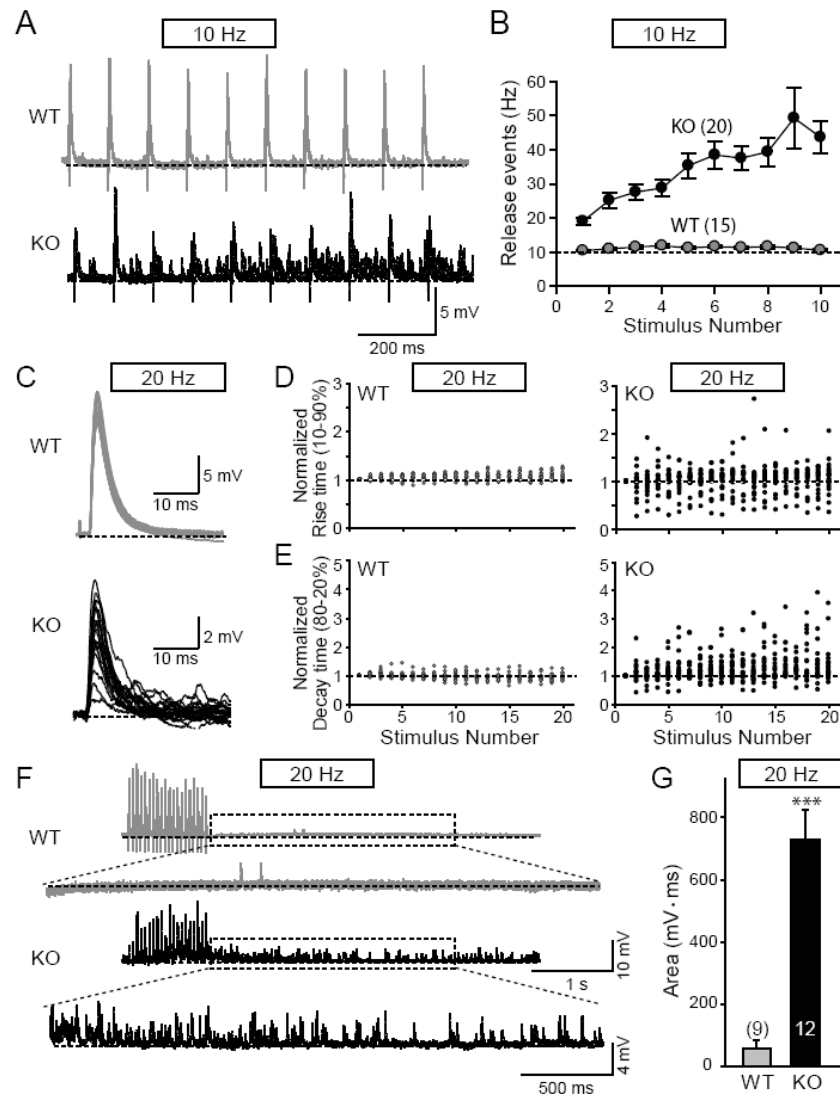


Figure 4-11 Desynchronization of EPPs during high-frequency stimulus trains in synaptotagmin-2 deficient NMJs.

A, Representative traces (superimposed 4 consecutive traces at 7s interval) of wildtype (WT) and synaptotagmin-2 KO when given 10 Hz stimulation to the phrenic nerve. **B**, Frequency of individual release events during 10 Hz stimulus trains plotted as a function of the stimulus number. Synaptic events were counted manually. **C**, Superimposed individual responses after phrenic nerve stimulation at 20 Hz for 1 s. **D & E**, Distributions of rise time (10-90%) and decay time (80-20%) normalized to the first response plotted as a function of stimulus number (WT: n=15, KO: n=19). **F**, Representative traces of repetitive stimulation at 20 Hz for wildtype and synaptotagmin-2 deficient NMJs. Lower traces represent enlargements of the traces for 3 s after 100 ms of the last stimulus. **G**, Integrated area under the peaks for 3 s after 50 ms of the last stimulus after a 1 s 20 Hz stimulus train. Integrated areas were plotted instead of event frequencies because the synaptotagmin-2 deficient NMJs have such high frequencies that they are impossible to accurately measure. Numbers of recordings are indicated above or within each bar. *** p<0.001.

stimulus train (Fig. 4-11B). Similar increases of synaptic release were seen at other stimulus frequencies (20, 50, 100 and 200 Hz, data not shown). Moreover, the evoked responses in wildtype NMJs remained completely synchronized throughout the stimulus trains (Fig. 4-11C) as revealed by plotting the 10-90% rise times and the 80-20% decay times as a function of stimulus numbers (Figs. 11D and 11E). In contrast, in synaptotagmin-2 deficient NMJs evoked responses became desynchronized as uncovered by the same plots which demonstrate that the rise and decay times become highly variable with increasing number of stimuli applied at 20 Hz (Figs. 11D and E), indicating the release is largely asynchronous. A similar desynchronization was seen in synaptotagmin-2 deficient NMJs under other frequencies stimulation (data not shown). These results suggest that during high stimulus trains, synchronous release is increasingly ineffective in synaptotagmin-2 deficient NMJs, and the accumulating Ca^{2+} during the stimulus train as a result begins to trigger more and more asynchronous release.

Our findings for the EPPs at the NMJ differ from those obtained with synaptotagmin-1 deficient cultured forebrain neurons where we observed no increase in asynchronous release during the stimulus trains, but increased ‘delayed’ release after the stimulus trains (Maximov and Sudhof, 2005). However, even in wildtype forebrain neurons asynchronous release becomes the dominant form of release during the stimulus trains (Hagler and Goda, 2001; Ohtsuka et al., 2002), suggesting that asynchronous release is already saturated during the stimulus train in wildtype neurons, and thus cannot be further increased in mutant neurons. Since delayed release observed after the stimulus trains is

significantly increased in synaptotagmin-1 deficient forebrain neurons (Maximov and Sudhof, 2005), we tested whether delayed release is also increased in NMJs lacking synaptotagmin-2 (Fig. 4-11F). We observed a dramatic (~10-fold) increase in delayed release in the NMJs (Fig. 4-11G). In these measurements, we integrated the area under the events for 3 s after a 1 s stimulus train applied at 20 Hz because individual release events could not be resolved due to their high frequency in synaptotagmin-2 deficient NMJs.

4.4 DISCUSSION

Synaptotagmin-1 and -2 are closely related synaptotagmin isoforms with similar, although slightly different Ca^{2+} -binding properties (Nagy et al., 2006; Sugita et al., 2002), but distinct expression patterns (Geppert et al., 1991; Marqueze et al., 1995; Perin et al., 1990; Ullrich et al., 1994). Rescue experiments of synaptotagmin-1 deficient neurons and chromaffin cells revealed that synaptotagmin-2 can rescue the synaptotagmin-1 deficiency phenotype (Nagy et al., 2006; Stevens and Sullivan, 2003). Moreover, a mutant mouse in which synaptotagmin-2 carries a point mutation exhibits a defect in synaptic transmission in selected synapses (Pang et al., 2006b). These experiments suggested that synaptotagmin-2 functions as a Ca^{2+} -sensor analogous to synaptotagmin-1 in release, but left open the question of the biological significance of synaptotagmin-2. Specifically, since no null mutant of synaptotagmin-2 was available, these previous experiments raised the question whether synaptotagmin-2 is an essential synaptotagmin isoform, and if so, what its essential functions are.

In the present study, we generated KO mice in which lacZ was knocked into exon 2 of the synaptotagmin-2 gene, creating a synaptotagmin-2 null allele that places expression of β -galactosidase under the control of the synaptotagmin-2 promoter. These mice allowed us to address four questions: 1. Where precisely is synaptotagmin-2 expressed in brain? 2. What is the consequence of deleting synaptotagmin-2 for mouse development, survival, and behavior? 3. What role does synaptotagmin-2 have in synapses formed by forebrain neurons that express synaptotagmin-2? 4. What is the role of synaptotagmin-2 in NMJ synapses formed by spinal cord neurons? Overall, our results support the previous hypothesis that synaptotagmin-2 functions as a Ca^{2+} -sensor in release similar to synaptotagmin-1, but reveal a vital biological difference between these two synaptotagmins: whereas synaptotagmin-1 is absolutely essential for fast Ca^{2+} -triggered release in excitatory and inhibitory cortical and hippocampal neurons, in those synapses that we studied here (synapses formed by neostriatal neurons and NMJ synapses formed by spinal cord neurons), synaptotagmin-2 contributes to fast Ca^{2+} -triggered release, but is not solely responsible for it. At least in the case of the NMJs, synaptotagmin-2 is complemented by co-expressed synaptotagmin-1. Thus, although synaptotagmin-1 and -2 likely perform similar functions, they perform these functions in a distinct biological context.

Expression pattern of synaptotagmin-2

Our data, in extension of previous studies that mapped the expression of synaptotagmin-2 by immunoblotting and *in situ* hybridization (Geppert et al., 1991; Marqueze et al., 1995; Ullrich et al., 1994), demonstrate that synaptotagmin-2 is

expressed in a restricted subset of forebrain neurons and in the majority of brainstem and spinal cord neurons. The forebrain and cerebellar expression pattern is interesting in that it appears to selectively involve inhibitory neurons, e.g. striatal neurons, neurons in the reticular nucleus of the thalamus, cerebellar Purkinje cells, and hypothalamic neurons. In some areas, most inhibitory neurons appear to express synaptotagmin-2 (e.g., striatum and cerebellar Purkinje cells), whereas in others, only a tiny percentage of inhibitory neurons seem to contain synaptotagmin-2 (e.g., cerebral cortex and hippocampus). In contrast to the forebrain, the majority of both excitatory and inhibitory neurons and cholinergic motoneurons in the brainstem and spinal cord express synaptotagmin-2. This leads to a strong expression of synaptotagmin-2 in NMJs. Somewhat surprisingly, we found that at least in the case of NMJs, synaptotagmin-2 and synaptotagmin-1 are co-expressed with an expression pattern that appears to be stochastic (Fig. 4-5) in that NMJs formed on the same muscle sometimes contain both synaptotagmin-1 and -2, and other times contain only synaptotagmin-2.

Synaptotagmin-2 is essential for survival of adolescent mice

Deletion of synaptotagmin-2 does not have a major effect on mouse survival or growth in the first postnatal week, but the mutant mice stop growing at the end of the second postnatal week, and die without exception in the third postnatal week. Thus synaptotagmin-2 is clearly not essential for fundamental nervous system activities such as breathing or feeding, a surprising result considering its prominent expression in motoneurons and the brainstem. The mice do not appear to have a developmental abnormality based on studies of brain morphology by light microscopy, and on the fact

that the protein composition of the brain and spinal cord is not significantly altered apart from a moderate increase in synaptotagmin-1 (Table 1). Immunofluorescence experiments indicated that there is no major developmental switch in synaptotagmin-2 expression in the second or third postnatal week that would explain the period of lethality of the synaptotagmin-2 deletion. Although it is at present unclear why synaptotagmin-2 KO mice initially appear normal, but then suffer from increasing weakness and die after three weeks, a plausible explanation based on the electrophysiological recordings and immunocytochemistry is that initially the co-expression of synaptotagmin-1 and -2 at least in the NMJ enables NMJs to compensate for the loss of synaptotagmin-2, but that in adolescent mice this compensation increasingly fails because the NMJs have to function more stringently as the mice become older.

Effect of the synaptotagmin-2 deficiency on inhibitory synaptic transmission in neostriatal neurons

We analyzed IPSCs elicited by action potentials in inter-neuronal synapses formed by cultured neostriatal neurons (Fig. 4-6). Deletion of synaptotagmin-2 caused a discrete release phenotype in these neurons: although the amplitude and charge transfer of the IPSCs was not significantly altered, the time course of release was significantly delayed in the synaptotagmin-2 deficient neurons than in littermate control neurons. The most dramatic change was a >2-fold increase in the time constant of the slow constituent of the IPSC. At the same time, the kinetics of spontaneous ‘mini’ IPSCs was unchanged, demonstrating that the delayed time course of evoked release in striatal synapses is not due to a change in receptor kinetics (Fig. 4-6 H-K). Thus synaptotagmin-2 is not essential

for neurotransmitter release in striatal neurons, but contributes dramatically to accelerate the release process, possibly because it is co-expressed with a second Ca^{2+} -sensor for fast release that almost completely compensates for the loss of synaptotagmin-2.

Synaptic transmission in NMJs from synaptotagmin-2 deficient mice

NMJ function exhibited six major changes in synaptotagmin-2 deficient mice:

1. Spontaneous release is increased >10-fold, independent of whether Ca^{2+} was chelated in the NMJ terminals or not (Fig. 4-7). This change is similar to the change we previously observed in mutant mice containing a point mutation in the synaptotagmin-2 gene (Pang et al., 2006b), demonstrating that this phenotype is not due to a particular strain or expression level of synaptotagmin-2.

2. The amplitude and quantal content of action potential-evoked synaptic release is dramatically decreased in mutant NMJs (Fig. 4-8). The scatter diagram in Fig. 4-8 shows that the variability among samples in the size of the synaptic responses was large; nevertheless, the average size of the amplitude and quantal content is decreased >2-fold. Moreover, similar to the cultured striatal neurons, the speed with which synaptic responses develop is decreased significantly in synaptotagmin-2 deficient NMJs.

3. In the mutant NMJs, the decrease in evoked release is accompanied by an increase in the paired-pulse ratio of synaptic responses (Fig. 4-9), indicating a reduction in synaptic release probability.

4. High-frequency stimulus trains (10, 20, or 50 Hz) produce a reliable synaptic response in wildtype mice, with only moderate facilitation or depression under the conditions used here (Fig. 4-10). In contrast, the same stimulus trains produce dramatic

facilitation in synaptotagmin-2 deficient NMJs at 10 or 20 Hz, whereas at 50 Hz no facilitation is observed, presumably because the NMJ membrane trafficking machinery becomes exhausted. These results are consistent with the notion that the release probability is reduced in synaptotagmin-2 deficient NMJs, but that the build-up of Ca^{2+} during the stimulus trains partially rescues the impairment of synaptic release (Fig. 4-10).

5. During high-frequency stimulus trains, vesicle release becomes highly asynchronous in synaptotagmin-2 deficient NMJs when residual Ca^{2+} accumulates (Fig. 4-11). This process becomes manifest by the large increase in the number of 'mini' events during the stimulus train (Fig. 4-11A and 11B), and the dramatic scattering of rise- and decay-times of EPPs during the train as a function of the number of stimuli applied (Figs. 11C-11E).

6. After a stimulus train, delayed release persists for several seconds in mutant NMJs, manifested as an increased number of spontaneous release events (Fig. 11F and 11G), which is similar to what we previously observed in cultured synaptotagmin-1 deficient cortical neurons (Maximov and Sudhof, 2005). These results indicate that similar to synaptotagmin-1, synaptotagmin-2 restricts delayed asynchronous release induced by residual Ca^{2+} after action potential trains.

In summary, our results demonstrate that synaptotagmin-2 plays an important role in the Ca^{2+} -triggering of neurotransmitter release in synapses formed by striatal neurons and in NMJ synapses, but that the loss of synaptotagmin-2 from these structures does not lead to a complete loss of release in these synapses. Although the reason for the

co-expression of multiple Ca^{2+} -sensing synaptotagmins in a particular synapse such as the NMJ or the synapses formed by striatal neurons remains unclear, it seems likely that the evolutionary diversification of synaptotagmin-1 into multiple similar isoforms that include synaptotagmin-2 served a regulatory role, possibly mediated by different regulatory properties of the different synaptotagmins. Future experiments will have to address this interesting and important question.

CHAPTER V: A TWO Ca^{2+} -SENSOR MODEL FOR NEUROTRANSMITTER RELEASE IN THE CALYX OF HELD SYNAPSE

5.1 Introduction

Two modes of Ca^{2+} -triggered neurotransmitter release were described. Fast synchronous release predominates in all synapses during low-frequency action-potential firing (Meinrenken et al., 2003; Schneggenburger and Neher, 2005). Slower asynchronous release mediates synaptic transmission in some synapses during high-frequency action-potential firing (Atluri and Regehr, 1998; Hagler and Goda, 2001; Hefft and Jonas, 2005; Lu and Trussell, 2000; Otsu et al., 2004), but remains a minor component in other synapses (Meinrenken et al., 2003; Schneggenburger and Neher, 2005). The most precise measurements of fast synchronous release were obtained in the calyx of Held synapse that allows simultaneous patching of pre- and postsynaptic neurons, and enables measurements of Ca^{2+} -currents and the capacitance of nerve terminals (Bollmann et al., 2000; Borst and Sakmann, 1996; Forsythe, 1994; Schneggenburger and Neher, 2000; Sun and Wu, 2001). Measurements of the apparent Ca^{2+} -affinity and -cooperativity of release in calyx synapses using Ca^{2+} -photolysis revealed that the Ca^{2+} -sensor for synchronous release exhibits an apparent cooperativity of ~ 5 , and an apparent K_d of ~ 10 (Bollmann et al., 2000) or $\sim 105 \mu\text{M}$ Ca^{2+} (Schneggenburger and Neher, 2000). In vertebrates, synaptotagmin-1, -2, and -9 function as Ca^{2+} -sensors for fast synchronous release (Fernandez-Chacon et al., 2001; Geppert et al., 1994; Nagy et al., 2006; Pang et al., 2006a; Stevens and Sullivan, 2003; Xu et al., 2007), with a binding stoichiometry of 5

Ca^{2+} -ions/molecule and an apparent micromolar Ca^{2+} -affinity that correlate well with that of synchronous release. Of these synaptotagmins, synaptotagmin-2 is a likely Ca^{2+} -sensor for synchronous release at the calyx synapse because a mutation that depresses synaptotagmin-2 levels decreases release from calyx terminals, although no null-mutants were examined (Pang et al., 2006b). The calyx Ca^{2+} -photolysis experiments allowed formulation of quantitative models of release that are based on the assumption of a single Ca^{2+} -sensor and are widely applicable (Bollmann et al., 2000; Schneggenburger and Neher, 2000). These models, however, are inaccurate for low Ca^{2+} -concentrations, and do not account for asynchronous release. To remedy this problem, a recent refined model proposes an allosterically modulated release machinery, but still does not account for asynchronous release and does not predict release at low Ca^{2+} -concentrations accurately (Lou et al., 2005). Thus at present, no accurate quantitative model for neurotransmitter release is available.

In synapses that exhibit predominantly asynchronous release during high-frequency action-potential trains, asynchronous release out-competes synchronous release during the stimulus train (Atluri and Regehr, 1998; Hagler and Goda, 2001; Hefft and Jonas, 2005; Lu and Trussell, 2000; Otsu et al., 2004). Measurements of asynchronous release suggested a higher apparent Ca^{2+} -affinity but the same Ca^{2+} -cooperativity as synchronous release (Goda and Stevens, 1994; Ravin et al., 1997), which would explain the ability of asynchronous release to outcompete synchronous release during high-frequency stimulus trains because accumulating residual Ca^{2+} would trigger asynchronous release in the intervals between action potentials at Ca^{2+} -levels at which

synchronous release cannot be induced. Consistent with this notion, Ca^{2+} -chelators such as EGTA abolish asynchronous release during high-frequency action potential trains but have less effect on synchronous release (Atluri and Regehr, 1998; Hagler and Goda, 2001; Hefft and Jonas, 2005; Lu and Trussell, 2000; Otsu et al., 2004). According to this view, synapses in which asynchronous release does not predominate during high-frequency trains, such as the calyx synapse, either lack asynchronous release entirely, and/or do not accumulate residual Ca^{2+} during stimulus trains because of efficient Ca^{2+} -buffers and Ca^{2+} -extrusion mechanisms (Chuhma and Ohmori, 2002; Schneggenburger and Forsythe, 2006). Moreover, the similar apparent Ca^{2+} -cooperativity of synchronous and asynchronous release suggested that asynchronous release could be a modification of synchronous release (Lou et al., 2005), suggesting that there is no separate universal asynchronous release pathway (Schneggenburger and Forsythe, 2006). Evaluating this fundamental issue in synaptic transmission is difficult because asynchronous release has primarily been characterized in synapses that have a strong synchronous release component which could have contaminated the measurements (Goda and Stevens, 1994; Ravin et al., 1997), and the biophysical properties of asynchronous release remain largely unknown. These questions have wide implications for our understanding of synaptic transmission because an accurate description of asynchronous release is required for any quantitative model of synaptic transmission. We now provide such a description in the calyx of Held synapse, and demonstrate that asynchronous release represents a separate and distinct release pathway that is likely to be universally present in synapses.

5.2 Material and Methods

5.2.1 Synaptotagmin-2 KO mice Mice lacking synaptotagmin-2 were described in detail earlier (Chapter IV), and were bred using standard mouse husbandry procedures. All analyses were performed on littermate offspring from heterozygous matings, with "wild-type mice" being either homo- or heterozygous for the wild-type allele.

5.2.2 Immunofluorescence labeling. Brainstems from mice at P5-P14 as indicated were removed after decapitation, immersed immediately in fresh 4% paraformaldehyde, and incubated overnight at 4 °C, followed by a second overnight incubation in 30% sucrose in phosphate-buffered saline. Sections (30 µm) were cut on a Leica CM3050S cryostat, incubated in primary antibodies (syt1: 41.1, 1:5,000; synaptotagmin-2: A320, 1:500; Synapsin: C110.22, 1:1,000 or E028, 1:1,000) again overnight at 4 °C, and then stained with Alexa Fluor conjugated secondary antibodies (Molecular Probes) at a dilution of 1:400 for 2 hrs at room temperature. Sections were washed, mounted, and viewed in a confocal microscope.

5.2.3 Slice electrophysiology. Brain slices (200 µm) containing MNTB were prepared in a parasagittal orientation from P7-P9 mice (for double patch or presynaptic cell-attached recording), or in a transverse orientation from P10-P14 mice (for fiber stimulation and purely post-synaptic recordings) were employed for single and/or double whole-cell recordings of nerve terminals and MNTB neurons largely as described (Sakaba and Neher, 2001; Sun et al., 2006). All experiments involved postsynaptic whole-cell recordings with an Axopatch 200B amplifier (Axon Instruments Inc., CA). Presynaptic whole-cell recordings were obtained with an EPC-9 amplifier (HEKA, Lambrecht,

Germany). The pre- and postsynaptic series resistances ($<15\text{ M}\Omega$ and $7\text{ M}\Omega$) were compensated by 60% and 98% (lag 10 ms), respectively. Both pre- and postsynaptic currents were low-pass filtered at 5 kHz and digitized at 20 kHz. Six recording configurations were employed:

- a.** Presynaptic cell-attached current injections to induce presynaptic action-potential trains with postsynaptic whole-cell recordings that monitor the evoked EPSCs (Fig. 4-1c). Stimulations were applied as 40 presynaptic current injections of 1 nA for 3 ms at 50 Hz.
- b.** Presynaptic afferent fiber stimulations with postsynaptic whole-cell voltage-clamp recordings (Fig. 5-2). Stimuli were applied with a bipolar electrode delivering 3-30 V for 0.1 ms.
- c.** Double-patch recordings by simultaneous pre- and postsynaptic whole-cell voltage-clamp recordings to measure the presynaptic RRP and Ca^{2+} -currents (Figs. 5-3a to 3g). Stimulations consist of a presynaptic 4 ms prepolarization to 70-80 mV, followed by 50 ms depolarization to 20 mV.
- d.** Sucrose stimulation with postsynaptic whole-cell voltage clamp recordings to measure the RRP (Figs. 5-3h and 3i). Stimulation involves puffing 2 M sucrose in bath solution onto the target terminal with a pipette that is located about 5 μm from the calyx.
- e.** Double patch experiments for simultaneous measurements of presynaptic $[\text{Ca}^{2+}]_i$ and postsynaptic EPSCs with manipulation of the presynaptic $[\text{Ca}^{2+}]_i$ (Fig. 4-4). Stimulations were effected either by dialysis of Ca^{2+} -containing

solutions into the terminal via the presynaptic pipette solution (Fig. 5-4**a,b**), or by flash photolysis of DM-nitrophen/ Ca^{2+} (Fig. 5-4**c,d**). Release rate was estimated by deconvolution (Sakaba and Neher 2001).

- f. Mini recordings were carried out under two conditions: 1). Standard recordings using a bath solution containing (in mM): 125 NaCl, 2.5 KCl, 1 MgCl_2 , 2 CaCl_2 , 25 dextrose, 1.25 NaH_2PO_4 , 0.4 ascorbic acid, 3 *myo*-inositol, 2 Na-pyruvate, 25 NaHCO_3 and 0.01 bicuculline, 0.01 strychnine, 0.05 D-AP5 (pH 7.4). 2). Under Ca^{2+} -free conditions using the same bath solution without Ca^{2+} , and additionally dialyzing via a patch pipette into the presynaptic terminal the following solution containing in mM: 125 K-gluconate, 20 KCl, 4 MgATP, 10 Na_2 -phosphocreatine, 0.3 GTP, 10.5 EGTA, 5 BAPTA and 10 HEPES-NaOH pH 7.2.

All recordings were performed in the presence of 50 μM D-AP5 in the bath; in addition, for the double-patch experiments in c and e, we added 0.1 mM cyclothiazide and 1 mM kynurenic acid (c) or 2 mM γ -DGG when strong flash photolysis was given resulting in $[\text{Ca}^{2+}]_i$ of $>3 \mu\text{M}$, in which case the obtained EPSCs were multiplied by 2 because control experiments determined that 2 mM γ -DGG decreased the EPSC amplitude 2-fold.

5.2.3 Ca^{2+} -uncaging and Ca^{2+} -imaging. The Ca^{2+} -uncaging and Ca^{2+} -imaging setup used an intense UV pulse from a frequency-tripled YAG-ND laser (355 nm, Surelite I, Continuum, CA) for Ca^{2+} -uncaging. Ca^{2+} -concentrations were measured *in situ* by ratiometric fluorescence imaging of nerve terminals filled with fura-2, fura-4F, or

fura-6F (Grynkiewicz et al., 1985). Ca^{2+} -indicator dyes were excited with a UV light source at 340 nm and 380 nm (energy $\leq 175\text{W}$) using a monochromator (DG-4, Sutter Instrument, CA). The laser pulse was coupled into the epifluorescence port of an Axioskop and combined with the UV light using a beam-splitter (customized 90%T/10%R for 355 nm with a bandwidth of <10 nm, Chroma Tech, VT). Both UV beams were collimated to optimize the intensity on the targeted terminal. A CCD camera (ORCA-ER, Hamamatsu, Japan) with on-chip binning was used to capture infrared images (300×300 pixels) and Ca^{2+} -images (19×19 pixels) of the terminal. The fluorescence in the measuring area with background fluorescence subtraction (off-line) was used to calculate the $[\text{Ca}^{2+}]_i$. Images were captured using MetaFluor software and analyzed by IgorPro (Wavemetrics). For *in vivo* calibration of Ca^{2+} -indicator signals, we introduced Ca^{2+} indicators with an intracellular K-Gluconate pipette solution into the terminal. For fura-2 imaging, we used exposure times of 100 ms with a 2 Hz capture rate. For fura-4F and fura-6F imaging, we used 10 ms exposure times with 2 Hz capture rates before the flash, and 10-30 Hz capture rates after the flash. Ca^{2+} -relaxation rates were modulated by the UV-illumination during the ratiometric Ca^{2+} -imaging procedure which was thus adjusted to maintain stable Ca^{2+} -levels.

5.2.4 Data processing and modeling. Release rates were calculated using the Neher deconvolution program (<http://www.mpibpc.mpg.de/groups/neher/software/index.html>) with an mEPSC size of 30 pA and a measured waveform (Sakaba and Neher, 2001).

5.2.5 Modeling. We applied the different kinetic models to fit the data in our experiments (Fig.5-5a,b). The conventional one Ca^{2+} -sensor kinetic model and the allosteric one Ca^{2+} -sensor kinetic model were simulated as described (Bollmann et al., 2000; Lou et al., 2005; Schneggenburger and Neher, 2000). In our two Ca^{2+} -sensor model, each vesicle in the RRP can be released via three independent pathways: 1) Ca^{2+} -independent fusion in the spontaneous mode, i.e. direct exocytosis of vesicles from the RRP with a release rate of γ_1 . An effectivity factor (C) to account for the change in spontaneous release rate in synaptotagmin-1 and -2 deficient synapses was included; 2) Synchronous Ca^{2+} -evoked fusion mode triggered by full occupancy of the 5 binding sites of the synchronous release Ca^{2+} -sensor (Bollmann et al., 2000; Lou et al., 2005); 3) Asynchronous Ca^{2+} -evoked release triggered by occupancy of 2 Ca^{2+} -binding sites of an unidentified Ca^{2+} -sensor. The Ca^{2+} binding states can be defined by $X_n Y_m(t)$, where X_n represents the state in which n binding sites of the Ca^{2+} -sensor for synchronous release have been occupied ($n=0-5$), and Y_m the state in which m binding sites of Ca^{2+} -sensor of asynchronous release have been occupied ($m=0-2$). α and β represent the binding and dissociation constants, respectively, of the Ca^{2+} -sensor for synchronous release, and χ and δ the binding constants for asynchronous release, respectively. b is the cooperativity factor (Heidelberger et al., 1994). Note that $X_0 Y_0|_{t=0} = \text{RRP}$. The kinetics of Ca^{2+} -binding states can be described as:

when $0 < n < 5, 0 < m < 2$:

$$d(X_n Y_m)/dt = \alpha \cdot (5-n+1) \cdot X_{n-1} Y_m \cdot [\text{Ca}^{2+}]_i + \beta \cdot b^n \cdot (n+1) \cdot X_{n+1} Y_m - \alpha \cdot (5-n) \cdot X_n Y_m \cdot [\text{Ca}^{2+}]_i$$

$$\begin{aligned}
& - \beta \cdot b^{n-1} \cdot n \cdot X_n Y_m + \chi \cdot (2-m+1) \cdot X_n Y_{m-1} \cdot [Ca^{2+}]_i + \delta \cdot b^m \cdot \\
& (m+1) \cdot X_n Y_{m+1} \\
& - \chi \cdot (2-m) \cdot X_n Y_m \cdot [Ca^{2+}]_i - \delta \cdot b^{m-1} \cdot m \cdot X_n Y_m
\end{aligned}$$

when n=0, m=0:

$$\begin{aligned}
d(X_0 Y_0)/dt = & \beta \cdot X_1 Y_0 - 5 \cdot \alpha \cdot X_0 Y_0 \cdot [Ca^{2+}]_i + \delta \cdot X_0 Y_1 - 2 \cdot \chi \cdot X_0 Y_0 \cdot [Ca^{2+}]_i - \\
& \gamma_1 \cdot X_0 Y_0
\end{aligned}$$

when n=5

$$\begin{aligned}
d(X_n Y_m)/dt = & \alpha \cdot (5-n+1) \cdot X_{n-1} Y_m \cdot [Ca^{2+}]_i + \beta \cdot b^n \cdot (n+1) \cdot X_{n+1} Y_m - \alpha \cdot (5- \\
& n) \cdot X_n Y_m \cdot [Ca^{2+}]_i
\end{aligned}$$

$$\begin{aligned}
& - \beta \cdot b^{n-1} \cdot n \cdot X_n Y_m + \chi \cdot (2-m+1) \cdot X_n Y_{m-1} \cdot [Ca^{2+}]_i + \delta \cdot b^m \cdot \\
& (m+1) \cdot X_n Y_{m+1} \\
& - \chi \cdot (2-m) \cdot X_n Y_m \cdot [Ca^{2+}]_i - \delta \cdot b^{m-1} \cdot m \cdot X_n Y_m - \gamma_2 \cdot (X_n Y_m)
\end{aligned}$$

when m=2

$$\begin{aligned}
d(X_n Y_m)/dt = & \alpha \cdot (5-n+1) \cdot X_{n-1} Y_m \cdot [Ca^{2+}]_i + \beta \cdot b^n \cdot (n+1) \cdot X_{n+1} Y_m - \alpha \cdot (5- \\
& n) \cdot X_n Y_m \cdot [Ca^{2+}]_i
\end{aligned}$$

$$\begin{aligned}
& - \beta \cdot b^{n-1} \cdot n \cdot X_n Y_m + \chi \cdot (2-m+1) \cdot X_n Y_{m-1} \cdot [Ca^{2+}]_i + \delta \cdot b^m \cdot \\
& (m+1) \cdot X_n Y_{m+1} \\
& - \chi \cdot (2-m) \cdot X_n Y_m \cdot [Ca^{2+}]_i - \delta \cdot b^{m-1} \cdot m \cdot X_n Y_m - \gamma_3 \cdot (X_n Y_m)
\end{aligned}$$

The total release within Δt :

$$\begin{aligned}
f_{use}(t, \Delta t) = & [\gamma_1 \cdot X_0 Y_0 + \gamma_2 \cdot (X_5 Y_0 + X_5 Y_1 + X_5 Y_2) + \gamma_3 \cdot (X_0 Y_2 + X_1 Y_2 + X_2 Y_2 + X_3 Y_2 \\
& + X_4 Y_2 + X_5 Y_2)] \cdot \Delta t
\end{aligned}$$

Where: spontaneous release= $\gamma_1 \cdot X_0 Y_0 \cdot \Delta t$

synchronized release= $\gamma_2 \cdot (X_5 Y_0 + X_5 Y_1 + X_5 Y_2) \cdot \Delta t$

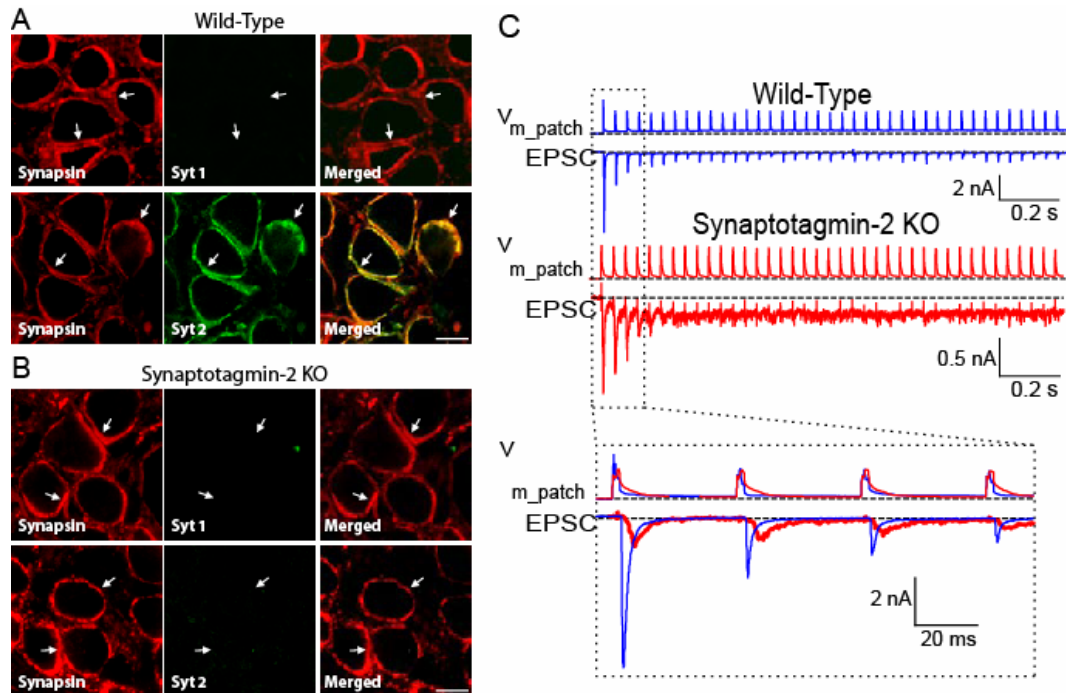
asynchronized release= $\gamma_3 \cdot (X_0 Y_2 + X_1 Y_2 + X_2 Y_2 + X_3 Y_2 + X_4 Y_2 + X_5 Y_2) \cdot \Delta t$

5.2.6 Miscellaneous. Immunofluorescence labeling and immunoblotting experiments were performed essentially as described (Pang et al., 2006a). All statistical analyses were performed using Student's t-test.

5.3. Results

5.3.1 *Synaptotagmin-2 deletion blocks synchronous release in calyx terminals*

Mice lacking synaptotagmin-2 initially develop normally, but perish after postnatal day 20 (P20), presumably because co-expression of synaptotagmin-1 in neuromuscular junctions and other essential synapses compensates for the loss of synaptotagmin-2 early in development, but fails to do so later (Pang et al., 2006a). Different from neuromuscular junctions, however, we detected no co-expression of synaptotagmin-1 with synaptotagmin-2 in the calyx of Held at any time between P5 and P14, or of synaptotagmin-9, which also serves as a Ca^{2+} -sensor for fast release (Xu et al., 2007) at P11 (Fig. 5-1a). Moreover, no compensatory increases of synaptotagmin-1 occur in calyces that lack synaptotagmin-2 (Fig. 5-1b). Thus, among the three synaptotagmins that serve as Ca^{2+} -sensors for synchronous release, the calyx expresses only synaptotagmin-2, presumably because synaptotagmin-2 is the fastest Ca^{2+} -sensor and the calyx synapse is specialized for precise fast responses.



Zhiping Pang and Jianyuan Sun

Figure 5- 1 Calyx synapses in synaptotagmin-2 deficient mice

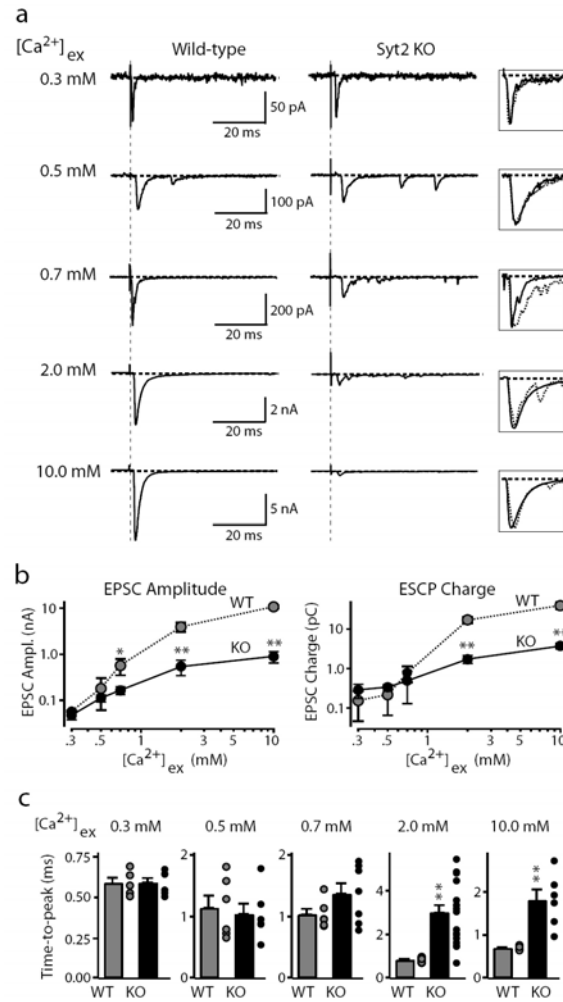
a. and b. Immunofluorescence analysis of brainstem sections from wild-type (a) and synaptotagmin-2 KO mice (b) at P11 with antibodies to synapsins (red; left panels) and synaptotagmin-1 or -2 (green; middle panels). Merged images are shown on the right with coincident staining in yellow. Scale bar = 10 μ m (applies to all panels); arrows point to synapses. Abbreviations: Syt1 and 2, synaptotagmin-1 and -2.

c. EPSCs recorded in response to 25 Hz action potential stimulation induced by a cell-attached presynaptic stimulation pipette (V_{m_patch} = extracellular voltage in the patched area). The insert at the bottom shows a superposition of wild-type and mutant traces.

To determine the effect of the synaptotagmin-2 deletion on release in calyx synapses, we examined brainstem slices from 7-9 day-old mice. Using cell-attached patches on calyx nerve terminals, we induced a train of presynaptic action potentials, and measured postsynaptic responses by whole-cell recordings (Fig. 5-1C). Strikingly, synaptic responses in synaptotagmin-2 deficient terminals were small and delayed, with

release being increasingly triggered in the inter-stimulus intervals during the stimulus train. These responses are consistent with the notion that in the absence of synaptotagmin-2 as the Ca^{2+} -sensor for synchronous release, accumulating Ca^{2+} during the stimulus train triggers asynchronous release.

To characterize the properties of this release, we evoked presynaptic action potentials by afferent fiber stimulations, and recorded EPSCs at different extracellular Ca^{2+} -concentrations ($[\text{Ca}^{2+}]_e = 0.3\text{-}10\text{ mM}$). At $0.3\text{-}0.7\text{ mM}$ $[\text{Ca}^{2+}]_e$, wild-type and mutant terminals exhibited similar amounts of release (Figs. 2a and 2b). At 2 mM and 10 mM $[\text{Ca}^{2+}]_e$, however, synaptotagmin-2 deficient terminals displayed >10-fold smaller EPSC amplitudes and charge transfers than wild-type terminals (Figs. 5-2a and 2b). Moreover, at 2 mM $[\text{Ca}^{2+}]_e$ (a nearly physiological concentration), synaptotagmin-2 deficient synapses were very slow: they required ~3-fold more time to reach the EPSC maximum (Fig. 4-2c), and exhibited ~5-fold slower release kinetics (measured as the time to achieve 50% synaptic charge transfer; WT = $4.9 \pm 0.7\text{ ms}$; Syt2 KO = $26.8 \pm 1.7\text{ ms}$; $p < 0.01$) We conclude that deletion of synaptotagmin-2 severely impairs synchronous release in the calyx of Held synapse but leaves a slower, asynchronous form of Ca^{2+} -triggered release intact.



Jianyuan Sun

Figure 5- 2 Synaptic transmission evoked by isolated action potentials

Postsynaptic voltage-clamp recordings of EPSCs evoked by afferent fiber stimulation in wild-type (left column) and synaptotagmin-2 deficient calyx synapses (right column) at the indicated $[Ca^{2+}]_{ex}$ in the presence of 50 μ M AP-5.

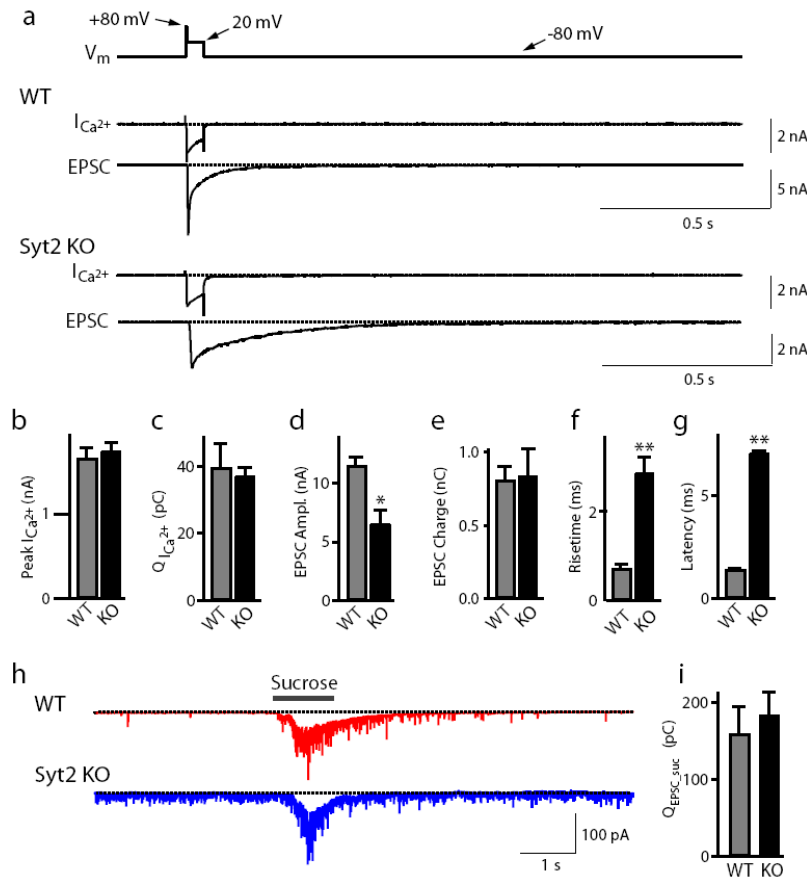
a. Representative EPSCs. Boxed traces on right display scaled superimposed EPSCs to illustrate EPSC kinetics.

b. Double-logarithmic plots of EPSC amplitudes (left panel) or EPSC charge transfer (right panel) as a function of $[Ca^{2+}]_{ex}$ (means \pm SEMs; number of recordings/ $[Ca^{2+}]_{ex}$: WT, 5/0.3 mM, 6/0.5 mM, 6/0.7 mM, 14/2 mM, 5/10 mM; KO, 6/0.3 mM, 6/0.5 mM, 7/0.7 mM, 17/2 mM, 6/10 mM).

c. Summary graphs of the time-to-peak of EPSCs recorded for the indicated $[Ca^{2+}]_{ex}$. For each Ca^{2+} -concentration, the bar depicts means \pm SEMs, and the dots on the right to the bar exhibit individual data points to illustrate the response variability in synaptotagmin-2 deficient terminals (*= $p < 0.05$; **= $p < 0.01$; Student's t-test).

In addition to blocking evoked synchronous release, the deletion of synaptotagmin-2, like that of synaptotagmin-1 in forebrain(Pang et al., 2006a)), increased the frequency of spontaneous release but did not alter the size and kinetics of spontaneous release events. Presynaptic introduction of 5 mM BAPTA/10 mM EGTA depressed the spontaneous release rate >5-fold both in wild-type and mutant calyx terminals. The frequency of the remaining Ca^{2+} -independent spontaneous release, however, was still 5-fold higher in synaptotagmin-2 deficient terminals than in wild-type terminals.

5.3.2 Synaptotagmin-2 deletion does not alter Ca^{2+} -currents and readily-releasable pool sizes. In presynaptic terminals of the calyx of Held, action potentials gate Ca^{2+} -influx via P/Q- and N-type Ca^{2+} -channels (Iwasaki and Takahashi, 1998; Wu et al., 1999). Since synaptotagmin-1 interacts with P/Q- and N-type Ca^{2+} -channels (Charvin et al., 1997; Leveque et al., 1994; Zhong et al., 1999), we tested whether deletion of synaptotagmin-2 impairs Ca^{2+} -channel function. We simultaneously patched presynaptic calyx terminals and postsynaptic MNTB neurons in the presence of tetrodotoxin (1 μM), kynurenic acid (1 mM), cyclothiazide (0.1 mM), and D-AP5 (50 μM), and recorded presynaptic Ca^{2+} -currents and postsynaptic EPSCs in response to prolonged depolarization using a standard prepolarization protocol (Sakaba and Neher, 2001) (4 ms prepolarization from -80 to +80 mV followed by 50 ms depolarization to +20 mV; Fig. 5-3a). Deletion of synaptotagmin-2 caused no detectable change in the peak Ca^{2+} -channel current (Fig. 5-3b) and electrical charge transfer mediated by presynaptic Ca^{2+} -



Jianyuan Sun

Figure 5- 3 RRP size, Ca^{2+} -currents, and release kinetics in synaptotagmin-2 deficient calyx synapses

a. Experimental protocol involving a short prepolarization followed by a long depolarization (top line), and representative traces of presynaptic Ca^{2+} -currents (I_{Ca}) and postsynaptic EPSCs induced by the depolarization in wild-type and synaptotagmin-2 deficient terminals (bottom traces). Experiments were performed by simultaneous pre- and postsynaptic voltage-clamp recordings in wild-type and synaptotagmin-2 deficient calyx terminals at P7–P9 in the presence of 0.1 μ M tetrodotoxin, 0.1 mM cyclothiazide, 1 mM kynurenic acid, and 50 μ M D-AP5.

b. and **c.** Quantitation of Ca^{2+} -currents and EPSC parameters induced by sustained presynaptic depolarization: Ca^{2+} -current amplitudes (**b**) and Ca^{2+} -current electrical charge (**c**, integrated over 100 ms).

d.-g. EPSC amplitudes (**d**), 20–80% rise times (**f**), latencies (**g**, from onset of Ca^{2+} -current to 10% of the EPSC), and charge (**e**, integrated over 2 s). Data shown are means \pm SEMs (WT: $n=12$; KO: $n=14$).

h. and **i.** Representative traces (**h**) and summary graphs of the electric charge transfer (**i**; integrated over 5 s) of synaptic responses induced by 1 s applications of 2 M sucrose via a glass pipette positioned ~ 5 μ m from the calyx (means \pm SEMs; WT: $n=10$; KO, $n=11$).

channels (Fig. 5-3c, integrated over 100 ms), suggesting that synaptotagmin-2 is not involved in regulating Ca^{2+} -channels.

The 50 ms depolarization in Fig. 4-3a depletes the readily-releasable pool (RRP) of vesicles by inducing a prolonged increase in intracellular $[\text{Ca}^{2+}]_i$ (Sakaba and Neher, 2001). Postsynaptic recordings of synaptic responses showed that deletion of synaptotagmin-2 depressed the peak amplitude of the depolarization-induced EPSC ~2-fold, slowed its risetime ~3-fold, and increased its latency ~5-fold (Figs. 5-3d,f). However, the synaptotagmin-2 deletion did not alter the total synaptic charge transfer (integrated over 2 s) induced by the 50 ms presynaptic depolarization (Fig. 5-3g). Thus, deletion of synaptotagmin-2 did not affect the size of the RRP, and asynchronous release can induce exocytosis of the entire RRP of vesicles in the absence of synaptotagmin-2, albeit with a much slower timecourse.

To compare the size of the RRP in wild-type and KO mice by an independent approach, we puffed 2 M sucrose solution onto the terminal for 1 s, and integrated the synaptic charge transfer of the induced EPSCs over 2 s (Figs. 5-3h and 3i). No difference between wild-type and synaptotagmin-2 deficient terminals was detected, confirming that the synaptotagmin-2 KO did not alter the size of the RRP. However, the absolute size of the RRP measured as the total postsynaptic charge transfer induced by sustained depolarization or by puffing of hypertonic sucrose was much larger in the case of the depolarization-induced EPSC than in the case of the sucrose-induced EPSC (Fig. 5-3). This difference may be due to the distinct measurement conditions used (EPSCs induced by depolarization but not by sucrose were monitored in the presence of cyclothiazide as a

blocker of receptor desensitization); in addition, Ca^{2+} -dependent mobilization of the RRP during the depolarization may have increased its size during the 2 s monitoring period (Stevens and Wesseling, 1998).

5.3.3 Ca^{2+} -dependence of synchronous and asynchronous release.

To characterize the Ca^{2+} -dependence of transmitter release at wild-type and synaptotagmin-2 deficient synapses, we determined the peak release rates in calyx terminals as a function of the presynaptic intracellular Ca^{2+} -concentration $[\text{Ca}^{2+}]_i$. For Ca^{2+} -concentrations of $<1 \mu\text{M}$, we injected terminals via the patch pipette with defined concentrations of CaCl_2 and Ca^{2+} -buffers. For Ca^{2+} -concentrations $>1 \mu\text{M}$, we injected terminals with caged Ca^{2+} (9 mM DM-nitrophen, 8.6 mM CaCl_2 , and various Ca^{2+} -buffers), and released the caged Ca^{2+} by flash photolysis with a laser pulse (Bollmann et al., 2000; Heidelberger et al., 1994; Mulkey and Zucker, 1991; Schneggenburger and Neher, 2000). This procedure produces a rapid and spatially uniform, defined rise in $[\text{Ca}^{2+}]_i$ that can be regulated by adjusting the charging voltage of the laser and the neutral density filter in the optic pathway. In all experiments, we monitored the intracellular Ca^{2+} -concentration in the terminals using co-injected Ca^{2+} -indicator dyes. In order to cover the entire range of Ca^{2+} -concentrations examined (0.1-15 μM), we employed three different Ca^{2+} -indicator dyes (Fura2, Fura-4F, and Fura-6F), and calibrated the Ca^{2+} -signals *in situ*. Finally, we quantified vesicle exocytosis by deconvolution of evoked EPSCs, using a measured miniature EPSC waveform to calculate the release rates (Sakaba and Neher, 2001).

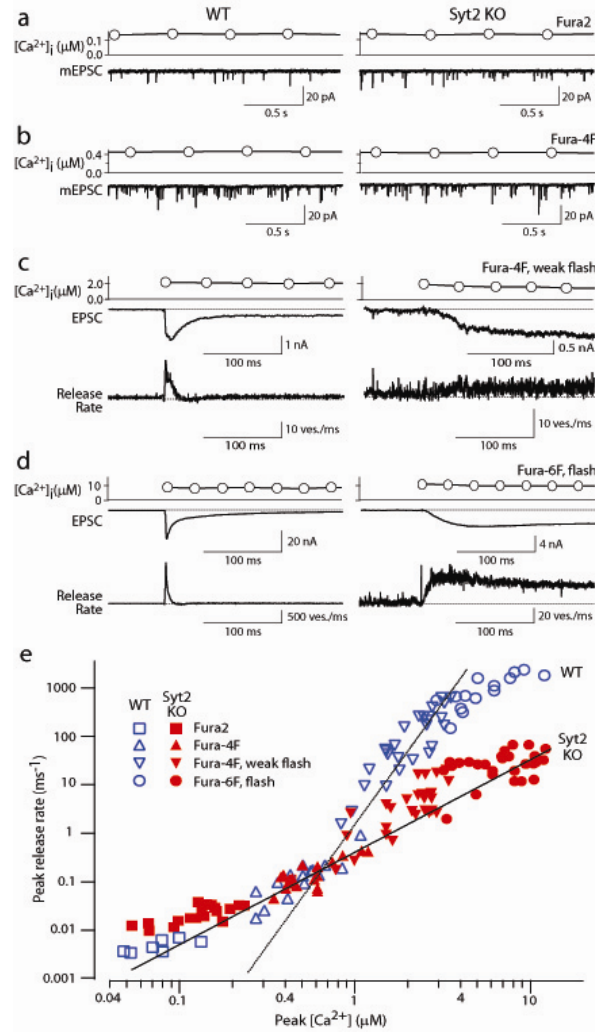


Figure 4
Sun et al.

Jianyuan Sun

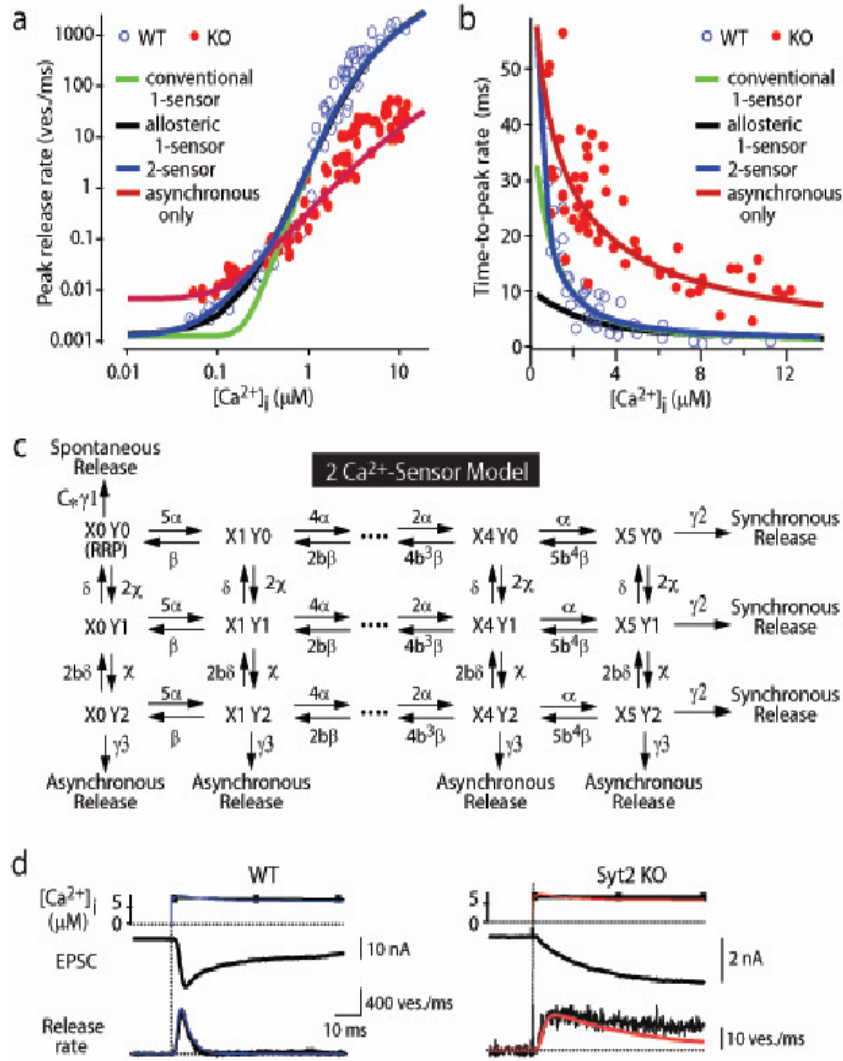
Figure 5- 4 Dependence of peak vesicular release rates on $[Ca^{2+}]_i$ in calyx terminals

EPSC were recorded in calyx synapses in the double-patch configuration at P7~P9 in the presence of 0.1 μ M tetrodotoxin, 0.1 mM cyclothiazide, 1 mM kynurenic acid, and 50 μ M D-AP5, and presynaptic $[Ca^{2+}]_i$ was simultaneously monitored optically using three different Ca^{2+} -sensitive dyes as indicated. Low $[Ca^{2+}]_i$ ($<1 \mu$ M) were achieved by dialysis of Ca^{2+} -buffers into the terminals via the patch pipette; higher $[Ca^{2+}]_i$ ($>1 \mu$ M) were achieved by photolysis of caged Ca^{2+} dialyzed into the terminal.

a-d. Representative experiments recorded in wild-type (left panels) and synaptotagmin-2 deficient calyces (right panels) at four characteristic Ca^{2+} -concentrations; the Ca^{2+} -indicator dyes used are shown on the right. In panels c and d, the vesicle release rate as calculated by deconvolution of EPSCs are also shown.

e. Summary graph of EPSC peak release rates and $[Ca^{2+}]_i$ ($n=63$ for wild-type [open symbols], 92 for synaptotagmin-2 deficient terminals [filled symbols]). The dashed line represents a fit of a 5th power function to the data from wild-type terminals at $[Ca^{2+}]_i$ of $>1 \mu$ M ($y=0.90 \cdot x^5$); the solid line a 2nd power function to the data from mutant terminals ($y=0.54 \cdot x^2$); note that the solid line also fits the wild-type responses at low $[Ca^{2+}]_i$.

We first elevated the $[Ca^{2+}]_i$ to concentrations between 0.05-1.0 μM . Increases of $[Ca^{2+}]_i$ to $<0.2 \mu M$ induced an enhancement in mEPSC frequency but no clearcut evoked EPSCs (Fig. 5-4a). At these Ca^{2+} -concentrations, release was slightly higher in synaptotagmin-2 deficient than in wild-type synapses (Fig. 5-4e), presumably because deletion of synaptotagmin-2 increases the resting frequency of mEPSCs. At $[Ca^{2+}]_i$ of 0.2-1.0 μM , the release rates converged between wild-type and synaptotagmin-2 deficient synapses (Figs. 5-4b and 4e). Thus, as observed for action potential-induced release at low $[Ca^{2+}]_e$ (Fig. 5-2), deletion of synaptotagmin-2 does not impair release evoked at low $[Ca^{2+}]_i$. This result suggests that even in wild-type synapses, release at low $[Ca^{2+}]_i$ is physiologically mediated by the asynchronous Ca^{2+} -sensor, a conclusion that is consistent with previously described properties of release induced by low $[Ca^{2+}]_i$ (Awatramani et al., 2005). We next examined larger increases in $[Ca^{2+}]_i$ produced by flash photolysis of caged Ca^{2+} . In wild-type neurons, a peak release rate of ~ 24 vesicles/ms was evoked when $[Ca^{2+}]_i$ was elevated to 2 μM by weak photolysis (Fig. 5-4c). The peak release rate steeply increased to ~ 1750 vesicles/ms when $[Ca^{2+}]_i$ was raised to 9.2 μM with a strong photolysis pulse, demonstrating a very high Ca^{2+} -cooperativity (Fig. 5-4d). In synaptotagmin-2 deficient synapses, conversely, a 2 μM $[Ca^{2+}]_i$ rise caused release with a peak rate of 3.7 vesicle/ms. Elevation of $[Ca^{2+}]_i$ to 10.5 μM only increased the release rate to 31 vesicles/ms, revealing a much lower Ca^{2+} -cooperativity.



Jianyuan Sun

Figure 5- 5 A two Ca^{2+} -sensor model for neurotransmitter release

a. and b. Fits of the Ca^{2+} -photolysis data from wild-type and synaptotagmin-2 deficient calyces for the peak release rate (a) and time-to-peak rate (b) to previously proposed models (the conventional 1-sensor model (Schneggenburger and Neher 2000; Bollmann et al. 2000), and allosteric 1-sensor model (Lou et al. 2005)), to the 2-sensor model, and to the 2-sensor model with inactivation of the synchronous Ca^{2+} -sensor. In all of the models, the RRP is set to 3000 vesicles(Schneggenburger and Neher 2000; Bollmann et al. 2000).

c. Reaction scheme. γ_1 , γ_2 , γ_3 = rates of spontaneous, synchronous, and asynchronous release, respectively (defined as the fraction of the RRP released per second); α and β , and χ and δ = k_{on} and k_{off} for synchronous and asynchronous release, respectively; X_0 - X_5 and Y_0 - Y_2 = Ca^{2+} -binding states of the Ca^{2+} -sensor for synchronous (X) and asynchronous release (Y), respectively (note that X_0Y_0 = RRP); b = cooperativity factor (Schneggenburger and Neher 2000; Bollmann et al. 2000). The following parameters were applied for curve fitting (only

γ_1 differs between wild-type and KO): $\alpha=1.53 \cdot 10^8 \text{ M}^{-1}\text{s}^{-1}$, $\beta=5800 \text{ s}^{-1}$, $b=0.25$; $\chi=2.94 \cdot 10^6 \text{ M}^{-1}\text{s}^{-1}$, $\delta=130 \text{ s}^{-1}$, $\gamma_1=0.417 \cdot 10^{-3} \text{ ms}^{-1}$ in wild-type and $2.23 \cdot 10^{-3} \text{ s}^{-1}$ in KO; $\gamma_2=6,000 \text{ s}^{-1}$; $\gamma_3=6,000 \text{ s}^{-1}$. Parameters for γ_1 were measured, for b and γ_2 were from ref. 11, and for γ_3 assumed to be equal to γ_2 based on the postulate that Ca^{2+} -binding to the asynchronous and synchronous release Ca^{2+} -sensors will trigger the same release rates since both empty the entire RRP. **d.** The predicted local $[\text{Ca}^{2+}]_i$ signal (for Ca^{2+} -relaxation model) and transmitter release rates predicted by the two Ca^{2+} -sensor model in WT (left) and synaptotagmin-2 KO calyces (right). Top panels: measured and predicted $[\text{Ca}^{2+}]_i$ (black and blue or red, respectively); middle panels: recorded EPSCs; lower panels: vesicular release rates obtained by deconvolution of EPSCs (black), and predicted by the model (blue or red).

Figure 5-4e demonstrates the Ca^{2+} -dependence of the peak release rate obtained from 63 wild-type (open symbols) and 92 synaptotagmin-2 deficient terminals (filled symbols), plotted on logarithmic coordinates. Whereas at $[\text{Ca}^{2+}]_i$ of $<1 \mu\text{M}$, the vesicular release rates are not decreased in synaptotagmin-2 deficient terminals, at $[\text{Ca}^{2+}]_i$ of $>2 \mu\text{M}$, deletion of synaptotagmin-2 reduced the peak transmitter release rate 10-40 fold compared to wild-type synapses. In the most dynamic range of $0.7\text{-}5 \mu\text{M}$ $[\text{Ca}^{2+}]_i$, the relation of the peak release rate to $[\text{Ca}^{2+}]_i$ follows a 5th power function in wild-type terminals, but only a 2nd power function in synaptotagmin-2 deficient terminals (Fig. 5-4e). At higher $[\text{Ca}^{2+}]_i$, release saturates in wild-type synapses, but not in KO synapses. Thus, whereas release triggered at $[\text{Ca}^{2+}]_i$ of $<1 \mu\text{M}$ exhibits a similarly low Ca^{2+} -cooperativity and magnitude in wild-type and synaptotagmin-2 deficient synapses, release triggered at $>1 \mu\text{M}$ $[\text{Ca}^{2+}]_i$ exhibits a dramatically different Ca^{2+} -cooperativity and magnitude in wild-type and mutant synapses.

A potential concern with a genetic study is that a compensatory developmental change could lead to the expression of a non-physiological Ca^{2+} -sensor in mutant synapses. However, the fact that release at low $[\text{Ca}^{2+}]_i$ is indistinguishable between wild-type and synaptotagmin-2 deficient synapses argues strongly against such a

developmental change since such a change should have affected the behavior of Ca^{2+} -triggered release at all Ca^{2+} -concentrations in the mutant terminals. Moreover, the good prediction of release in both wild-type and mutant synapses by our quantitative model described below argues against such a change.

5.3.4 A two Ca^{2+} -sensor model of neurotransmitter release.

Initial Ca^{2+} -photolysis studies on calyx synapses allowed the formulation of quantitative models of neurotransmitter release (referred to here as ‘conventional 1-sensor model’) (Bollmann et al., 2000; Schneggenburger and Neher, 2000). These models, however, were unable to predict release at low $[\text{Ca}^{2+}]_i$ as shown in Figure 5-5a, presumably because this release – as depicted in Figures 5-2 and 5-4 – is primarily carried by the asynchronous Ca^{2+} -sensor. In part to remedy this problem, and in part to account for the change in release induced by phorbol esters, an allosteric model of release was proposed (Lou et al., 2005) that provides an improved prediction of the Ca^{2+} -dependence of peak release rates (Fig. 5-5a). The allosteric model, however, again operates with a single Ca^{2+} -sensor, and significantly underestimates the time-to-peak rate (Fig. 5-5b). To formulate a more accurate model of Ca^{2+} -triggered neurotransmitter release, we developed a two Ca^{2+} -sensor kinetic model (Fig. 5-5c). This model postulates that (1) synchronous release is triggered by Ca^{2+} -binding to a Ca^{2+} -sensor with a Ca^{2+} -cooperativity of ~ 5 , i.e. synaptotagmin-2 in the calyx and synaptotagmin-1 in forebrain, consistent with earlier studies (Bollmann et al., 2000; Schneggenburger and Neher, 2000); (2) asynchronous release is triggered by Ca^{2+} -binding to an unidentified Ca^{2+} -sensor with

a Ca^{2+} -cooperativity of ~ 2 (Fig. 5-4); and (3) spontaneous release occurs Ca^{2+} -independently and includes an effective factor C to account for the change in spontaneous release in synaptotagmin-deficient synapses. The two Ca^{2+} -sensor model assumes that these three release pathways compete with each other, and operate on the same vesicle pools.

The two Ca^{2+} -sensor model allows a satisfactory description of all of our Ca^{2+} -photolysis data, both for the Ca^{2+} -dependence of the peak release rates and of the time-to-peak rate for wild-type and synaptotagmin-2 deficient synapses (Figs. 5-5a and 5-5b). Moreover, the two Ca^{2+} -sensor model accurately predicts the kinetics of Ca^{2+} -dependent vesicle release in wild-type and synaptotagmin-2 deficient calyx synapses (Figs. 5-5d and 5-5e). The two Ca^{2+} -sensor model calculates that synchronous release exhibits an apparent Ca^{2+} -affinity of $\sim 38 \mu\text{M}$ a Ca^{2+} -cooperativity of ~ 5 , and an apparent k_{on} rate of $\alpha = 1.53 \cdot 10^8 \text{ M}^{-1}\text{s}^{-1}$. In contrast, although asynchronous release exhibits an apparent Ca^{2+} -affinity of $\sim 44 \mu\text{M}$ that is similar to that of synchronous release, asynchronous release displays a much lower Ca^{2+} -cooperativity of ~ 2 , and a much slower k_{on} rate of $\chi = 2.94 \cdot 10^6 \text{ M}^{-1}\text{s}^{-1}$ (Fig. 5-5). Our parameters for synchronous release are squarely in the middle between the two previous estimates in calyx synapses (Bollmann et al., 2000; Schneggenburger and Neher, 2000), but the parameters for asynchronous release that we determined differ from previous suggestions (Goda and Stevens, 1994; Ravin et al., 1997), probably because previous suggestions were based on extrapolations of asynchronous release in the continued presence of synchronous release that may have contaminated the estimates. Although the two Ca^{2+} -sensor model thus reveals that asynchronous release exhibits a

relatively low apparent Ca^{2+} -affinity, the model still predicts that asynchronous release is the major physiological mode of synaptic transmission at low $[\text{Ca}^{2+}]_i$ because its lower degree of Ca^{2+} -cooperativity renders asynchronous release more effective at low $[\text{Ca}^{2+}]_i$. At high $[\text{Ca}^{2+}]_i$, conversely, synchronous release dominates because the predicted k_{on} for synchronous release is ~100-fold higher than that for asynchronous release (Fig. 5-5).

5.4 Discussions

Here we show that among synaptotagmin isoforms that mediate synchronous release (synaptotagmin-1, -2, and -9), calyx terminals only express synaptotagmin-2 (Fig. 5-1). We demonstrate that synaptotagmin-2 is selectively essential for Ca^{2+} -triggering of fast synchronous release (Fig. 5-2) without being required for Ca^{2+} -influx or vesicle priming into the RRP in calyx terminals (Fig. 5-3). Thus, synaptotagmin-2 – as suggested for synaptotagmin-1 in forebrain synapses (Geppert et al., 1994)– is selectively required for Ca^{2+} -triggering of fast release. We show that although asynchronous release contributes little to action potential-induced release in calyx synapses at physiological $[\text{Ca}^{2+}]_e$, asynchronous release empties the entire RRP upon prolonged increases in $[\text{Ca}^{2+}]_i$ (Fig. 5-3). This finding indicates that the synchronous and asynchronous release act on the same vesicle pools. Moreover, release at low Ca^{2+} -concentrations (Awatramani et al., 2005) exhibits a similar magnitude and Ca^{2+} -dependence in wild-type and synaptotagmin-2 deficient synapses, suggesting that release at low Ca^{2+} -concentrations is normally driven by the asynchronous Ca^{2+} -sensor, and that asynchronous release does not change in the KO mice.

Traditionally, asynchronous release is explained by two competing hypotheses. (1) Asynchronous and synchronous release share the same Ca^{2+} -sensor, but differ in the coupling of vesicles to Ca^{2+} -channels, the state of the vesicles, and/or the Ca^{2+} -buffering mechanisms involved (Lou et al., 2005; Schneggenburger and Forsythe, 2006; Taschenberger et al., 2005); (2) different Ca^{2+} -sensors with distinct properties mediate synchronous and asynchronous release (Geppert et al., 1994). In demonstrating that synchronous release exhibits an unexpectedly low Ca^{2+} -affinity and a Ca^{2+} -cooperativity that is different from that of synchronous release, our results support the second hypothesis. The definition of the biophysical properties of asynchronous Ca^{2+} -triggered release made it possible to formulate a quantitative model for neurotransmitter release that applies to all synapses, and resolves limitations of previous models which could not fully account for the Ca^{2+} -dependence of release (Bollmann et al., 2000; Lou et al., 2005; Schneggenburger and Neher, 2000). Our model indicates that the Ca^{2+} -sensors for synchronous and asynchronous release operate in competition with each other at all stages, with the asynchronous Ca^{2+} -sensor being slower but able to bind Ca^{2+} at lower concentrations, whereas the synchronous Ca^{2+} -sensor is faster with a higher Ca^{2+} -cooperativity. As a result, in this competition the synchronous Ca^{2+} -sensor ‘wins’ during pulses of high Ca^{2+} -concentrations, while the asynchronous Ca^{2+} -sensor prevails during sustained phases of lower Ca^{2+} -concentrations (Fig. 5-5). Within this framework, differences between synapses are primarily determined by which synaptotagmin isoform is being used as Ca^{2+} -sensor for synchronous release, and by the accumulation of residual Ca^{2+} in the intervals between action potentials during stimulus trains (i.e., by the Ca^{2+} -

buffering properties) (Awatramani et al., 2005; Bollmann et al., 2000; Heidelberger et al., 1994; Taschenberger et al., 2005). It is of interest here that the calyx terminals with their exquisitely fast release properties uses as a synchronous Ca^{2+} -sensor only synaptotagmin-2, the fastest of the three Ca^{2+} -sensors for synchronous release(Xu et al., 2007).

CHAPTER VI: DISCUSSION AND CONCLUSIONS

Synaptic vesicle release occurs in at least two modes: a fast synchronous release and slow asynchronous release (Geppert et al., 1994; Goda and Stevens, 1994; Maximov and Sudhof, 2005). Fast synchronous release is a tightly regulated process triggered by action potential evoked Ca^{2+} influx, which is essential for temporally precise neuronal communication. Slow release is delayed release of neurotransmitter after action potential triggered Ca^{2+} influx, and usually become obvious after a high-frequency action potential train (Maximov and Sudhof, 2005). Although the computational role of slow release is unclear it may be important for the temporal summation of information. A central question about these release modes concerns how fast and slow release are coupled to Ca^{2+} elevation in nerve terminals and specifically what molecules accomplish this coupling. Synaptotagmin-1 is believed to act as the fast synchronous release sensor (Geppert et al., 1994; Maximov and Sudhof, 2005; Nishiki and Augustine, 2004). Two pieces of evidences strongly support this model: first, when synaptotagmin-1 is knocked-out in mice (Geppert et al., 1994), or from invertebrates such as *C. elegans* (Nonet et al., 1993) and *Drosophila* (Littleton et al., 1993b), fast synchronous release disappears; second, a milestone study from the Südhof lab indicated that by decreasing the Ca^{2+} binding affinities of synaptotagmin-1, fast synchronous release probability is reduced (Fernandez-Chacon et al., 2001). However, there are several central questions that need to be addressed in detailing the mechanism of Ca^{2+} control of synaptic vesicle release which I pursued in my thesis research: 1) Is Ca^{2+} -dependent synaptotagmin-1/SNARE

binding important for evoked synaptic release? 2) Is synaptotagmin-2 another fast Ca^{2+} -sensor? 3) What is the nature of slow asynchronous release?

6.1 Ca^{2+} -dependent Synaptotagmin 1/SNARE binding is important for synaptic vesicle release

Synaptotagmin-1 binds to plasma membranes containing acidic phospholipids and to the neuronal SNARE complexes in a Ca^{2+} -dependent manner. Using two knock-in mouse lines each with single amino-acid substitution, namely D232N and D238N, we studied these lines using biochemical and electrophysiological methods. We found that the D232N substitution in synaptotagmin-1 increases Ca^{2+} -dependent SNARE bindings but leaves phospholipid binding unchanged, whereas the D238N mutant slightly decreased phospholipid binding but leaves SNARE binding insignificantly changed. Furthermore, we found that evoked release in D232N mutant neuronal cultures is significantly increased, whereas in D238N cultures release is slightly but significantly decreased. Ca^{2+} titration curves indicated the apparent Ca^{2+} affinity for vesicle release significantly increased in D232N synapses. In combination with previous data, the current study indicates that both Ca^{2+} dependent synaptotagmin-1/SNARE binding and synaptotagmin-1/phospholipids binding are important for synaptic vesicle release.

6.2 Synaptotagmin is a fast Ca^{2+} -sensor for synaptic vesicle release in Calyx and Neuromuscular junctions

Among all the members of synaptotagmin family, synaptotagmin-2 shares the highest sequence homology with synaptotagmin 1. Biochemically, both synaptotagmins bind to phospholipids and SNARE proteins in a Ca^{2+} dependent manner. Synaptotagmin-

2 is predominantly expressed in the hindbrain including the cerebellum, brainstem and spinal cord. Synaptotagmin 1 is predominantly expressed in the forebrain.

Synaptotagmin-2 has long been implicated as a fast Ca^{2+} -sensor for synaptic vesicle release, but this suggestion has never been tested genetically. To test this, we used two genetically modified mouse lines: one is synaptotagmin-2^{I377N} which came from a chemical induced mutagenesis screen; the other one is synaptotagmin-2 knockout.

I377N substitution largely destabilized synaptotagmin-2 protein in in vitro experiments. In synaptotagmin-2^{I377N} mice, synaptotagmin-2 expression decreased to ~30% in the brain stem. In Calyx of Held synapses, this mutation causes a delay and a decrease in Ca^{2+} -induced but not in hypertonic sucrose-induced release, suggesting that synaptotagmin-2 mediates Ca^{2+} -triggering of evoked release in brainstem synapses.

Moreover, we have also generated mice in which the 5' end of the synaptotagmin-2 gene was replaced by lacZ. Using β -galactosidase as a marker, we show that consistent with previous studies, synaptotagmin-2 is widely expressed in the spinal cord, brainstem, and cerebellum, but is additionally present in selected forebrain neurons, including most striatal neurons and a small subset of hypothalamic, cortical, and hippocampal neurons. Synaptotagmin-2 deficient mice were indistinguishable from wildtype littermates at birth, but subsequently developed severe motor dysfunction, and perished at ~3 weeks of age. Electrophysiological studies in cultured striatal neurons revealed that the synaptotagmin-2 deletion slowed the kinetics of evoked neurotransmitter release without altering the total amount of release. In contrast, synaptotagmin-2 deficient NMJs suffered from a large reduction in evoked release and a major increase in short-term synaptic plasticity. Viewed together, our results demonstrate that the synaptotagmin-2 deficiency causes a lethal impairment in synaptic transmission in selected

synapses. This impairment, however, is less severe than that produced in forebrain neurons by deletion of synaptotagmin 1, presumably because at least in NMJs, synaptotagmin 1 is co-expressed with synaptotagmin-2, and both together mediate fast Ca^{2+} -triggered release.

Unexpectedly, we additionally observed in synaptotagmin-2^{1377N} synapses and synaptotagmin-2 deficient NMJs the frequency of spontaneous miniature release events was increased both at rest and during stimulus trains. At the same time, synaptotagmin-1 deficient excitatory and inhibitory cortical synapses also displayed a large increase in spontaneous release, demonstrating that this effect was shared among synaptotagmins 1 and 2. Our data suggest that synaptotagmin 1 and 2 perform equivalent functions in the Ca^{2+} -triggering of action potential-induced release and in the restriction of spontaneous release, consistent with a general role of synaptotagmins in controlling ‘release slots’ for synaptic vesicles at the active zone.

Thus synaptotagmin-2 is an essential synaptotagmin isoform that functions in concert with other synaptotagmins in the Ca^{2+} -triggering of neurotransmitter release.

6.3 A two- Ca^{2+} -sensor model for synaptic vesicle release

These above studies expanded our understanding of the molecular control of synchronous release but did not illuminate the molecular mechanism of asynchronous neurotransmission. To address this we exploited a fortuitous discovery: synaptotagmin-2 but not synaptotagmin-1 is expressed in the Calyx of Held. This fact enabled us to study a synapse that lacked both known Ca^{2+} -sensors for fast synchronous release. Using electrophysiological recording combined with Ca^{2+} uncaging experiments we studied the

properties of asynchronous release. Ca^{2+} uncaging allowed us to precisely control the Ca^{2+} concentration optically in presynaptic terminal in a temporally defined manner. Using this method, we mapped increasing Ca^{2+} concentrations in relation to neurotransmitter release and built a comprehensive mathematical model for the Ca^{2+} control of synaptic vesicle fusion. We found compelling evidence for the existence of two Ca^{2+} -sensors: one (synaptotagmin-2 in Calyx of Held) is responsible for fast synchronous release, and the other one is responsible for slow delayed synaptic release. The slow Ca^{2+} -sensor has two Ca^{2+} binding sites. Surprisingly, we found the two Ca^{2+} -sensors have similar apparent Ca^{2+} affinities. This study showed clearly that synaptotagmin-2 is a fast Ca^{2+} -sensor, and gave us a prediction that narrows down the potential candidate for the slow Ca^{2+} -sensor.

6.5. Future directions in searching for slow asynchronous Ca^{2+} -sensor(s)

Our findings suggest that asynchronous Ca^{2+} -triggered release is universal, and not a particular phenomenon of a subset of synapses. A molecular hypothesis of the release pathways is illustrated in Figure 6-1. According to this hypothesis, primed vesicles contain partially assembled SNARE complexes (maybe corresponding to the ‘reluctantly releasable vesicles’ of Neher and co-workers) (Trommershauser et al., 2003), and ‘superprimed’ vesicles SNARE complexes forced into a poised, fully assembled state by complexin binding. Both states are subject to Ca^{2+} -triggering by the unidentified asynchronous release Ca^{2+} -sensor and by synaptotagmin as the synchronous release Ca^{2+} -sensor, although complexin-bound SNARE- complexes exhibit a much higher efficiency of synaptotagmin-action. An alternative molecular hypothesis would have been that the

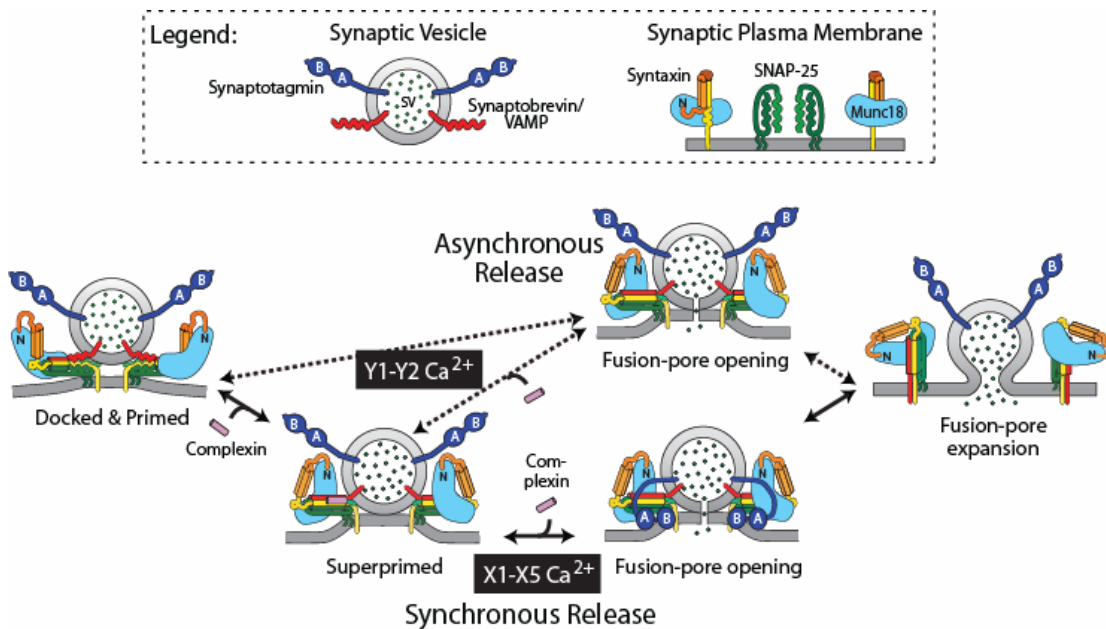


Figure 6- 1 **A molecular hypothesis describing the two Ca^{2+} -sensor model of neurotransmitter release.**

Vesicles are primed by assembly of a complex composed of partially formed SNARE-complexes containing bound Munc18-1 (left). Binding of complexins to the partially assembled SNARE-complexes forces completion of SNARE-complex formation, energizing the vesicle/plasma membrane interface and arresting fusion. Binding of five Ca^{2+} -ions to synaptotagmin, the Ca^{2+} -sensor of synchronous release (X1-X5) then triggers synaptotagmin-binding to phospholipids and to SNARE-complexes with displacement of complexins, which together opens the fusion pore. Binding of two Ca^{2+} -ions to the unknown Ca^{2+} -sensor for asynchronous release also triggers fusion-pore opening by a complexin-independent mechanism. During physiological action potential-induced Ca^{2+} -influx into terminals ($[\text{Ca}^{2+}]_i = >1 \mu\text{M}$), synchronous release prevails despite similar apparent Ca^{2+} -affinities of the two Ca^{2+} -sensors because the synchronous Ca^{2+} -sensor acts more rapidly than the asynchronous Ca^{2+} -sensor. However, at $[\text{Ca}^{2+}]_i = 0.2\text{-}1.0 \mu\text{M}$ (for example, when residual Ca^{2+} accumulates during high-frequency stimulus trains), asynchronous release dominates because the asynchronous Ca^{2+} -sensor has a lower Ca^{2+} -cooperativity, and thus is more sensitive to low Ca^{2+} -concentrations.

asynchronous release Ca^{2+} -sensor accelerates an upstream priming step, and that it induces release by increasing the number of primed vesicles that then spontaneously fuse. It is likely that priming is accelerated by Ca^{2+} (Stevens and Wesseling, 1998), nevertheless, this effect cannot explain asynchronous release as defined here (Fig. 5-4). Moreover, the observation that the entire RRP can be triggered for exocytosis by the asynchronous Ca^{2+} -sensor within 100 ms argues against a role of the asynchronous Ca^{2+} -sensor only in accelerating an upstream priming step. Although the asynchronous Ca^{2+} -sensor is unknown, it is probably not a synaptotagmin isoform because of its low Ca^{2+} -cooperativity, but more likely represents a protein with a single C_2 -domain or EF-hand, such as piccolo, phospholipase C, or diacylglycerol kinase.

BIBLIOGRAPHY

Aikawa, Y., and Martin, T.F. (2003). ARF6 regulates a plasma membrane pool of phosphatidylinositol(4,5)bispophosphate required for regulated exocytosis. *J Cell Biol* 162, 647-659.

Antonin, W., Fasshauer, D., Becker, S., Jahn, R., and Schneider, T.R. (2002). Crystal structure of the endosomal SNARE complex reveals common structural principles of all SNAREs. *Nature structural biology* 9, 107-111.

Arac, D., Murphy, T., and Rizo, J. (2003). Facile detection of protein-protein interactions by one-dimensional NMR spectroscopy. *Biochemistry* 42, 2774-2780.

Atluri, P.P., and Regehr, W.G. (1998). Delayed release of neurotransmitter from cerebellar granule cells. *J Neurosci* 18, 8214-8227.

Awatramani, G.B., Price, G.D., and Trussell, L.O. (2005). Modulation of transmitter release by presynaptic resting potential and background calcium levels. *Neuron* 48, 109-121.

Bai, J., Wang, C.T., Richards, D.A., Jackson, M.B., and Chapman, E.R. (2004). Fusion pore dynamics are regulated by synaptotagmin**t*-SNARE interactions. *Neuron* 41, 929-942.

Banerjee, A., Kowalchyk, J.A., DasGupta, B.R., and Martin, T.F. (1996). SNAP-25 is required for a late postdocking step in Ca²⁺-dependent exocytosis. *J Biol Chem* 271, 20227-20230.

Baram, D., Adachi, R., Medalia, O., Tuvim, M., Dickey, B.F., Mekori, Y.A., and Sagi-Eisenberg, R. (1999). Synaptotagmin II negatively regulates Ca²⁺-triggered exocytosis of lysosomes in mast cells. *J Exp Med* 189, 1649-1658.

Barrett, E.F., and Stevens, C.F. (1972). The kinetics of transmitter release at the frog neuromuscular junction. *J Physiol* 227, 691-708.

Benfenati, F., Greengard, P., Brunner, J., and Bahler, M. (1989). Electrostatic and hydrophobic interactions of synapsin I and synapsin I fragments with phospholipid bilayers. *J Cell Biol* 108, 1851-1862.

Bennett, M.K., Calakos, N., and Scheller, R.H. (1992). Syntaxin: a synaptic protein implicated in docking of synaptic vesicles at presynaptic active zones. *Science* 257, 255-259.

Berton, F., Iborra, C., Boudier, J.A., Seagar, M.J., and Marqueze, B. (1997). Developmental regulation of synaptotagmin I, II, III, and IV mRNAs in the rat CNS. *J Neurosci* 17, 1206-1216.

Betz, A., Okamoto, M., Benseler, F., and Brose, N. (1997). Direct interaction of the rat unc-13 homologue Munc13-1 with the N terminus of syntaxin. *J Biol Chem* 272, 2520-2526.

Betz, W.J., Mao, F., and Smith, C.B. (1996). Imaging exocytosis and endocytosis. *Current opinion in neurobiology* 6, 365-371.

Bollmann, J.H., Sakmann, B., and Borst, J.G. (2000). Calcium sensitivity of glutamate release in a calyx-type terminal. *Science* 289, 953-957.

Borst, J.G., Helmchen, F., and Sakmann, B. (1995). Pre- and postsynaptic whole-cell recordings in the medial nucleus of the trapezoid body of the rat. *J Physiol* 489 (Pt 3), 825-840.

Borst, J.G., and Sakmann, B. (1996). Calcium influx and transmitter release in a fast CNS synapse. *Nature* 383, 431-434.

Bowen, M.E., Weninger, K., Ernst, J., Chu, S., and Brunger, A.T. (2005). Single-molecule studies of synaptotagmin and complexin binding to the SNARE complex. *Biophys J* 89, 690-702.

Broadie, K., Bellen, H.J., DiAntonio, A., Littleton, J.T., and Schwarz, T.L. (1994). Absence of synaptotagmin disrupts excitation-secretion coupling during synaptic transmission. *Proc Natl Acad Sci U S A* 91, 10727-10731.

Brose, N., Petrenko, A.G., Sudhof, T.C., and Jahn, R. (1992). Synaptotagmin: a calcium sensor on the synaptic vesicle surface. *Science* 256, 1021-1025.

Brunger, A.T. (2005). Structure and function of SNARE and SNARE-interacting proteins. *Q Rev Biophys* 38, 1-47.

Buffelli, M., Burgess, R.W., Feng, G., Lobe, C.G., Lichtman, J.W., and Sanes, J.R. (2003). Genetic evidence that relative synaptic efficacy biases the outcome of synaptic competition. *Nature* 424, 430-434.

Cajal, R.y. (1937). *Recuerdos de mi Vida* (Cambridge, MIT press).

Chapman, E.R., An, S., Edwardson, J.M., and Jahn, R. (1996). A novel function for the second C2 domain of synaptotagmin. Ca²⁺-triggered dimerization. *J Biol Chem* 271, 5844-5849.

Chapman, E.R., Desai, R.C., Davis, A.F., and Tornehl, C.K. (1998). Delineation of the oligomerization, AP-2 binding, and synprint binding region of the C2B domain of synaptotagmin. *J Biol Chem* 273, 32966-32972.

- Chapman, E.R., Hanson, P.I., An, S., and Jahn, R. (1995). Ca^{2+} regulates the interaction between synaptotagmin and syntaxin 1. *J Biol Chem* 270, 23667-23671.
- Chapman, E.R., and Jahn, R. (1994). Calcium-dependent interaction of the cytoplasmic region of synaptotagmin with membranes. Autonomous function of a single C2-homologous domain. *J Biol Chem* 269, 5735-5741.
- Charvin, N., L'Eveque, C., Walker, D., Berton, F., Raymond, C., Kataoka, M., Shoji-Kasai, Y., Takahashi, M., De Waard, M., and Seagar, M.J. (1997). Direct interaction of the calcium sensor protein synaptotagmin I with a cytoplasmic domain of the $\alpha 1A$ subunit of the P/Q-type calcium channel. *Embo J* 16, 4591-4596.
- Chen, X.L., Zhong, Z.G., Yokoyama, S., Bark, C., Meister, B., Berggren, P.O., Roder, J., Higashida, H., and Jeromin, A. (2001). Overexpression of rat neuronal calcium sensor-1 in rodent NG108-15 cells enhances synapse formation and transmission. *J Physiol* 532, 649-659.
- Chuhma, N., and Ohmori, H. (2002). Role of Ca^{2+} in the synchronization of transmitter release at calyceal synapses in the auditory system of rat. *Journal of neurophysiology* 87, 222-228.
- Connors, B.W., and Long, M.A. (2004). Electrical synapses in the mammalian brain. *Annu Rev Neurosci* 27, 393-418.
- Cruz, L.J., Gray, W.R., Olivera, B.M., Zeikus, R.D., Kerr, L., Yoshikami, D., and Moczydlowski, E. (1985). Conus geographus toxins that discriminate between neuronal and muscle sodium channels. *J Biol Chem* 260, 9280-9288.
- Cummings, D.D., Wilcox, K.S., and Dichter, M.A. (1996). Calcium-dependent paired-pulse facilitation of miniature EPSC frequency accompanies depression of EPSCs at hippocampal synapses in culture. *J Neurosci* 16, 5312-5323.
- Davis, A.F., Bai, J., Fasshauer, D., Wolowick, M.J., Lewis, J.L., and Chapman, E.R. (1999). Kinetics of synaptotagmin responses to Ca^{2+} and assembly with the core SNARE complex onto membranes. *Neuron* 24, 363-376.
- Davletov, B., Sontag, J.M., Hata, Y., Petrenko, A.G., Fykse, E.M., Jahn, R., and Sudhof, T.C. (1993). Phosphorylation of synaptotagmin I by casein kinase II. *J Biol Chem* 268, 6816-6822.
- Davletov, B.A., and Sudhof, T.C. (1993). A single C2 domain from synaptotagmin I is sufficient for high affinity Ca^{2+} /phospholipid binding. *J Biol Chem* 268, 26386-26390.
- Deutsch, J.W., and Kelly, R.B. (1981). Lipids of synaptic vesicles: relevance to the mechanism of membrane fusion. *Biochemistry* 20, 378-385.

- DiAntonio, A., Parfitt, K.D., and Schwarz, T.L. (1993). Synaptic transmission persists in synaptotagmin mutants of *Drosophila*. *Cell* 73, 1281-1290.
- DiAntonio, A., and Schwarz, T.L. (1994). The effect on synaptic physiology of synaptotagmin mutations in *Drosophila*. *Neuron* 12, 909-920.
- Ernst, J.A., and Brunger, A.T. (2003). High resolution structure, stability, and synaptotagmin binding of a truncated neuronal SNARE complex. *J Biol Chem* 278, 8630-8636.
- Fasshauer, D., Eliason, W.K., Brunger, A.T., and Jahn, R. (1998). Identification of a minimal core of the synaptic SNARE complex sufficient for reversible assembly and disassembly. *Biochemistry* 37, 10354-10362.
- Fenster, S.D., Chung, W.J., Zhai, R., Cases-Langhoff, C., Voss, B., Garner, A.M., Kaempf, U., Kindler, S., Gundelfinger, E.D., and Garner, C.C. (2000). Piccolo, a presynaptic zinc finger protein structurally related to bassoon. *Neuron* 25, 203-214.
- Fernandez-Chacon, R., Konigstorfer, A., Gerber, S.H., Garcia, J., Matos, M.F., Stevens, C.F., Brose, N., Rizo, J., Rosenmund, C., and Sudhof, T.C. (2001). Synaptotagmin I functions as a calcium regulator of release probability. *Nature* 410, 41-49.
- Fernandez-Chacon, R., Shin, O.H., Konigstorfer, A., Matos, M.F., Meyer, A.C., Garcia, J., Gerber, S.H., Rizo, J., Sudhof, T.C., and Rosenmund, C. (2002). Structure/function analysis of Ca²⁺ binding to the C2A domain of synaptotagmin 1. *J Neurosci* 22, 8438-8446.
- Fernandez, I., Arac, D., Ubach, J., Gerber, S.H., Shin, O., Gao, Y., Anderson, R.G., Sudhof, T.C., and Rizo, J. (2001). Three-dimensional structure of the synaptotagmin 1 C2B-domain: synaptotagmin 1 as a phospholipid binding machine. *Neuron* 32, 1057-1069.
- Fernandez, I., Ubach, J., Dulubova, I., Zhang, X., Sudhof, T.C., and Rizo, J. (1998). Three-dimensional structure of an evolutionarily conserved N-terminal domain of syntaxin 1A. *Cell* 94, 841-849.
- Forsythe, I.D. (1994). Direct patch recording from identified presynaptic terminals mediating glutamatergic EPSCs in the rat CNS, in vitro. *J Physiol* 479 (Pt 3), 381-387.
- Fowler, S.C., Birkestrand, B.R., Chen, R., Moss, S.J., Vorontsova, E., Wang, G., and Zarcone, T.J. (2001). A force-plate actometer for quantitating rodent behaviors: illustrative data on locomotion, rotation, spatial patterning, stereotypies, and tremor. *J Neurosci Methods* 107, 107-124.

Frazier, A.A., Roller, C.R., Havelka, J.J., Hinderliter, A., and Cafiso, D.S. (2003). Membrane-bound orientation and position of the synaptotagmin I C2A domain by site-directed spin labeling. *Biochemistry* 42, 96-105.

Geppert, M., Archer, B.T., 3rd, and Sudhof, T.C. (1991). Synaptotagmin II. A novel differentially distributed form of synaptotagmin. *J Biol Chem* 266, 13548-13552.

Geppert, M., Goda, Y., Hammer, R.E., Li, C., Rosahl, T.W., Stevens, C.F., and Sudhof, T.C. (1994). Synaptotagmin I: a major Ca^{2+} sensor for transmitter release at a central synapse. *Cell* 79, 717-727.

Gerber, S.H., Rizo, J., and Sudhof, T.C. (2002). Role of electrostatic and hydrophobic interactions in Ca^{2+} -dependent phospholipid binding by the C(2)A-domain from synaptotagmin I. *Diabetes* 51 Suppl 1, S12-18.

Goda, Y., and Stevens, C.F. (1994). Two components of transmitter release at a central synapse. *Proc Natl Acad Sci U S A* 91, 12942-12946.

Goldhamer, D.J., Faerman, A., Shani, M., and Emerson, C.P., Jr. (1992). Regulatory elements that control the lineage-specific expression of myoD. *Science* 256, 538-542.

Gromada, J., Bark, C., Smidt, K., Efanov, A.M., Janson, J., Mandic, S.A., Webb, D.L., Zhang, W., Meister, B., Jeromin, A., *et al.* (2005). Neuronal calcium sensor-1 potentiates glucose-dependent exocytosis in pancreatic beta cells through activation of phosphatidylinositol 4-kinase beta. *Proc Natl Acad Sci U S A* 102, 10303-10308.

Grynkiewicz, G., Poenie, M., and Tsien, R.Y. (1985). A new generation of Ca^{2+} indicators with greatly improved fluorescence properties. *J Biol Chem* 260, 3440-3450.

Hagler, D.J., Jr., and Goda, Y. (2001). Properties of synchronous and asynchronous release during pulse train depression in cultured hippocampal neurons. *Journal of neurophysiology* 85, 2324-2334.

Hayashi, T., McMahon, H., Yamasaki, S., Binz, T., Hata, Y., Sudhof, T.C., and Niemann, H. (1994). Synaptic vesicle membrane fusion complex: action of clostridial neurotoxins on assembly. *Embo J* 13, 5051-5061.

Hefft, S., and Jonas, P. (2005). Asynchronous GABA release generates long-lasting inhibition at a hippocampal interneuron-principal neuron synapse. *Nat Neurosci* 8, 1319-1328.

Heidelberger, R., Heinemann, C., Neher, E., and Matthews, G. (1994). Calcium dependence of the rate of exocytosis in a synaptic terminal. *Nature* 371, 513-515.

- Hendricks, K.B., Wang, B.Q., Schnieders, E.A., and Thorner, J. (1999). Yeast homologue of neuronal frequenin is a regulator of phosphatidylinositol-4-OH kinase. *Nature cell biology* *1*, 234-241.
- Herrick, D.Z., Sterbling, S., Rasch, K.A., Hinderliter, A., and Cafiso, D.S. (2006). Position of synaptotagmin I at the membrane interface: cooperative interactions of tandem C2 domains. *Biochemistry* *45*, 9668-9674.
- Hilfiker, S., Pieribone, V.A., Nordstedt, C., Greengard, P., and Czernik, A.J. (1999). Regulation of synaptotagmin I phosphorylation by multiple protein kinases. *J Neurochem* *73*, 921-932.
- Holz, R.W., Hlubek, M.D., Sorensen, S.D., Fisher, S.K., Balla, T., Ozaki, S., Prestwich, G.D., Stuenkel, E.L., and Bittner, M.A. (2000). A pleckstrin homology domain specific for phosphatidylinositol 4, 5-bisphosphate (PtdIns-4,5-P₂) and fused to green fluorescent protein identifies plasma membrane PtdIns-4,5-P₂ as being important in exocytosis. *J Biol Chem* *275*, 17878-17885.
- Hu, C., Ahmed, M., Melia, T.J., Sollner, T.H., Mayer, T., and Rothman, J.E. (2003). Fusion of cells by flipped SNAREs. *Science* *300*, 1745-1749.
- Hui, E., Bai, J., and Chapman, E.R. (2006). Ca²⁺-triggered simultaneous membrane penetration of the tandem C2-domains of synaptotagmin I. *Biophys J* *91*, 1767-1777.
- Hui, E., Bai, J., Wang, P., Sugimori, M., Llinas, R.R., and Chapman, E.R. (2005). Three distinct kinetic groupings of the synaptotagmin family: candidate sensors for rapid and delayed exocytosis. *Proc Natl Acad Sci U S A* *102*, 5210-5214.
- Iwasaki, S., and Takahashi, T. (1998). Developmental changes in calcium channel types mediating synaptic transmission in rat auditory brainstem. *J Physiol* *509* (Pt 2), 419-423.
- Jahn, R., Lang, T., and Sudhof, T.C. (2003). Membrane fusion. *Cell* *112*, 519-533.
- Jahn, R., and Sudhof, T.C. (1999). Membrane fusion and exocytosis. *Annual review of biochemistry* *68*, 863-911.
- Janz, R., Goda, Y., Geppert, M., Missler, M., and Sudhof, T.C. (1999). SV2A and SV2B function as redundant Ca²⁺ regulators in neurotransmitter release. *Neuron* *24*, 1003-1016.
- Kandel, E.R., Schwartz, J.H., and Jessell, T.M. (2000). *Principles of Neural Science*, 4/e (McGraw-Hill companies, Inc.).
- Katz, B. (1966). *Nerve, Muscle, and Synapse*, 1st edn (New York, McGraw-Hill).

Katz, B., and Miledi, R. (1967a). Ionic requirements of synaptic transmitter release. *Nature* 215, 651.

Katz, B., and Miledi, R. (1967b). The timing of calcium action during neuromuscular transmission. *J Physiol* 189, 535-544.

Katz, B., and Miledi, R. (1968). The role of calcium in neuromuscular facilitation. *J Physiol* 195, 481-492.

Kee, Y., and Scheller, R.H. (1996). Localization of synaptotagmin-binding domains on syntaxin. *J Neurosci* 16, 1975-1981.

Kerr, A.M., Reisinger, E., Fakler, B., and Jonas, P.M. (2006). Synaptotagmin-1 is not required for fast, synchronous synaptic transmission at inhibitory synapses between parvalbumin-expressing basket cells and granule cells in hippocampus. Paper presented at: Soc Neurosci Abstr.

Kim, D.K., and Catterall, W.A. (1997). Ca^{2+} -dependent and -independent interactions of the isoforms of the $\alpha 1A$ subunit of brain Ca^{2+} channels with presynaptic SNARE proteins. *Proc Natl Acad Sci U S A* 94, 14782-14786.

Lee, B.H., Min, X., Heise, C.J., Xu, B.E., Chen, S., Shu, H., Luby-Phelps, K., Goldsmith, E.J., and Cobb, M.H. (2004). WNK1 phosphorylates synaptotagmin 2 and modulates its membrane binding. *Mol Cell* 15, 741-751.

Leveque, C., el Far, O., Martin-Moutot, N., Sato, K., Kato, R., Takahashi, M., and Seagar, M.J. (1994). Purification of the N-type calcium channel associated with syntaxin and synaptotagmin. A complex implicated in synaptic vesicle exocytosis. *J Biol Chem* 269, 6306-6312.

Lewit-Bentley, A., Rety, S., Sopkova-de Oliveira Santos, J., and Gerke, V. (2000). S100-annexin complexes: some insights from structural studies. *Cell biology international* 24, 799-802.

Li, C., Davletov, B.A., and Sudhof, T.C. (1995a). Distinct Ca^{2+} and Sr^{2+} binding properties of synaptotagmins. Definition of candidate Ca^{2+} sensors for the fast and slow components of neurotransmitter release. *J Biol Chem* 270, 24898-24902.

Li, C., Ullrich, B., Zhang, J.Z., Anderson, R.G., Brose, N., and Sudhof, T.C. (1995b). Ca^{2+} -dependent and -independent activities of neural and non-neural synaptotagmins. *Nature* 375, 594-599.

Li, L., Shin, O.H., Rhee, J.S., Arac, D., Rah, J.C., Rizo, J., Sudhof, T., and Rosenmund, C. (2006). Phosphatidylinositol phosphates as co-activators of Ca^{2+} binding to C2 domains of synaptotagmin 1. *J Biol Chem* 281, 15845-15852.

- Liley, A.W. (1956). The quantal components of the mammalian end-plate potential. *J Physiol* *133*, 571-587.
- Lin, R.C., and Scheller, R.H. (2000). Mechanisms of synaptic vesicle exocytosis. *Annu Rev Cell Dev Biol* *16*, 19-49.
- Littleton, J.T., Bellen, H.J., and Perin, M.S. (1993a). Expression of synaptotagmin in *Drosophila* reveals transport and localization of synaptic vesicles to the synapse. *Development* *118*, 1077-1088.
- Littleton, J.T., Stern, M., Schulze, K., Perin, M., and Bellen, H.J. (1993b). Mutational analysis of *Drosophila* synaptotagmin demonstrates its essential role in Ca^{2+} -activated neurotransmitter release. *Cell* *74*, 1125-1134.
- Lou, X., Scheuss, V., and Schneggenburger, R. (2005). Allosteric modulation of the presynaptic Ca^{2+} sensor for vesicle fusion. *Nature* *435*, 497-501.
- Lu, T., and Trussell, L.O. (2000). Inhibitory transmission mediated by asynchronous transmitter release. *Neuron* *26*, 683-694.
- Mao, L., and Wang, J.Q. (2001). Upregulation of preprodynorphin and preproenkephalin mRNA expression by selective activation of group I metabotropic glutamate receptors in characterized primary cultures of rat striatal neurons. *Brain research* *86*, 125-137.
- Marek, K.W., and Davis, G.W. (2002). Transgenically encoded protein photoinactivation (FlAsH-FALI): acute inactivation of synaptotagmin I. *Neuron* *36*, 805-813.
- Marqueze, B., Boudier, J.A., Mizuta, M., Inagaki, N., Seino, S., and Seagar, M. (1995). Cellular localization of synaptotagmin I, II, and III mRNAs in the central nervous system and pituitary and adrenal glands of the rat. *J Neurosci* *15*, 4906-4917.
- Matthew, W.D., Tsavaler, L., and Reichardt, L.F. (1981). Identification of a synaptic vesicle-specific membrane protein with a wide distribution in neuronal and neurosecretory tissue. *J Cell Biol* *91*, 257-269.
- Maximov, A., Pang, Z.P., Tervo, D.G., and Sudhof, T.C. (2007a). Monitoring synaptic transmission in primary neuronal cultures using local extracellular stimulation. *J Neurosci Methods* *161*, 75-87.
- Maximov, A., Shin, O.H., Liu, X., and Sudhof, T.C. (2007b). Synaptotagmin-12, a synaptic vesicle phosphoprotein that modulates spontaneous neurotransmitter release. *J Cell Biol* *176*, 113-124.

Maximov, A., and Sudhof, T.C. (2005). Autonomous function of synaptotagmin 1 in triggering synchronous release independent of asynchronous release. *Neuron* 48, 547-554.

McFerran, B.W., Graham, M.E., and Burgoyne, R.D. (1998). Neuronal Ca²⁺ sensor 1, the mammalian homologue of frequenin, is expressed in chromaffin and PC12 cells and regulates neurosecretion from dense-core granules. *J Biol Chem* 273, 22768-22772.

McMahon, H.T., Missler, M., Li, C., and Sudhof, T.C. (1995). Complexins: cytosolic proteins that regulate SNAP receptor function. *Cell* 83, 111-119.

McNew, J.A., Weber, T., Parlati, F., Johnston, R.J., Melia, T.J., Sollner, T.H., and Rothman, J.E. (2000). Close is not enough: SNARE-dependent membrane fusion requires an active mechanism that transduces force to membrane anchors. *J Cell Biol* 150, 105-117.

Means, A.R. (2000). Regulatory cascades involving calmodulin-dependent protein kinases. *Molecular endocrinology* (Baltimore, Md 14, 4-13.

Meinrenken, C.J., Borst, J.G., and Sakmann, B. (2003). Local routes revisited: the space and time dependence of the Ca²⁺ signal for phasic transmitter release at the rat calyx of Held. *J Physiol* 547, 665-689.

Milosevic, I., Sorensen, J.B., Lang, T., Krauss, M., Nagy, G., Haucke, V., Jahn, R., and Neher, E. (2005). Plasmalemmal phosphatidylinositol-4,5-bisphosphate level regulates the releasable vesicle pool size in chromaffin cells. *J Neurosci* 25, 2557-2565.

Morimoto, T., Wang, X.H., and Poo, M.M. (1998). Overexpression of synaptotagmin modulates short-term synaptic plasticity at developing neuromuscular junctions. *Neuroscience* 82, 969-978.

Mulkey, R.M., and Zucker, R.S. (1991). Action potentials must admit calcium to evoke transmitter release. *Nature* 350, 153-155.

Muller, M., Felmy, F., Schwaller, B., and Schneggenburger, R. (2007). Parvalbumin is a mobile presynaptic Ca²⁺ buffer in the calyx of held that accelerates the decay of Ca²⁺ and short-term facilitation. *J Neurosci* 27, 2261-2271.

Nagy, G., Kim, J.H., Pang, Z.P., Matti, U., Rettig, J., Sudhof, T.C., and Sorensen, J.B. (2006). Different effects on fast exocytosis induced by synaptotagmin 1 and 2 isoforms and abundance, but not by phosphorylation. *J Neurosci* (in press).

Nishiki, T., and Augustine, G.J. (2004). Synaptotagmin I synchronizes transmitter release in mouse hippocampal neurons. *J Neurosci* 24, 6127-6132.

Nonet, M.L., Grundahl, K., Meyer, B.J., and Rand, J.B. (1993). Synaptic function is impaired but not eliminated in *C. elegans* mutants lacking synaptotagmin. *Cell* 73, 1291-1305.

Ohtsuka, T., Takao-Rikitsu, E., Inoue, E., Inoue, M., Takeuchi, M., Matsubara, K., Deguchi-Tawarada, M., Satoh, K., Morimoto, K., Nakanishi, H., *et al.* (2002). Cast: a novel protein of the cytomatrix at the active zone of synapses that forms a ternary complex with RIM1 and munc13-1. *J Cell Biol* 158, 577-590.

Osborne, S.L., Herreros, J., Bastiaens, P.I., and Schiavo, G. (1999). Calcium-dependent oligomerization of synaptotagmins I and II. Synaptotagmins I and II are localized on the same synaptic vesicle and heterodimerize in the presence of calcium. *J Biol Chem* 274, 59-66.

Otsu, Y., Shahrezaei, V., Li, B., Raymond, L.A., Delaney, K.R., and Murphy, T.H. (2004). Competition between phasic and asynchronous release for recovered synaptic vesicles at developing hippocampal autaptic synapses. *J Neurosci* 24, 420-433.

Pang, Z.P., Melicoff, E., Padgett, D., Liu, Y., Teich, A.F., Dickey, B.F., Lin, W., Adachi, R., and Sudhof, T.C. (2006a). Synaptotagmin-2 is essential for survival and contributes to Ca²⁺ triggering of neurotransmitter release in central and neuromuscular synapses. *J Neurosci* 26, 13493-13504.

Pang, Z.P., Sun, J., Rizo, J., Maximov, A., and Sudhof, T.C. (2006b). Genetic analysis of synaptotagmin 2 in spontaneous and Ca²⁺-triggered neurotransmitter release. *Embo J* 25, 2039-2050.

Parlati, F., McNew, J.A., Fukuda, R., Miller, R., Sollner, T.H., and Rothman, J.E. (2000). Topological restriction of SNARE-dependent membrane fusion. *Nature* 407, 194-198.

Perin, M.S., Brose, N., Jahn, R., and Sudhof, T.C. (1991). Domain structure of synaptotagmin (p65). *J Biol Chem* 266, 623-629.

Perin, M.S., Fried, V.A., Mignery, G.A., Jahn, R., and Sudhof, T.C. (1990). Phospholipid binding by a synaptic vesicle protein homologous to the regulatory region of protein kinase C. *Nature* 345, 260-263.

Pongs, O., Lindemeier, J., Zhu, X.R., Theil, T., Engelkamp, D., Krah-Jentgens, I., Lambrecht, H.G., Koch, K.W., Schwemer, J., Rivosecchi, R., *et al.* (1993). Frequentin--a novel calcium-binding protein that modulates synaptic efficacy in the *Drosophila* nervous system. *Neuron* 11, 15-28.

Popoli, M. (1993). Synaptotagmin is endogenously phosphorylated by Ca²⁺/calmodulin protein kinase II in synaptic vesicles. *FEBS Lett* 317, 85-88.

- Pucharcos, C., Casas, C., Nadal, M., Estivill, X., and de la Luna, S. (2001). The human intersectin genes and their spliced variants are differentially expressed. *Biochim Biophys Acta* 1521, 1-11.
- Rajebhosale, M., Greenwood, S., Vidugiriene, J., Jeromin, A., and Hilfiker, S. (2003). Phosphatidylinositol 4-OH kinase is a downstream target of neuronal calcium sensor-1 in enhancing exocytosis in neuroendocrine cells. *J Biol Chem* 278, 6075-6084.
- Ravin, R., Spira, M.E., Parnas, H., and Parnas, I. (1997). Simultaneous measurement of intracellular Ca^{2+} and asynchronous transmitter release from the same crayfish bouton. *J Physiol* 501 (Pt 2), 251-262.
- Reim, K., Mansour, M., Varoqueaux, F., McMahon, H.T., Sudhof, T.C., Brose, N., and Rosenmund, C. (2001). Complexins regulate a late step in Ca^{2+} -dependent neurotransmitter release. *Cell* 104, 71-81.
- Rhee, J.S., Li, L.Y., Shin, O.H., Rah, J.C., Rizo, J., Sudhof, T.C., and Rosenmund, C. (2005). Augmenting neurotransmitter release by enhancing the apparent Ca^{2+} affinity of synaptotagmin 1. *Proc Natl Acad Sci U S A* 102, 18664-18669.
- Rickman, C., Archer, D.A., Meunier, F.A., Craxton, M., Fukuda, M., Burgoyne, R.D., and Davletov, B. (2004). Synaptotagmin interaction with the syntaxin/SNAP-25 dimer is mediated by an evolutionarily conserved motif and is sensitive to inositol hexakisphosphate. *J Biol Chem* 279, 12574-12579.
- Rickman, C., and Davletov, B. (2003). Mechanism of calcium-independent synaptotagmin binding to target SNAREs. *J Biol Chem* 278, 5501-5504.
- Rivosecchi, R., Pongs, O., Theil, T., and Mallart, A. (1994). Implication of frequenin in the facilitation of transmitter release in *Drosophila*. *J Physiol* 474, 223-232.
- Rizo, J., and Sudhof, T.C. (2002). Snares and Munc18 in synaptic vesicle fusion. *Nat Rev Neurosci* 3, 641-653.
- Robinson, I.M., Ranjan, R., and Schwarz, T.L. (2002). Synaptotagmins I and IV promote transmitter release independently of Ca^{2+} binding in the C(2)A domain. *Nature* 418, 336-340.
- Rosenmund, C., and Stevens, C.F. (1996). Definition of the readily releasable pool of vesicles at hippocampal synapses. *Neuron* 16, 1197-1207.
- Roux, I., Safieddine, S., Nouvian, R., Grati, M., Simmler, M.C., Bahloul, A., Perfettini, I., Le Gall, M., Rostaing, P., Hamard, G., *et al.* (2006). Otoferlin, defective in a human deafness form, is essential for exocytosis at the auditory ribbon synapse. *Cell* 127, 277-289.

Rufener, E., Frazier, A.A., Wieser, C.M., Hinderliter, A., and Cafiso, D.S. (2005). Membrane-bound orientation and position of the synaptotagmin C2B domain determined by site-directed spin labeling. *Biochemistry* 44, 18-28.

Russ, A., Stumm, G., Augustin, M., Sedlmeier, R., Wattler, S., and Nehls, M. (2002). Random mutagenesis in the mouse as a tool in drug discovery. *Drug Discov Today* 7, 1175-1183.

Sakaba, T., and Neher, E. (2001). Quantitative relationship between transmitter release and calcium current at the calyx of held synapse. *J Neurosci* 21, 462-476.

Schiavo, G., Gmachl, M.J., Stenbeck, G., Sollner, T.H., and Rothman, J.E. (1995). A possible docking and fusion particle for synaptic transmission. *Nature* 378, 733-736.

Schiavo, G., Stenbeck, G., Rothman, J.E., and Sollner, T.H. (1997). Binding of the synaptic vesicle v-SNARE, synaptotagmin, to the plasma membrane t-SNARE, SNAP-25, can explain docked vesicles at neurotoxin-treated synapses. *Proc Natl Acad Sci U S A* 94, 997-1001.

Schneggenburger, R., and Forsythe, I.D. (2006). The calyx of Held. *Cell and tissue research* 326, 311-337.

Schneggenburger, R., and Neher, E. (2000). Intracellular calcium dependence of transmitter release rates at a fast central synapse. *Nature* 406, 889-893.

Schneggenburger, R., and Neher, E. (2005). Presynaptic calcium and control of vesicle fusion. *Current opinion in neurobiology* 15, 266-274.

Schoch, S., Deak, F., Konigstorfer, A., Mozhayeva, M., Sara, Y., Sudhof, T.C., and Kavalali, E.T. (2001). SNARE function analyzed in synaptobrevin/VAMP knockout mice. *Science* 294, 1117-1122.

Shao, X., Li, C., Fernandez, I., Zhang, X., Sudhof, T.C., and Rizo, J. (1997). Synaptotagmin-syntaxin interaction: the C2 domain as a Ca²⁺-dependent electrostatic switch. *Neuron* 18, 133-142.

Sheng, Z.H., Yokoyama, C.T., and Catterall, W.A. (1997). Interaction of the synprint site of N-type Ca²⁺ channels with the C2B domain of synaptotagmin I. *Proc Natl Acad Sci U S A* 94, 5405-5410.

Shin, O.H., Han, W., Wang, Y., and Sudhof, T.C. (2005). Evolutionarily conserved multiple C2 domain proteins with two transmembrane regions (MCTPs) and unusual Ca²⁺ binding properties. *J Biol Chem* 280, 1641-1651.

Shin, O.H., Rhee, J.S., Tang, J., Sugita, S., Rosenmund, C., and Sudhof, T.C. (2003). Sr^{2+} binding to the Ca^{2+} binding site of the synaptotagmin 1 C2B domain triggers fast exocytosis without stimulating SNARE interactions. *Neuron* 37, 99-108.

Shin, O.H., Rizo, J., and Sudhof, T.C. (2002). Synaptotagmin function in dense core vesicle exocytosis studied in cracked PC12 cells. *Nat Neurosci* 5, 649-656.

Sippy, T., Cruz-Martin, A., Jeromin, A., and Schweizer, F.E. (2003). Acute changes in short-term plasticity at synapses with elevated levels of neuronal calcium sensor-1. *Nat Neurosci* 6, 1031-1038.

Sommer, I., Lingenhohl, K., and Friauf, E. (1993). Principal cells of the rat medial nucleus of the trapezoid body: an intracellular in vivo study of their physiology and morphology. *Exp Brain Res* 95, 223-239.

Sorensen, J.B. (2005). SNARE complexes prepare for membrane fusion. *Trends Neurosci* 28, 453-455.

Sorensen, J.B., Fernandez-Chacon, R., Sudhof, T.C., and Neher, E. (2003). Examining synaptotagmin 1 function in dense core vesicle exocytosis under direct control of Ca^{2+} . *J Gen Physiol* 122, 265-276.

Stevens, C.F., and Sullivan, J.M. (2003). The synaptotagmin C2A domain is part of the calcium sensor controlling fast synaptic transmission. *Neuron* 39, 299-308.

Stevens, C.F., and Wesseling, J.F. (1998). Activity-dependent modulation of the rate at which synaptic vesicles become available to undergo exocytosis. *Neuron* 21, 415-424.

Stumm, G., Russ, A., and Nehls, M. (2002). Deductive genomics: a functional approach to identify innovative drug targets in the post-genome era. *Am J Pharmacogenomics* 2, 263-271.

Sudhof, T.C. (2002). Synaptotagmins: why so many? *J Biol Chem* 277, 7629-7632.

Sudhof, T.C. (2004). The synaptic vesicle cycle. *Annu Rev Neurosci* 27, 509-547.

Sudhof, T.C., De Camilli, P., Niemann, H., and Jahn, R. (1993). Membrane fusion machinery: insights from synaptic proteins. *Cell* 75, 1-4.

Sugita, S., Han, W., Butz, S., Liu, X., Fernandez-Chacon, R., Lao, Y., and Sudhof, T.C. (2001). Synaptotagmin VII as a plasma membrane Ca^{2+} sensor in exocytosis. *Neuron* 30, 459-473.

Sugita, S., Hata, Y., and Sudhof, T.C. (1996). Distinct Ca^{2+} -dependent properties of the first and second C2-domains of synaptotagmin I. *J Biol Chem* 271, 1262-1265.

Sugita, S., Shin, O.H., Han, W., Lao, Y., and Sudhof, T.C. (2002). Synaptotagmins form a hierarchy of exocytotic Ca(2+) sensors with distinct Ca(2+) affinities. *Embo J* 21, 270-280.

Sun, J., Bronk, P., Liu, X., Han, W., and Sudhof, T.C. (2006). Synapsins regulate use-dependent synaptic plasticity in the calyx of Held by a Ca2+/calmodulin-dependent pathway. *Proc Natl Acad Sci U S A* 103, 2880-2885.

Sun, J.Y., and Wu, L.G. (2001). Fast kinetics of exocytosis revealed by simultaneous measurements of presynaptic capacitance and postsynaptic currents at a central synapse. *Neuron* 30, 171-182.

Sutton, R.B., Fasshauer, D., Jahn, R., and Brunger, A.T. (1998). Crystal structure of a SNARE complex involved in synaptic exocytosis at 2.4 Å resolution. *Nature* 395, 347-353.

Tang, J., Maximov, A., Shin, O.H., Dai, H., Rizo, J., and Sudhof, T.C. (2006). A complexin/synaptotagmin 1 switch controls fast synaptic vesicle exocytosis. *Cell* 126, 1175-1187.

Taschenberger, H., Scheuss, V., and Neher, E. (2005). Release kinetics, quantal parameters and their modulation during short-term depression at a developing synapse in the rat CNS. *J Physiol* 568, 513-537.

Taverna, E., Francolini, M., Jeromin, A., Hilfiker, S., Roder, J., and Rosa, P. (2002). Neuronal calcium sensor 1 and phosphatidylinositol 4-OH kinase beta interact in neuronal cells and are translocated to membranes during nucleotide-evoked exocytosis. *Journal of cell science* 115, 3909-3922.

Toutenhoofd, S.L., and Strehler, E.E. (2000). The calmodulin multigene family as a unique case of genetic redundancy: multiple levels of regulation to provide spatial and temporal control of calmodulin pools? *Cell calcium* 28, 83-96.

Trommershauser, J., Schneggenburger, R., Zippelius, A., and Neher, E. (2003). Heterogeneous presynaptic release probabilities: functional relevance for short-term plasticity. *Biophys J* 84, 1563-1579.

Ubach, J., Lao, Y., Fernandez, I., Arac, D., Sudhof, T.C., and Rizo, J. (2001). The C2B domain of synaptotagmin I is a Ca2+-binding module. *Biochemistry* 40, 5854-5860.

Ubach, J., Zhang, X., Shao, X., Sudhof, T.C., and Rizo, J. (1998). Ca2+ binding to synaptotagmin: how many Ca2+ ions bind to the tip of a C2-domain? *Embo J* 17, 3921-3930.

Ullrich, B., Li, C., Zhang, J.Z., McMahon, H., Anderson, R.G., Geppert, M., and Sudhof, T.C. (1994). Functional properties of multiple synaptotagmins in brain. *Neuron* 13, 1281-1291.

Wang, C.T., Grishanin, R., Earles, C.A., Chang, P.Y., Martin, T.F., Chapman, E.R., and Jackson, M.B. (2001). Synaptotagmin modulation of fusion pore kinetics in regulated exocytosis of dense-core vesicles. *Science* 294, 1111-1115.

Wang, X., Kibschull, M., Laue, M.M., Lichte, B., Petrasch-Parwez, E., and Kilimann, M.W. (1999). Aczonin, a 550-kD putative scaffolding protein of presynaptic active zones, shares homology regions with Rim and Bassoon and binds profilin. *J Cell Biol* 147, 151-162.

Wang, Y., and Sudhof, T.C. (2003). Genomic definition of RIM proteins: evolutionary amplification of a family of synaptic regulatory proteins(small star, filled). *Genomics* 81, 126-137.

Washbourne, P., Thompson, P.M., Carta, M., Costa, E.T., Mathews, J.R., Lopez-Bendito, G., Molnar, Z., Becher, M.W., Valenzuela, C.F., Partridge, L.D., *et al.* (2002). Genetic ablation of the t-SNARE SNAP-25 distinguishes mechanisms of neuroexocytosis. *Nat Neurosci* 5, 19-26.

Weber, T., Zemelman, B.V., McNew, J.A., Westermann, B., Gmachl, M., Parlati, F., Sollner, T.H., and Rothman, J.E. (1998). SNAREpins: minimal machinery for membrane fusion. *Cell* 92, 759-772.

Wilson, M.C., Mehta, P.P., and Hess, E.J. (1996). SNAP-25, enSNAREd in neurotransmission and regulation of behaviour. *Biochem Soc Trans* 24, 670-676.

Wu, L.G., and Borst, J.G. (1999). The reduced release probability of releasable vesicles during recovery from short-term synaptic depression. *Neuron* 23, 821-832.

Wu, L.G., Westenbroek, R.E., Borst, J.G., Catterall, W.A., and Sakmann, B. (1999). Calcium channel types with distinct presynaptic localization couple differentially to transmitter release in single calyx-type synapses. *J Neurosci* 19, 726-736.

Xu-Friedman, M.A., and Regehr, W.G. (2000). Probing fundamental aspects of synaptic transmission with strontium. *J Neurosci* 20, 4414-4422.

Xu, J., Mashimo, T., and Sudhof, T.C. (2007). Synaptotagmin-1, -2, and -9: Ca(2+) sensors for fast release that specify distinct presynaptic properties in subsets of neurons. *Neuron* 54, 567-581.

Yoshida, A., Oho, C., Omori, A., Kuwahara, R., Ito, T., and Takahashi, M. (1992). HPC-1 is associated with synaptotagmin and omega-conotoxin receptor. *J Biol Chem* 267, 24925-24928.

Yoshihara, M., and Littleton, J.T. (2002). Synaptotagmin I functions as a calcium sensor to synchronize neurotransmitter release. *Neuron* 36, 897-908.

Zhang, J.Z., Davletov, B.A., Sudhof, T.C., and Anderson, R.G. (1994). Synaptotagmin I is a high affinity receptor for clathrin AP-2: implications for membrane recycling. *Cell* 78, 751-760.

Zhang, X., Kim-Miller, M.J., Fukuda, M., Kowalchuk, J.A., and Martin, T.F. (2002). Ca^{2+} -dependent synaptotagmin binding to SNAP-25 is essential for Ca^{2+} -triggered exocytosis. *Neuron* 34, 599-611.

Zhang, X., Rizo, J., and Sudhof, T.C. (1998). Mechanism of phospholipid binding by the C2A-domain of synaptotagmin I. *Biochemistry* 37, 12395-12403.

Zhao, X., Varnai, P., Tuymetova, G., Balla, A., Toth, Z.E., Oker-Blom, C., Roder, J., Jeromin, A., and Balla, T. (2001). Interaction of neuronal calcium sensor-1 (NCS-1) with phosphatidylinositol 4-kinase beta stimulates lipid kinase activity and affects membrane trafficking in COS-7 cells. *J Biol Chem* 276, 40183-40189.

Zhong, H., Yokoyama, C.T., Scheuer, T., and Catterall, W.A. (1999). Reciprocal regulation of P/Q-type Ca^{2+} channels by SNAP-25, syntaxin and synaptotagmin. *Nat Neurosci* 2, 939-941.

Zucker, R.S., and Regehr, W.G. (2002). Short-term synaptic plasticity. *Annu Rev Physiol* 64, 355-405.

VITAE

Zhiping Pang was born in Dongzhi, Anhui, China on Sept. 27th, 1973, the second child of Longxi Pang and Guizhen Cao. After completing his studies in Dongliu High School, Anhui in 1990, he entered the Fourth Military Medical University at Xi'an, Shaanxi. He received the degree of Bachelor of Medicine (Equivalent to M.D. degree in the US) in 1995. He subsequently obtained a Master of Science degree majored in Neuroscience from the same institute in 1997. From 1998 to 1999, he was a visiting scientist at Department of Physiology of Kyushu University, Fukuoka, Japan. From 2000 to 2003, he was a research associate at Indiana University School of Medicine at Indianapolis. Since July 2003, he is a graduate student for Ph.D. degree in UT Southwestern Medical Center at Dallas. In 2001, he married to Yan Lin from Beijing.

Permanent Address: 2913 Elmridge Drive,
Flower Mound, TX 75022